How proteins search for their targets on DNA

A THESIS

SUBMITTED TO THE FACULTY OF THE GRADUATE SCHOOL

OF THE UNIVERSITY OF MINNESOTA

BY

Tao Hu

IN PARTIAL FULFILLMENT OF THE REQUIREMENTS

FOR THE DEGREE OF

DOCTOR OF PHILOSOPHY

May, 2008

Acknowledgements

Of all the people who have helped me through my five years at the University of Minnesota, undoubtedly the first one to whom I am extremely grateful is my advisor, Professor Boris I. Shklovskii. It is Boris who brought me into the fantastic world of theoretical condensed matter and biological physics. He guided me like a strict father, being critical to my work, caring so much about my life and future career plans. I can not imagine I could go so far to the fulfilment of my Phd with out his numerous help.

I must also thank Professor Alexander Yu. Grosberg. I benefit numerously from collaboration with him. Whenever I ask him a question, no matter how trivial it is, he explained to me in every detail with great patience. He is also a great lecturer. I really enjoyed taking three of his graduate courses.

I thank Professor Lenid I. Glazman for his kind guidance during my search for graduate advisor. I also thank him and Professor Vincent Noriax for their help in my postdoctoral position seeking.

I am grateful to Xinjie Qiu, who is the first person who welcomed me in the new country. He picked me up at the airport upon my first arrival and arranged temporary housing for me. I received tons of help from him since then. I bet my life would be much harder without his generous help.

During my research and postdoctoral position searching, Jingshan Zhang offered me big help. Discussion with him about Physics is always interesting. I appreciate his kind hosting when I visited Boston.

Also I am very lucky to have these friends Yu Chen, Xiaoqi Liu, Baolin Liu, Wenhao zhang, Zekun Deng, Jian Qin, Rui Zhang and Longhua Hu who gave me much help in various aspects. I would like to express my thank to them here.

A special world goes to my wife Kai Xie. Her love, patience, and encouragement have given my life immense purpose, joy, and meaning. My achievement at current stage would have no meaning or satisfaction without having her with me to share it.

Finally, I must thank all the members of family to whom this work is dedicated. Their encoragement and understanding through out my education have always been the very important support for me.

To my wife, my family, and my friends for all of their love, support and most importantly their patience.

Abstract

It is known since the early days of molecular biology that proteins locate their specific targets on DNA up to two orders-of-magnitude faster than the Smoluchowski three-dimensional (3D) diffusion rate. An accepted explanation of this fact is that proteins are nonspecifically adsorbed on DNA, and sliding along DNA provides for the faster one-dimensional (1D) search. We explicitly addressed the role of DNA conformation and the dispersion of nonspecific adsorption energies. We identified a wealth of new different scaling regimes and found that the maximum on the rate-versus-ionic strength curve is asymmetric.

We also studied the other facilitating mechanism termed intersegment transferwhere proteins which have two DNA binding sites can transfer from one DNA segment to another without dissociation to water. We proposed a scaling theory which combines the effects of protein 3D diffusion, 1D sliding, intersegment transfer and DNA motion.

A direct application of our work on target search problem is the kinetics of viral self-assembly. We show that due to the 1D sliding of capsid proteins on the unassembled chain of single-stranded RNA, the self-assembly is more than ten times faster than the case involving only three-dimensional diffusion.

We further extended our theory to the macroscopic diffusion coefficient of

proteins in a semi-dilute solution of DNA pieces and the effective conductivity of a composite made of well conducting nanowires suspended in some poor conducting medium.

Table of Contents

List of Tables

List of Figures

Chapter 1

Introduction

Imagine that while you are reading these lines a λ-phage injects its DNA into a cell. For the infected cell, this sets a race against time: its hope to survive depends entirely on the ability of the proper restriction enzyme to find and recognize the specific site on viral DNA and then cut it, thus rendering viral DNA inoperable and harmless. If restriction enzyme takes too long to locate its target, then the cell is dead.

This is, of course, just an example. Essentially all of molecular biology is about various enzymes operating with the specific places on DNA, and each enzyme must locate its target site quickly and reliably. How can they accomplish the task? It was recognized very early on that the search by free diffusion through the 3D solution is far too slow and proteins somehow do it faster. Indeed, the rate at which diffusing particles find the target was determined by M. Smoluchowski

as early as in 1917 [1], it is equal to $4\pi D_3 bc$, where b is the target radius, D_3 and c are, respectively, the diffusion coefficient and concentration of diffusing particles, in our case - proteins (see also appendix A for a simple derivation). Although Smoluchowski result sets the rigid upper bound for the possible diffusion controlled rate, proteins at least in some instances somehow manage to do it up to about two orders of magnitude faster - see, for instance, [2, 3]. The idea to resolve this paradox goes back to Delbrück [4] who suggested that proteins can fairly quickly adsorb on a non-specific random place on DNA and then 1D sliding along DNA can be much faster than the 3D diffusion. In fact, the idea that reduced dimension speeds up chemical reaction can be traced even further back to Langmuir [5], who noticed that adsorbtion of reagents on a 2D surface can facilitate their diffusive finding each other.

The field attracted intensive attention for many years. Early studies [2, 3] seemed to corroborate the Delbrück model. A nice recent review of various strategies employed to address the problem experimentally can be found in the paper Ref. [6]. Based on the summary of experimental evidence, authors of this review conclude, that the process is not just the naive 1D sliding, but rather a delicately weighted mixture of 1D sliding over some distances and 3D diffusion. A theorist also could have guessed the presence of a cross-over between 1D sliding and 3D diffusion, because sliding along coiled DNA becomes very inefficient at large scale: having moved by about $t^{1/2}$ along DNA after 1D diffusion over some time

t, protein moves in space by only $t^{1/4}$ if DNA is a Gaussian coil. This is very slow subdiffusion. That is the situation requiring theoretical attention to understand how 3D and 1D diffusion can be combined and how their combination should be manifested in experiments.

On the theoretical front, major contribution to the field is due to Berg, Winter and von Hippel (BWH) [7]. As an outcome of their theory, these authors formulated the following nice prediction, partially confirmed by their later *in vitro* experiments [8]: the rate at which proteins find their specific target site on DNA depends in a non-monotonic fashion on the ionic strength of the solution. In this context, ionic strength is believed to tune the strength of non-specific adsorbtion of proteins on DNA, presumably because a protein adsorbs to DNA via positively charged patch on its surface. Thus, in essence one should speak of the non-monotonous dependence of the rate on the energy of non-specific adsorbtion of proteins on DNA.

Although qualitatively consistent with experiment, BWH theory [7] leaves several questions open. First and foremost, how does the search time of proteins finding their target, or the corresponding rate, depend on the DNA conformation? In particular, is it important that the DNA is coiled at the length scale larger than the persistence length? Is it important that DNA coil may not fit in the volume available, and then DNA must be a globule, like in the nucleoid in a procaryotic cell *in vivo* or under experimental conditions *in vitro* [9]? Second,

closely related aspect is that BWH theory [7] does not answer the experimentally most relevant question [6] of the interplay between 1D sliding and 3D diffusion. In particular, one of the questions raised by experiments and not answered by the BWH theory [7] is about the correlations between the place where a protein departs from DNA and the place where it re-adsorbs. Third aspect, although of a lesser importance and more taste-dependent, BWH theory [7] does not yield simple intuitive explanation for non-monotonic dependence of the rate on the strength of non-specific adsorbtion, and one may want to know whether there exists simple qualitative description of the rate at least in some limits.

More recent refinement of the theory is given in the work Ref. [10]. The authors of this work follow BWH in that they treat DNA in terms of "domains" - a concept having no unambiguous definition in the physics of DNA. Also, the paper Ref. [10] makes it very explicit that BWH [7] and subsequent theories neglect correlations between the place where protein desorbs from DNA and the place where it adsorbs again - the approximation that clearly defies the polymeric nature and fractal properties of DNA. At the same time, this approximation leaves unanswered the experimentally motivated question of the interplay between 1D and 3D components of the search process.

In the recent years, the problem was revisited by physicists several times [11, 12, 13], but the disturbing fact was that all of them attributed quite different results and statements to BWH: the paper Ref. [11] says that according to BWH,

the search time scales as DNA lengths L rather than L^2 as in 1D diffusion along DNA; the work Ref. [12] states that proteins slide along DNA some distance which is independent of DNA conformation, regardless even of the DNA fractal properties; the article Ref. [13], although concentrates on the role of the non-uniform DNA sequence, claims that the time for 3D diffusion must be about the same as time for 1D diffusion along DNA. Further, possibly even more disturbing fact is that neither of the papers [7, 10, 11, 13] makes any clearly articulated explicit assumption about DNA conformation. Is it straight, or Gaussian coil with proper persistence length, or what? Does the result depend on the DNA conformation? Interestingly, experimenters do discuss in their works (see [6] and references therein) the issue of correlated vs. uncorrelated re-adsorbtion, these discussions call for theoretical attention and theoretical description in terms of correlations in fractal DNA, but so far proper theory was not suggested.

Motivated by these considerations, we in this work set out to re-examine the problem from the very beginning. The plan is as follows. In Chapter 2, we explicitly take into account that DNA is fairly straight at the length scale smaller than persistence length, it is Gaussian coil on the larger length scale. We also consider the possibility that DNA is confined within such a volume where Gaussian coil does not fit (as it does not fit into a typical procaryotic cell, for instance), in which case DNA must be a globule. In Chapter 3, we extend our theory to the case where the proteins have two DNA binding sites and can transfer from one DNA

segment to another without dissociation to water. We calculate the target search rate for such proteins in a dense globular DNA, taking into account intersegment transfer working in conjunction with DNA motion and protein sliding along DNA. We continue in Chapter 4 by looking at the role of the dispersion of nonspecific adsorption energies of proteins along DNA due to its quasi random sequence. In Chapter 5, we further applied our theory to the kinetics of the viral self-assembly. Finally, in Chapter 6 we calculate the macroscopic diffusion coefficient of protein in a solution of DNA pieces. We also find the effective conductivity of a composite made of well conducting nanowires suspended in a poor conducting medium.

Chapter 2

Role of DNA Conformation

2.1 Model, approach, and limitations

We assume that within some volume v some (double helical) DNA is confined, with contour length L, persistence length p, and with the target site of the size b.

We further assume that protein can be non-specifically adsorbed on any place of the DNA, and that non-specific adsorbtion energy ϵ, or the corresponding constant $y = e^{\epsilon/k_B T}$, is the same everywhere on the DNA and does not depend on the DNA sequence. We assume that every protein molecule has just one site capable to adsorb on the DNA. There are proteins with two such sites, they can adsorb on two separate pieces of DNA at the same time and thus serve as a cross-linker for the DNA itself. We do not consider this possibility in this chapter.

We assume that there is only one molecule of DNA. In reality, macroscopic

sample of DNA solution at certain concentration is used in any *in vitro* experiment. From the theoretical standpoint, DNA solution with concentration of $1/v$ (in units of DNA chains per unit volume) is equivalent to the system of one DNA considered here. We also assume that DNA has only one target site on it, which is not always true in reality [6].

We assume that non-specifically bound protein can diffuse (slide) along DNA with the diffusion coefficient D_1, while protein dissolved in surrounding water diffuses in 3D with diffusion constant D_3. Thus, we have a unitless parameter related to the diffusion coefficients, it is $d = D_1/D_3$. In the simpler version of the theory, which we shall consider first, we assume $D_1 = D_3$, or $d = 1$. For simplicity, we assume that while protein is diffusing, either in 3D or along the DNA, DNA itself remains immobile.

The quantity of our interest is the time needed for the target site to be found by a protein (consider e.g., an example of restriction enzyme attacking viral DNA intruder). One should imagine certain concentration c of proteins randomly introduced into the system, and ask what is the time needed for the *first* of these proteins to arrive to the target site. We will only address the mean time, averaged over both thermal noise and DNA conformation. For this averaged quantity, since the DNA is assumed immobile, the problem can be addressed in a simple way, by looking at the stationary *rate*. Namely, we should consider that there is a sink of proteins in the place of the specific target site, and that it consumes proteins

with the rate J proportional to concentration c, which should be supported on a constant level by an influx to maintain stationarity. Obviously then, the averaged time is just $1/J$. At the end of the chapter, in section 2.5.1 we show how to re-derive all our results in terms of a single protein, thus avoiding an artificial assumption that there is a sink of proteins at the place of the target.

In this chapter, we calculate the rate J assuming concentration c an arbitrary constant. In order to compare the predicted rate to the Smoluchowski rate $J_s = 4\pi D_3 cb$, we shall mainly look at the ratio

$$\frac{J}{J_s} = \frac{J}{4\pi D_3 cb} \sim \frac{J}{D_3 cb} \ , \tag{2.1}$$

which characterizes the acceleration of the reaction rate achieved due to the sliding along DNA.

We will be mainly interested in scaling dependence of the rate J or acceleration J/J_s on major system parameters, such as y, L, and v. In this context, we will use symbol "$\sim$" to mean "equal up to a numerical coefficient of order one", while symbols $>$ and $<$ mean $\gg$ and $\ll$, respectively.

Along with dropping out all numerical coefficients in our scaling estimates, we also make several assumptions driven by pure desire to make formulae simpler and to clarify major physical ideas. We assume that all the "microscopic" length scales are of the same order, namely, about target size b: protein diameter, double helical

DNA diameter, and the distance from DNA at which non-specific adsorbtion takes place. These assumptions are easy to relax.

Throughout this work we disregard the excluded volume of DNA, considering DNA coil as Gaussian and *not* the swollen coil, described by the Flory index 3/5. This is a reasonable approximation for most realistic cases [14]. Indeed, for many real DNAs, such as, e.g., λ-DNA, it is justified because of a large persistence length-to-diameter ratio of the double helix: excluded volume in the coil remains unimportant up to DNA length about $L < p^3/b^2$ (up to about 100000 base pairs under normal non-exotic ionic conditions). We further assume that the volume fraction of DNA inside volume v, which is about Lb^2/v, is sufficiently small even when DNA is a globule. In particular, we assume $Lb^2/v < b/p$, because in a denser system liquid crystalline nematic ordering of DNA segments becomes likely [14]. Of course, real nucleoid is a rather complex structure involving much more sophisticated features than just orientational ordering, they are caused by structural and other proteins, by entanglements, etc - see the recent experimental work [9] and references therein. In this work we shall touch neither of these issues, guided by the prejudice that simple questions should be addressed first.

The plan of this chapter is as follows. In section 2.2 we consider first the relatively simple cases when DNA is a Gaussian coil and 1D sliding of proteins along DNA involves only a small part of DNA length. Already in this situation we will be able to explain the effect of correlated re-adsorbtion and arrive at a

number of new results, such as, for instance, possible asymmetric character of the maximum on the curve of the rate as a function of adsorbtion strength. These results are also derived through the electrostatic analogy in the appendix (B). In the section 2.3 we present a summary of all possible scaling regimes. We then discuss them in more details (section 2.4). We start this by looking at the rate saturation when 1D sliding involves entire DNA length (section 2.4.1). We then consider a delicate case when DNA as a whole is a globule (section 2.4.2); in this case, we found that even the 3D transport of proteins is in many cases realized through the sliding of adsorbed proteins along DNA and using DNA as a network of 1D transport ways. We continue in section 2.4.3 by looking at the situations when diffusion coefficient of the proteins along DNA is either smaller or larger than their diffusion coefficient in the surrounding bulk water. In section 2.5.1 we re-derive all our major results using the language of single protein search time instead of a stationary process and flux. Finally, we conclude with comparison of our results to those of earlier works and the discussion of possible further implications of our work (section 2.5).

2.2 Simple case: straight antenna vs. Gaussian coil antenna

The reason why non-specific adsorbtion on DNA can speed up the finding of target is illustrated in Fig. 2.1 (a) and (b): it is because DNA forms a kind of an antenna around the target thus increasing the size of the "effective target". How should we determine the size of this antenna? The simplest argument is this. Suppose antenna size is ξ and contour length of DNA inside antenna is λ. It is worth to emphasize that ξ and λ do not define any sharp border, but rather a smooth cross-over, such that transport outside antenna is *mainly* due to the 3D diffusion, while inside antenna transport is *dominated* by the sliding, or 1D diffusion along DNA. The advantage of thinking about *stationary* process is that under stationary conditions, the flux of particles delivered by the 3D diffusion into the ξ-sphere of antenna must be equal to the flux of particles delivered by 1D diffusion into the target. The former rate is given by the Smoluchowski formula (see appendix A) for the target size ξ and for the concentration of "free" (not adsorbed) proteins $c_{\rm free}$, it is $\sim D_3 c_{\rm free}\xi$. To estimate the latter rate, we note that the time of 1D diffusion into the target site from a distance of order λ is about λ^2/D_1; therefore, the rate can be written as $(\lambda c_{\rm ads})\,/\,(\lambda^2/D_1)$, where $\lambda c_{\rm ads}$ is the number of proteins non-specifically adsorbed on the piece of DNA of the length

λ. Thus, our main *balance* equation for the rate J reads

$$J \sim D_3 c_{\rm free} \xi \sim \frac{D_1 c_{\rm ads}}{\lambda} \ . \tag{2.2}$$

Formally, this equation follows from the continuity equation, which says that divergence of flux must vanish everywhere for the stationary process, flux must be a potential field.

Notice that the balance equation (2.2) depends on the relation between ξ and λ - between the size of antenna measured in space (ξ) and measured along the DNA (λ). Here, we already see why fractal properties of DNA conformations enter our problem.

To determine the one-dimensional concentration of non-specifically adsorbed proteins, $c_{\rm ads}$, and concentration of proteins remaining free in solution $c_{\rm free}$, we now argue that as long as antenna is only a small part of the DNA present, every protein in the system will adsorb and desorb many times on DNA before it locates the target, therefore, there is statistical equilibrium between adsorbed and desorbed proteins. Assuming that we know the adsorbtion energy ϵ or the corresponding constant $y = e^{\epsilon/k_B T}$, and remembering that adsorbed proteins are confined within distance or order b from the DNA, we can write down the equilibrium condition as

$$c_{\rm ads}/c_{\rm free} b^2 = y \ , \tag{2.3}$$

which must be complemented by the particle counting condition

$$c_{\rm ads}L + c_{\rm free}\left(v - Lb^2\right) = cv \ . \tag{2.4}$$

Since volume fraction of DNA is always small, $Lb^2 \ll v$, standard algebra then yields

$$\begin{aligned} c_{\rm ads} &\simeq \frac{cvyb^2}{yLb^2+v} \sim \begin{cases} cyb^2 & \text{if} \quad y < v/Lb^2 \\ cv/L & \text{if} \quad y > v/Lb^2 \end{cases} , \\ c_{\rm free} &\simeq \frac{cv}{yLb^2+v} \sim \begin{cases} c & \text{if} \quad y < v/Lb^2 \\ cv/Lb^2y & \text{if} \quad y > v/Lb^2 \end{cases} . \end{aligned} \tag{2.5}$$

Note that at the length scales smaller than persistence length p DNA double helix is practically straight, while on the length scales greater than p, double helix as a whole is a Gaussian coil. That means, if we take a piece of double helix of the contour length λ, then its size in space scales as

$$\xi \sim \begin{cases} \lambda & \text{when} \quad \lambda < p \\ \sqrt{\lambda p} & \text{when} \quad \lambda > p \end{cases} . \tag{2.6}$$

Substituting this result into the balance equation (2.2), we can determine the antenna size and then, automatically, the rate, the latter being either side of the balance equation. We have to be careful, because we see that there are already

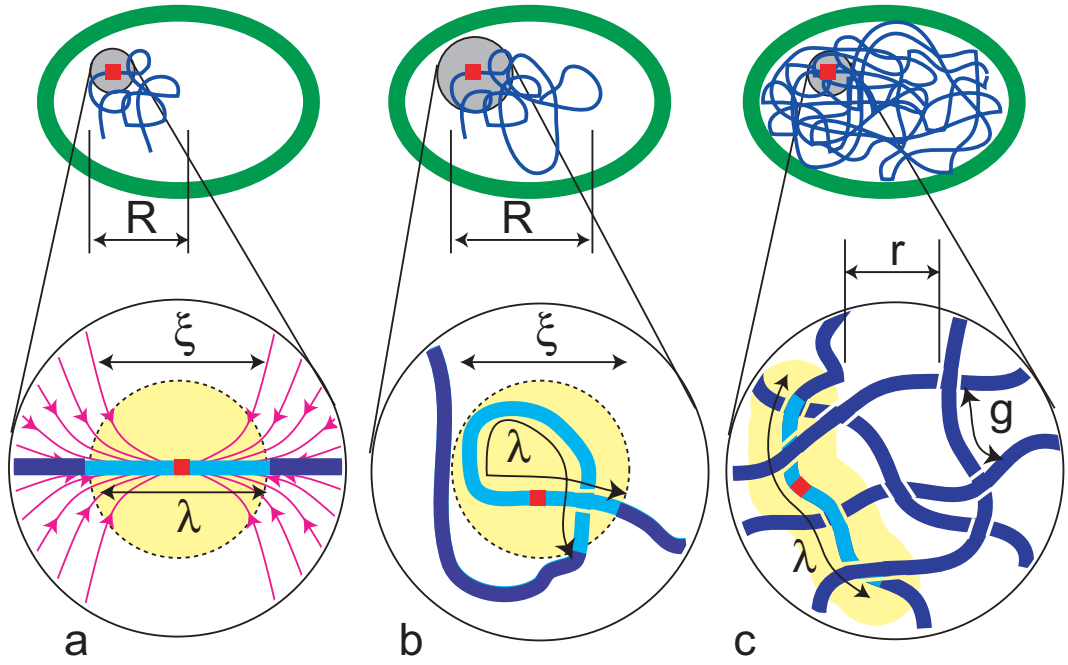

Figure 2.1: Antenna in a variety of cases. The upper part of every figure represents a poor man's idea of a prokaryotic cell. In figures a and b, DNA in the cell is a coil, because coil size R is smaller than the cell dimension; alternatively, one can think of dilute solution of DNA in which R is much smaller than the distance to other coils (not shown). In figure c, the amount of DNA is so large, that the coil size would have exceeded the cell diameter, and so DNA is a globule; alternatively, one can think of a semi-dilute solution [15] of strongly overlapping DNA coils. The lower figures represent blow up view of the region around the target site on DNA. The antenna part of DNA around the target is shown in lighter color than the rest of DNA. The space region below the crossover length scale is shadowed. This space region is roughly spherical in cases a and b, it is sausage shaped in case c. Figure a also shows the averaged flow lines of the diffusion, which go in 3D far away from the target and go mostly along DNA within antenna length scale (they are equivalent to electric field lines in terms of electrostatic analogy, Appendix B). In figures b and c flow lines are not shown, simply because it is difficult to draw them. In figure c, we see that DNA globule locally looks like a temporal network, with the mesh size r. In this case, antenna might be much longer that one mesh. In the figure, mesh size is not larger than persistence length, so the length of DNA in the mesh g is about the same as r; at lesser density, mesh size might be longer, and then DNA in the mesh would be wiggly, with $g \gg r$.

as many as four different scaling regimes, due to equations (2.5) and (2.6):

- Regime A - antenna is straight (upper line of Eq. (2.6)), adsorbtion is relatively weak (upper lines in the Eq. (2.5));
- Regime B - antenna is Gaussian (lower line in the Eq. (2.6), but adsorbtion is still relatively weak;
- Regime C - antenna is Gaussian and adsorbtion is relatively strong (lower lines in the Eqs. (2.5));
- Regime D - Straight antenna and strong adsorbtion.

Later we will find plenty more regimes, but now let us consider just these ones, one by one.

To begin with, suppose antenna is straight ($\lambda < p$, so $\lambda \sim \xi$, see Fig. 2.1, (a)) and non-specific adsorbtion relatively weak ($y < v/Lb^2$, so $c_{\rm ads} \sim cyb^2$). In this case, balance equation yields $\lambda \sim b(yd)^{1/2}$, or for the rate

$$J \sim c\sqrt{D_3 D_1}\, y^{1/2} b \ ; \tag{2.7}$$

in other words, for the ratio of this rate to the Smoluchowski rate $J_s \sim D_3 cb$, we obtain

$$\frac{J}{J_s} \sim (yd)^{1/2} \qquad \text{(regime A)}. \tag{2.8}$$

This result remains correct as long as antenna remains shorter than persistence length, and since we know λ, we obtain this condition explicitly: $y < p^2/b^2 d$.

Let us now suppose that non-specific adsorbtion is still relatively weak ($y < v/Lb^2$, so $c_{\text{ads}} \sim cyb^2$), but it is strong enough such that antenna is longer than persistence length ($\lambda > p$, so that $\xi \sim \sqrt{\lambda p}$, see Fig. 2.1, (b)). Then our balance equation yields $\lambda \sim (yd)^{2/3} p^{-1/3} b^{4/3}$ or

$$\frac{J}{J_s} \sim \left(\frac{ypd}{b}\right)^{1/3} \qquad \text{(regime B)}. \tag{2.9}$$

One should check that this new result for λ implies that $\lambda > p$ at $y > p^2/b^2 d$, and so $y \sim p^2/b^2 d$ is the cross-over line between the two regimes, A and B. In both regimes, and as expected, the rate grows with the strength of non-specific adsorbtion, y, because increasing y increases the size of antenna. However, the functional scaling dependence of the rate on y is significantly different, reflecting the difference in DNA fractality at different length scales.

Before we proceed with analysis of other scaling regimes, it is useful to make the following comment. The balance equation (2.2) describes the fact that every protein going through the 3D diffusion far away must then also go through the 1D diffusion closer to the target. In other words, balance equation (2.2) describes the self-establishing match between 3D and 1D parts of the process. But we can also look at the situation differently: suppose that one particular protein is

adsorbed on DNA in a random place, and let us estimate the distance it can diffuse along DNA before it desorbs due to a thermal fluctuation. Since probability of thermally activated desorbtion is proportional to $e^{-\epsilon/k_BT} = 1/y$, the time protein spends adsorbed must be about $b^2 y/D_3$. During this time, protein diffuses along DNA by the distance about $\sqrt{D_1 b^2 y/D_3} = b\sqrt{yd}$. Following [10, 12], we call it *sliding distance*. We see, therefore, that antenna length λ is just about sliding distance for the straight DNA, but $\lambda \gg \ell_{\text{slide}}$ for the coiled DNA. This seems for the first glance like a very weird result: how can possibly be antenna longer than the distance over which protein can slide? In fact antenna does become longer than the bare sliding distance, and this happens because for the coiled DNA every protein, desorbed after sliding the distance of the order of ℓ_{slide}, has a significant chance to re-adsorb nearby. Such correlated re-adsorbtion gets more likely as we consider more and more crumpled conformations of DNA. Indeed, if we in general assume that $\xi \sim \lambda^\nu$, then balance equation yields $\lambda \sim y^{1/(1+\nu)}$, which means that λ grows with y *faster* than $\ell_{\text{slide}} \sim y^{1/2}$ at every $\nu < 1$. This growth of λ with y gets increasingly fast as ν decreases, which corresponds to more crumpled conformations. We should emphasize that this mechanism of correlated re-adsorbtion is impossible to see as long as DNA polymeric and fractal properties are not considered explicitly, that is why this mechanism has been overlooked in previous works.

With further increase of either non-specific adsorbtion strength y or DNA

overall length L, we ran into the situation when most of the proteins are adsorbed on the DNA. In other words, if one prefers to think in terms of a single protein diffusion, then this single protein molecule spends most of the time adsorbed on DNA far away from the target. For this case, we have to use the lower lines of the formulae (2.5) and substitute it into the balance equation (2.2). Since equilibrium condition (2.3) is still satisfied, the result $\lambda\xi \sim ydb^2$ remains unchanged. Depending on whether antenna length λ is longer or shorter than persistence length, we obtain the regimes C and D.

For regime C, we have $\lambda > p$, antenna is a Gaussian coil and $\xi \sim \sqrt{\lambda p}$, yielding $\lambda \sim (yd)^{2/3} p^{-1/3} b^{4/3}$ and

$$\frac{J}{J_s} \sim \frac{v(pd)^{1/3}}{Lb^{7/3}y^{2/3}} \qquad \text{(regime C)}. \tag{2.10}$$

Given our expression for λ, the condition $\lambda > p$ implies the familiar $y > p^2/b^2 d$, and another condition for this regime is that most proteins are adsorbed, or $y > v/Lb^2$, see Eqs. (2.5).

For regime D, antenna is straight, so $\xi \sim \lambda$, and we get $\lambda \sim b(yd)^{1/2}$, just as in the regime A. For the rate however substitution of lower lines of the Eqs. (2.5) into the balance equation (2.2) yields

$$\frac{J}{J_s} \sim \frac{vd^{1/2}}{Lb^2 y^{1/2}} \qquad \text{(regime D)}. \tag{2.11}$$

According to our discussion, this regime should exist when $y < p^2/b^2 d$ and $y > v/Lb^2$. As we shall see later, in the section 2.4.3, these two conditions can be met together and the room for this regime exists only if $d < 1$, which means when 1D diffusion along DNA is slower than 3D diffusion in space.

In both regimes C and D, overall rate decreases with the increase of non-specific adsorbtion, y, because 3D transport to the antenna is slowed down by the lack of free proteins.

We have so far discussed four of the scaling regimes, our results are equations (2.8), (2.9), (2.10) and (2.11). Already at this stage, we gained simple understanding of the non-monotonic dependence of the rate on y - phenomenon formally predicted in [7] and observed in [8], but previously not explained qualitatively: at the beginning, increasing y helps the process because it leads to increasing antenna length; further increase of y is detrimental for the rate because it leads to an unproductive adsorbtion of most of the proteins. We have also obtained a new feature, absent in previous works: the shape of the maximum on the $J(y)$ curve is asymmetric, at least if DNA is not too long: in the regimes B and C, rate grows as $y^{1/3}$ and then falls off as $y^{-2/3}$.

Since there are quite a few more scaling regimes, it is easier to understand them if we now interrupt and offer the summary of all regimes as presented in Figure 2.2 and Table 2.1.

2.3 Summary of the results: scaling regimes

Our results are summarized in Fig. 2.2 and in the Table 2.1. Figure 2.2 represents the log-log plane of parameters L and y, and each line on this plane marks a cross-over between scaling regimes. This figure gives the diagram of scaling regimes for the specific case $d = 1$ (or $D_1 = D_3$); later on, in the section 2.4.3 we will return to the more general situation and present corresponding diagrams for both $d < 1$ and $d > 1$ cases.

To be systematic, let us start our review of scaling regimes from the two trivial cases, which correspond to the axes in Fig. 2.2. When $y \leq 1$, there is no non-specific binding of proteins to the DNA, and no sliding along DNA. Proteins find their specific target at the rate which is equal to the Smoluchowski rate, or $J/J_s = 1$. Similarly, if the DNA is very short, as short as the specific target site itself, or $L \sim b$, then once again $J/J_s = 1$ for trivial reason. Since we assume that there is some non-specific adsorbtion, or $y \geq 1$, and since DNA length is obviously always greater than the target size b, our diagram in Fig. 2.2 presents only the $y > 1$ and $L/b > 1$ region, which is why pure Smoluchowski regime is seen only on the axes.

If we increase y and consider $y > 1$ situation, then we have significant non-specific adsorbtion of proteins on DNA, which increases the rate due to the antenna effect. If y remains moderate, the antenna is shorter than DNA persistence

Table 2.1: The summary of rates and antenna lengths in various regimes. In labelling regimes, we skip J and L to avoid confusion with the rate and DNA length.

Regime	Description	J/J_s	λ
Axes	Smoluchowski: no antenna	1	b
A	straight antenna, few proteins adsorbed	$(yd)^{1/2}$	$b(yd)^{1/2}$
B	coiled antenna, few proteins adsorbed	$(ypd/b)^{1/3}$	$(yd)^{2/3}\,p^{-1/3}b^{4/3}$
C	coiled antenna, most proteins adsorbed	$\frac{v(pd)^{1/3}}{Lb^{7/3}y^{2/3}}$	$(yd)^{2/3}\,p^{-1/3}b^{4/3}$
D ($d<1$)	straight antenna, most proteins adsorbed	$\frac{vd^{1/2}}{Lb^2y^{1/2}}$	$b(yd)^{1/2}$
E	whole DNA as straight antenna, few proteins adsorbed	L/b	L
F	whole DNA as coiled antenna, few proteins adsorbed	$(Lp/b^2)^{1/2}$	L
G	whole DNA as antenna, most proteins adsorbed	$\frac{vd}{L^2b}$	L
H	antenna with coiled mesh, most proteins adsorbed	$\frac{p}{b^2}\left(\frac{vd}{Ly}\right)^{1/2}$	$\frac{b}{p}\left(\frac{vyd}{L}\right)^{1/2}$
I	antenna with straight mesh, most proteins adsorbed	$\frac{vd^{1/2}}{Lb^2y^{1/2}}$	$b\,(yd)^{1/2}$
K ($d>1$)	antenna with straight mesh, few proteins adsorbed	$(yd)^{1/2}$	$b\,(yd)^{1/2}$
M ($d>1$)	antenna with coiled mesh, few proteins adsorbed	$p\left(\frac{Lyd}{v}\right)^{1/2}$	$\frac{b}{p}\left(\frac{vyd}{L}\right)^{1/2}$

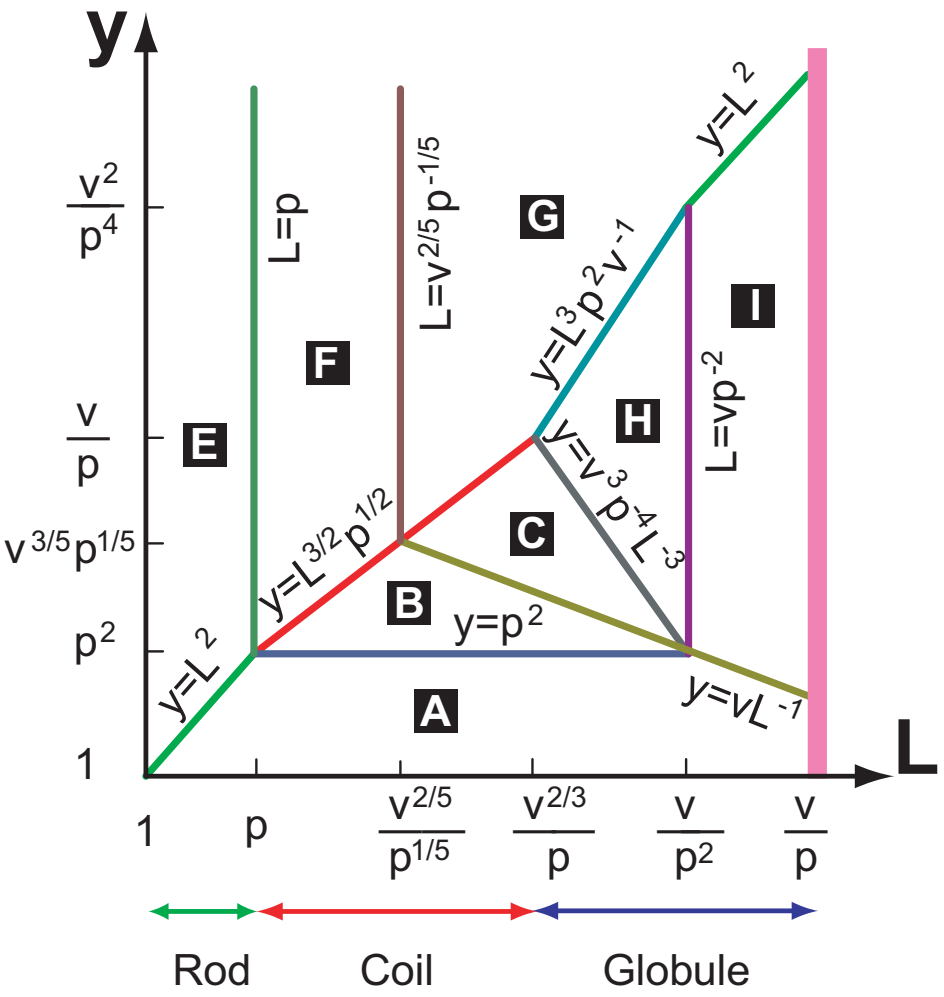

Figure 2.2: Diagram of scaling regimes for the case $d = 1$, when diffusion along DNA has the same diffusion constant as diffusion in surrounding water. Both L and y axes are in the logarithmic scale. When DNA is shorter than persistence length ($b < L < p$) DNA is essentially a rod, DNA is a Gaussian coil as long as it is longer than persistence length, but coil size is smaller than the restriction volume v ($p < L < v^{2/3}/p$), DNA is globular at $L > v^{2/3}/p$, and we only consider L up to about v/pb, because at larger L DNA segments start forming liquid crystalline order. Summary of the rates for each regime is found in Table 2.1. Here, as well as in the other figures, to make formulae look shorter, all lengths are measured in the units of b, meaning that L, p, and v stand for L/b, p/b, and v/b^3.

length, it is straight. This is regime labelled A in Fig. 2.2 and described by formula (2.8). With further increase of y, when $y > p^2/b^2d$, we cross-over into the regime labelled B and described by formula (2.9), in this regime antenna is so long that it is a Gaussian coil. From the regime B, we can cross over the line $y = v/Lb^2$ and get into the regime labelled C and described by the formula (2.10). One can cross-over into the regime C by either increasing y or increasing L, because increasing either of these variables promotes unproductive non-specific adsorbtion of proteins on far away pieces of DNA and thus slows down the transport to the specific target.

From regime A, we can also cross over the line $y = v/Lb^2$, but as long as $d = 1$ this does not bring us to the regime D, instead we get to the new regime labelled I, which we will explain a few lines below.

To understand all other scaling regimes, we have to remember that our previous consideration throughout Section 2.2 was restricted in two respects. First, we assumed that the entire DNA in the form of Gaussian coil fits within volume v, which is true only as long as $L < v^{1/3}$ and $\sqrt{Lp} < v^{1/3}$, where $v^{1/3}$ stands for the linear dimension of the restriction volume. To relax this assumption, we will have to consider a long DNA which is many times reflected by the walls of volume v and inside volume v represents a globule, locally looking like a semi-dilute solution of separate DNA pieces, as illustrated in Fig. 2.1 (c). For such long DNA, we shall find two more regimes labelled H and I in Fig. 2.2. Second, we assumed that the

antenna length λ was smaller than full DNA length L; the consequence of this was our statement (2.3) that there is equilibrium between adsorbed and dissolved proteins. Relaxing this assumption, we will have to discuss regimes labelled E, F, and G on Fig. 2.2.

In Figure 5.4, we present a schematic y-dependence of the rate for a number of values of DNA lengths L. Each curve is labelled with the corresponding value of L. To be specific, we have chosen the lengths which correspond to various cross-overs and are marked on the scaling regimes diagram, Figure 2.2. Note that in many cases our result for the rate exhibits a maximum and saturation beyond the maximum - features first described in the work BWH, Ref. [7]. Unlike BWH, we find that the maximum is asymmetric and, even more importantly, J/J_s can become much smaller than unity, i.e., one can observe deceleration in comparison with Smoluchowski rate. We also find a number of other features, such as specific power law scaling behavior of the rate.

Thus, we have to discuss one by one all the new regimes E, F, G, H, I. This is what we do in the next section 2.4.

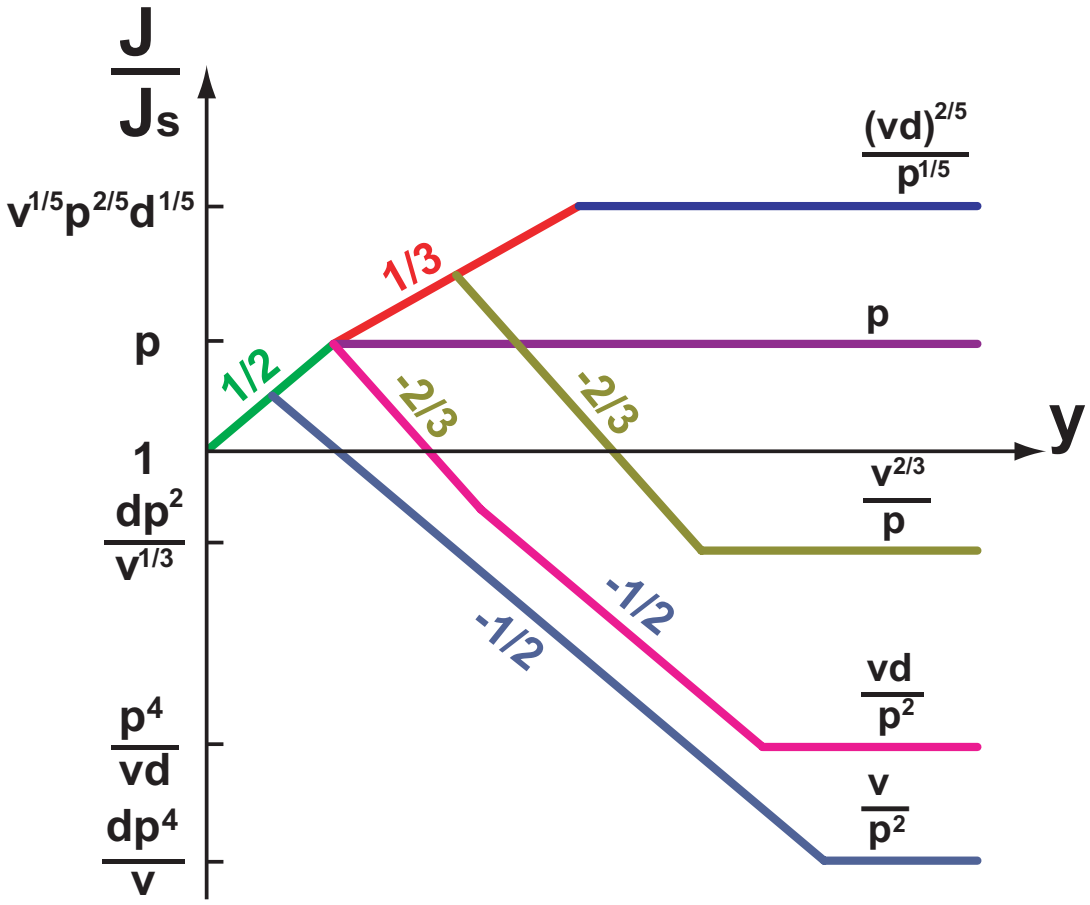

Figure 2.3: Schematic representation of rate dependence on y. Both the rate J and y are given in logarithmic scale. The fraction next to each curve shows its slope, which is the power of $J(y)$ dependence. Each curve corresponds to the specified value of DNA length L, also indicated in Figure 2.2, the length L is shown above the right end of each curve. Experimentally, the value of y can be controlled through the salt concentration, because non-specific adsorbtion of proteins is controlled by Coulomb interaction between negative DNA and positive patch on the protein surface; for instance, if the salt is KCl, then it is believed [8, 11] that $y = 10\,[\mathrm{KCl}] + 2.5$, where [KCl] is the molar concentration of the salt. Note that we recover the possibility, first indicated in [7], that the rate goes through the maximum and then saturates, but in our case maximum is in many cases asymmetric, while at large y the rate becomes very small $J/J_s \ll 1$, particularly for long DNA. Here, as well as in the other figures, to make formulae look shorter, all lengths are measured in the units of b, meaning that L, p, and v stand for L/b, p/b, and v/b^3.

2.4 Systematic consideration of scaling regimes

2.4.1 DNA is not long enough for full antenna

If DNA is too short for antenna, then proteins already adsorbed on DNA can find their target faster than new proteins can be delivered to the DNA from solution. There is no adsorbtion equilibrium any longer, and instead of formula (2.3) we can only claim that $c_{\rm ads} < y c_{\rm free} b^2$. Therefore, the amount of adsorbed proteins under stationary conditions is physically determined by the stationarity itself, which means, we have to look at formula (2.2) as *two* equations. In doing so, we have to replace λ in the right hand side (one-dimensional rate) by L, because we don't have more DNA than L, and we have to replace ξ in the left hand side, which is the antenna size for 3D transport, by R - overall size of DNA coil. Of course, particle counting equation (2.4) is still valid, it is the third equation. Thus, our equations read:

$$\begin{aligned} &\frac{J}{J_s} \sim \frac{c_{\rm free} R}{cb} \ ; \\ &c_{\rm free} R \sim \frac{c_{\rm ads} d}{L} \ ; \\ &c_{\rm ads} L + c_{\rm free} v \sim cv \ . \end{aligned} \tag{2.12}$$

From here, we find

$$\frac{J}{J_s} = \frac{vRd/b}{RL^2 + vd} \ . \tag{2.13}$$

We can now easily address all possible scaling regimes in which antenna is longer than DNA.

To begin with, it is possible that DNA length is shorter than DNA persistence length $L < p$, such that the entire DNA is essentially straight, and then $R \simeq L$. Assuming also $L^3 < v$, we arrive at the scaling regime labelled E in Fig. 2.2, in this regime

$$\frac{J}{J_s} \sim \frac{L}{b} \qquad \text{(regime E)}. \tag{2.14}$$

The borderline of this regime can be established from the condition that since entire DNA is smaller than "equilibrium" antenna, we must expect that c_{ads} is smaller than its equilibrium value, or $c_{\text{ads}}/c_{\text{free}}b^2 \leq y$. Since according to the second of the formulae (2.12) we have $c_{\text{ads}}/c_{\text{free}} = LR/d$, so we have the condition $LR/d < yb^2$; at $L < p$ this yields $y > L^2/b^2d$. At the same condition we can also arrive from the other side of the crossover, by noting that regime A continues as long as antenna is shorter than entire DNA, $\lambda < L$; using our result for λ for the regime A, this produces the same cross-over line between regimes A and E.

For longer DNA, when $L > p$, entire DNA is Gaussian coil, its size is $R \sim (Lp)^{1/2}$. Still assuming that the second term dominates in the denominator in formula (2.13), we arrive at

$$\frac{J}{J_s} \sim \left(\frac{Lp}{b^2}\right)^{1/2} \qquad \text{(regime F)}. \tag{2.15}$$

This regime is labelled F in Fig. 2.2. Its borderline with regime E is obviously vertical line $L = p$. As regards cross-over to the regime B, once again it can be established either from $c_{\rm ads}/c_{\rm free} = LR/d < y$ for the regime F or from $\lambda < L$ for the regime B. In either way we arrive at the cross-over condition $y = L^{3/2}p^{1/2}/b^2d$.

For even longer DNA, the antenna length becomes equal to the length of entire DNA only at so large y, that the system is already in the regime C, with rate falling down with increasing y because of the unproductive adsorbtion of proteins. Since antenna length λ in the regime C is given by the same formula as in the regime B, so the upper border line of the regime C is the continuation of the corresponding line bordering regime B, it is $y = L^{3/2}p^{1/2}/b^2d$. However, when we cross this line upwards from the regime C, we arrive at the new situation, because now the first term dominates in the denominator of the equation (2.13), meaning that most of the proteins are adsorbed on DNA, such that we obtain

$$\frac{J}{J_s} \sim \frac{vd}{L^2 b} \qquad \text{(regime G)}. \tag{2.16}$$

The cross-over between this regime and regime F is vertical line at which both terms are comparable in the denominator of equation (2.13), it is $L = (vd)^{2/5}/p^{1/5}$. Crossover line with the regime C can once again be established from the condition $c_{\rm ads}/c_{\rm free} = LR/d < y$.

In all regimes E, F, and G the rate saturates with increasing y. For the regimes

E and F this happens after just initial growth of rate; for the regime G saturation occurs after rate goes through the maximum and starts decreasing. In all cases saturation is due to the fact that increasing adsorbtion strength does not lead to any increase of the antenna size, because already the entire DNA is employed as antenna and antenna has nowhere to grow.

2.4.2 Cell is not big enough to house DNA Gaussian coil

When DNA is very long for a given volume, specifically, when $(Lp)^{1/2} > v^{1/3}$, DNA cannot remain just a coil, it must be a globule, as it is forced to return many times back into the volume after touching the walls (see, for instance, [14]).

For the purposes of this work, it is sufficient to keep assuming that excluded volume of DNA is not important, because volume fraction of DNA within confinement volume v is still small, and even small compared at b/p. Nevertheless, the system locally looks like a so-called semi-dilute solution of DNA, or transient network with certain mesh size (see Figure 2.1c).

We should remind some basic facts regarding the semi-dilute solution of transient network [14, 15]. Let us denote r the characteristic length scale of a mesh in the network, it is in the scaling sense the same as the characteristic radius of

density-density correlation (see Figure 2.1c). Let us further denote g the characteristic length along the polymer corresponding to the spatial distance r. Quantities r and g can be estimated from the following physical argument [14, 15]. Consider a piece of polymer of the length g starting from some particular monomer, it occupies region $\sim r^3$ and makes density about $\sim g/r^3$; this density must be about overall average density, which for our system is of the order of L/v. Thus, $g/r^3 \sim L/v$. Second relation between g and r is similar to formula (2.6), it depends on whether mesh size is bigger or smaller than persistence length p:

$$r \sim \begin{cases} g & \text{if} \quad g < p \\ \sqrt{gp} & \text{if} \quad g > p \end{cases} . \tag{2.17}$$

Accordingly, we obtain after some algebra

$$\begin{array}{llll} g \sim \sqrt{\frac{v}{L}} \, , & r \sim \sqrt{\frac{v}{L}} & \text{if} & L > \frac{v}{p^2} \\ g \sim \frac{v^2}{L^2 p^3} \, , & r \sim \frac{v}{Lp} & \text{if} & \frac{v^{2/3}}{p} < L < \frac{v}{p^2} \end{array} . \tag{2.18}$$

The upper line corresponds to the network so dense that every mesh is shorter than persistence length and polymer is essentially straight within each mesh. The lower line describes much less concentrated network, in which every mesh is represented by a little Gaussian coil.

Returning to our problem, we should realize that the antenna length λ can in

fact be longer than the mesh size g, as illustrated in Fig. 2.1 (c). To estimate the antenna size for this case, we should remember that desorbtion from antenna does not necessarily completely breaks the sliding along DNA, because protein can still re-adsorb on a nearby place of DNA, more generally - on a *correlated* place on DNA. To account for this, let us imagine that the antenna part of DNA is decorated by a tube of the radius r. Since r is the correlation length in the DNA solution, protein remains correlated with antenna as long as it remains within this tube around antenna. Accordingly, our main balance equation (2.2) must be modified to account for the fact that 3D transport on the scales larger than r is now realized through DNA network and, therefore, the task of regular 3D diffusion is only to deliver proteins over the length scale of order of one mesh size r, into any one of the λ/g network meshes along the antenna. The rate of delivery into one such mesh would be $\sim D_3 c_{\rm free} r$, so overall delivery rate into the antenna tube scales as $\sim D_3 c_{\rm free} r\lambda/g$. As usual, this must be equal to the rate of 1D delivery along antenna into the specific target, so instead of (2.2) we finally get

$$J \sim D_3 c_{\rm free} r \frac{\lambda}{g} \sim D_1 \frac{c_{\rm ads}}{\lambda} \ . \tag{2.19}$$

As long as antenna is shorter than the entire DNA, the relation between $c_{\rm free}$ and

c_{ads} equilibrates and obeys (2.3-2.5), so we finally get

$$\lambda^2 \sim b^2 \frac{gyd}{r} \ , \tag{2.20}$$

and

$$\frac{J}{J_s} \sim \frac{c_{\text{free}}}{c} \frac{r\lambda}{g} \sim \frac{v}{Lb^2} \left(\frac{rd}{yg} \right)^{1/2} \ . \tag{2.21}$$

What is nice about this formula is that it remains correct in a variety of circumstances - when antenna is straight ($\lambda < p$), or antenna is Gaussian ($p < \lambda < v^{2/3}/p$), or antenna is a globule ($\lambda > v^{2/3}/p$).

Taking r and g from the formulae (2.18), we finally obtain two new regimes. When every mesh is Gaussian,

$$\frac{J}{J_s} \sim \frac{p}{b^2} \left(\frac{vd}{Ly} \right)^{1/2} \qquad \text{(regime H)}. \tag{2.22}$$

This regime borders regime C along the line where antenna size is equal to the mesh size, $\lambda = g$, which reads $y = v^3/(L^3 p^4 b^2 d)$. Regime H also borders regime G along the line where antenna size is as long as the entire DNA, $\lambda = L$, or $y = L^3 p^2 / v b^2 d$. Finally, regime H also borders another regime I along the vertical line $L = v/p^2$, which corresponds to DNA within every mesh becoming straight (shorter than persistence length). For this regime, we have to use upper line in

formulae (2.18), thus obtaining

$$\frac{J}{J_s} \sim \frac{vd^{1/2}}{Lb^2y^{1/2}} \qquad \text{(regime I)}. \tag{2.23}$$

This regime borders saturation regime G along the line $y = L^2/b^2d$ where $\lambda = L$.

As regards the lower border of the regime I, it corresponds to the situation when antenna becomes straight, which happens at $y = v/Lb^2d$. However, as long as $d = 1$, which is the case presented in Figure 2.2, this line coincides with the line $y = v/Lb^2$ below which most proteins are desorbed and free in solution. That is why at $d = 1$, there is no room for the regime D, in which antenna is straight, but most proteins adsorbed. Indeed, when $d = 1$, then 3D transport is mostly realized by sliding along the network edges as soon as most proteins are adsorbed, which precisely means that regime A crosses over directly to regime I.

As we see, in both H and I regimes the rate J decreases with growing y, but does so slower than in the regime C, only as $y^{-1/2}$ instead of $y^{-2/3}$. This happens because adsorbed proteins are not just taken away from the process, as in the regime C, but they participate in 3D transport through the network, albeit this transport is still pretty slow.

This completes our scaling analysis for the $d = 1$ case shown in Fig. 2.2.

2.4.3 Diffusion rate along DNA is different from that in surrounding water

Let us now relax the $d = 1$ condition and examine the cases when diffusion along DNA is either slower ($d < 1$) or faster ($d > 1$) than in surrounding water.

First let us consider $d < 1$ case, when diffusion along DNA is slower than that in the surrounding water ($D_1 < D_3$), corresponding scaling regimes are summarized in the diagram Figure 2.4. Most of the diagram is topologically similar to that in the Figure 2.2, and we do not repeat corresponding analysis. Of course, there are now powers of d in all equations, but the major qualitative novelty is that there is now a room for the regime D sandwiched between regimes A and I. The formal reason why this regime now exists in a separate region is because the line $y = v/Lb^2d$ goes above the line $y = v/Lb^2$. To understand the more meaningful physical difference, let us recall that the line $y = v/Lb^2$ marks the cross-over above which most of the proteins are adsorbed, but it is not enough for the sliding-along-network mechanism to dominate in the 3D transport at $d < 1$.

Interestingly, the rate for both regimes D and I is given by the same formula - compare Eqs. (2.11) and (2.23). This happens because antenna is straight for the regime D and, while antenna is not straight for the regime I, it still consists of a number of essentially straight pieces, each representing one mesh. The major

difference between regimes D and I, despite similar scaling of the rate, is in the mechanism of diffusion: in the regime D, proteins diffuse through the water in a usual manner, while in the regime I they are mostly transported along the network of DNA, with only short "switches" on the scale of one mesh size r between sliding tours. This is why straight pieces of DNA in different meshes independently add together to yield the same overall formula for rate as in the regime D.

Let us now switch to the opposite limit and consider the $d > 1$ case, for which the results are summarized in Figure 2.5. This diagram is quite similar to the previously considered ones in Figures 2.2 and 2.4, except there are now two new regimes labelled K and M (in alphabetical labelling of the regimes we skip J and L to avoid confusion with rate and DNA length). These regimes are both below the line $y = v/Lb^2$, which means, most of the proteins are not adsorbed. However, since $d > 1$, the new physical feature of the situation is that adsorbed proteins, although they are in minority, can nevertheless dominate in 3D transport by sliding along DNA network, because sliding is now so fast at $d > 1$. Thus, regimes K and M are the ones in which effective diffusion along DNA network dominates, so we have to use formula (2.19) for the rate and antenna size, while for the concentrations of free and adsorbed proteins we have to use upper lines in the formulae (2.5). In the regime K, local concentration of DNA segments is so high, that every mesh in DNA network contains an essentially straight piece of DNA, so we have to use the upper line in formula (2.18), yielding (after some

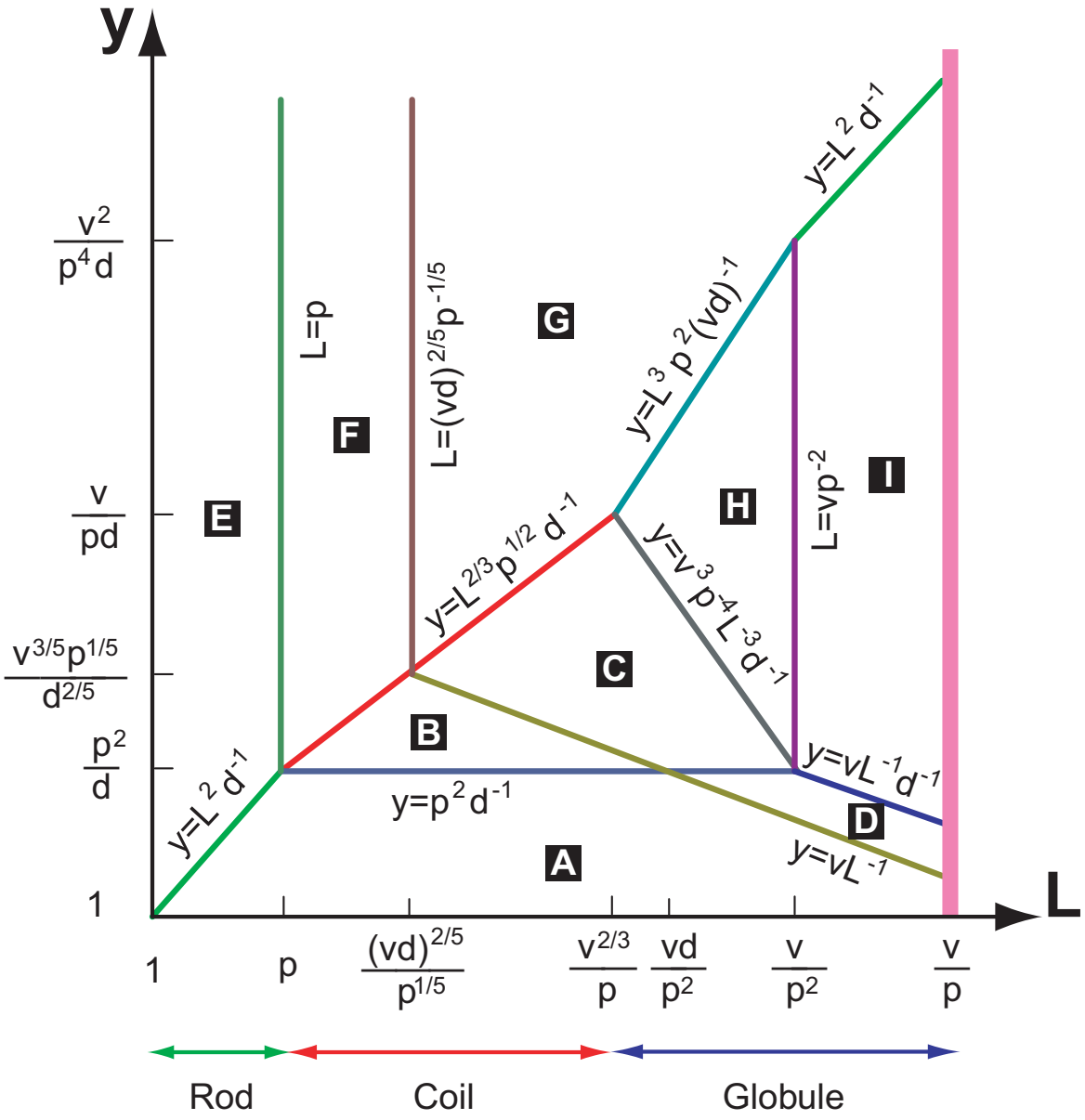

Figure 2.4: Scaling regimes for the case $d < 1$. The major difference from the $d = 1$ case is the presence of regime D, in which majority of proteins are adsorbed, but still the dominant 3D transport is the usual diffusion through the surrounding water, because sliding along DNA is too slow ($D_1 < D_3$). In this figure, as well as in the other figures, to make formulae look shorter, all lengths are measured in the units of b, meaning that L, p, and v stand for L/b, p/b, and v/b^3.

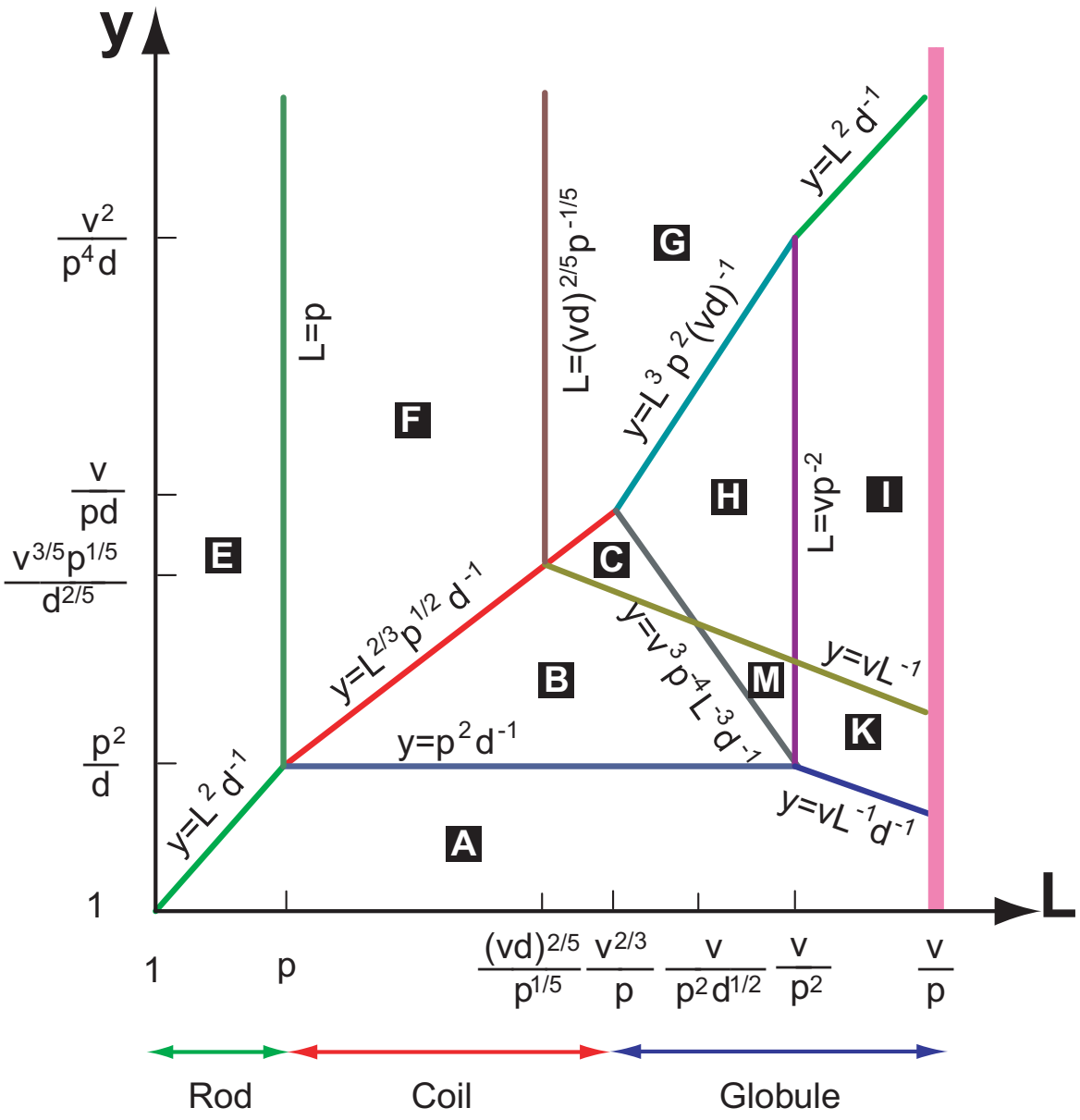

Figure 2.5: Scaling regimes for the case $d > 1$. The major new feature of this diagram compared to previous ones is the presence of regimes K and M. In these regimes the majority of proteins are not adsorbed, but still the dominant 3D transport mechanism is the sliding of minority proteins along DNA network, because it is so much faster ($D_1 > D_3$). We skip J and L in labelling regimes to avoid confusion with rate J and DNA length L. In this figure, as well as in the other figures, to make formulae look shorter, all lengths are measured in the units of b, meaning that L, p, and v stand for L/b, p/b, and v/b^3.

algebra)

$$\frac{J}{J_s} \sim (yd)^{1/2} \qquad \text{(regime K)}. \tag{2.24}$$

Similarly, in the regime M mesh of the DNA network is Gaussian, we have to use lower line in equation (2.18), and this produces

$$\frac{J}{J_s} \sim p\left(\frac{Lyd}{v}\right)^{1/2} \qquad \text{(regime M)}. \tag{2.25}$$

Since the majority of proteins are not adsorbed, it is not surprising that rate grows with y in both regimes K and M. Notice that the rate is given by the same formula for the regimes A and K - compare (2.8) and (2.24). This is similar to the situation with regimes D and I, as discussed before, because although rate is given by the same formula, the underlying diffusion mechanism is fundamentally different. In both cases of D and I or A and K, it is possible that although scaling laws are the same, the numerical pre-factors are different.

It is also interesting to note that the cross-over between regimes B and M takes place on the line $y = v^3/p^4L^3b^2d$ where antenna length is equal to the DNA length in one mesh: on the side of B regime, antenna is shorter than one mesh, and transport to antenna must be through water; on the side of M, antenna is longer than one mesh, and effective transport along DNA network is at play.

2.4.4 Maximal rate

To finalize our discussion of scaling regimes, it is reasonable to ask: what is the maximal possible rate? According to our results, the maximal rate is achieved on the border between regimes F and G, that is, at $L \sim (vd)^{2/5}/p^{1/5}$ and at $y \geq v^{3/5}p^{1/5}/b^2d^{2/5}$. Maximal possible acceleration compared to Smoluchowski rate is about $(vp^2d/b^5)^{1/5}$. It is interesting to note that the "optimal strategy" in achieving the maximal rate at the minimal possible y requires to have the adsorbtion strength y right at the level at which the probability of non-specific adsorbtion for every protein is about 1/2 (on the line $y \sim v/L$).

It is interesting that the maximal possible acceleration grows with overall volume v, which may seem counterintuitive. This result is due to the fact that total amount of DNA grows with increasing v, and, according to our assumption, all this DNA has still just one target.

2.5 Discussion

2.5.1 Single protein view

Many of the previous theoretical works [10, 11, 12, 13] looked at the situation in terms of a single protein molecule diffusing to its target. In this view, one should imagine that a protein molecule is initially introduced into a random place within

volume v, and then one should ask what is the first passage time [16] needed for the protein to arrive to the specific target site on DNA. The mean first passage time τ can of course be found using our results for the rate J by inverting the value of the rate and assuming that on average there is just one protein molecule in the system at any time: $\tau = 1/J|_{c=1/v}$. However, we want to re-derive all our results directly in terms of τ in order to build bridges to the works of other authors. The re-derivation turns out also quite illuminating.

First let us consider that DNA is a globule, $L > v^{2/3}/p$ (or semi-dilute solution), and look at the regimes H, I, K, and M; unlike stationary diffusion approach above, in the single protein language the derivation for the globular DNA case is actually simpler. Following [13], we imagine that the search process for the given single protein consists of tours of 1D sliding along DNA followed by diffusion in 3D, followed by 1D sliding, etc. If in one tour of 1D sliding protein moves some distance λ along DNA, then it takes time about λ^2/D_1. The length λ here is, of course, our familiar antenna length, but we will re-derive it here, so we *do not* assume it known. As regards the tour of 3D diffusion, it breaks correlation of the 1D sliding if it carries protein over a distance larger or about the correlation length in the DNA system, which is r - mesh (or blob) size. Thus, the longevity of one tour of 3D diffusion is about r^2/D_3.

The next step of our argument is this. On its way to the target, the protein will go through great many adsorbtion and de-sorbtion cycles, therefore, the ratio

of times protein spends adsorbed and de-sorbed should simply follow equilibrium Boltzmann statistics:

$$\frac{\lambda^2/D_1}{r^2/D_3} \sim \frac{yLb^2}{v} \ . \tag{2.26}$$

(Here, we note parenthetically that there is an approximation underlying our argument: one tour of "correlated 1D sliding" does include small 3D excursions of the protein into water, but they are small in the sense that they do not go beyond the cross-over correlation distance and, therefore, re-adsorbtion after excursion occurs on a correlated place on DNA. Accordingly, these excursions make only marginal contribution to the sliding time which is correctly estimated as $\sim \lambda^2/D_1$.)

The final part of the argument is most clearly formulated by Bruinsma in the work ref. [11]: since subsequent tours of 1D sliding occur over uncorrelated parts of DNA, full search requires about L/λ rounds. Therefore, the total search time τ can be written as

$$\tau \sim \frac{L}{\lambda}\left[\frac{\lambda^2}{D_1} + \frac{r^2}{D_3}\right] \ . \tag{2.27}$$

Equations (2.26) and (2.27) solve the problem for all regimes of globular DNA if we remember that mesh (or blob) size r is given by the formula (2.18). Notice that formula (2.26) gives a new interpretation to the line $y \sim v/Lb^2$ on any of our diagrams Fig. 2.2, 2.4, 2.5: for the parameters below this line most of the overall search time is spent in 3D diffusion, while for the system with parameters

above the line the major time consuming part is 1D sliding. It is close to this line where the result of the work ref. [13] applies and these two times are of the same order. And let us remind that it is also close to this line where the maximal possible rate is achieved (see section 2.4.4).

Thus, four regimes H, I, K, and M result from two possibilities for r in Eq. (2.18) (straight or Gaussian DNA within a mesh) and two possibilities of either first or second term dominance in formula (2.27).

Let us now turn to the regimes A, B, C, and D, when DNA is a coil. In this case, we still essentially rely on the equations similar to (2.26) and (2.27), except some effort is now needed to understand the time of 3D diffusion.

Our argument for this case starts from noticing that there is a cross-over spatial scale ξ, such that correlated sliding takes place inside scale ξ, while regular 3D diffusion in water occurs on a larger length scale, as it breaks correlations between desorbtion and subsequent re-adsorbtion. Thus, the time of one tour of 3D diffusion is the mean first passage time into any one of the L/λ balls of the size ξ (here λ is the contour length of DNA accommodated by one ball of the size ξ; once again, we *pretend* that we do not know ξ and λ, we will re-derive them in this single-protein language). The arrival time into one such ball is the Smoluchowski time (discussed in the appendix A) for the target of size ξ, it is about $v/D_3\xi$; the arrival time into any one of the L/λ balls is L/λ times smaller: $\sim v\,/D_3\xi(L/\lambda)$

In order to present our equations for λ and overall search time τ in the form similar to Eqs. (2.26) and (2.27), we define distance r_{eff} such that $r_{\text{eff}}^2 \sim D_3 \left[v \, / D_3 \xi(L/\lambda) \right] = v\lambda / L\xi$ and then we obtain

$$\frac{\lambda^2 / D_1}{r_{\text{eff}}^2 / D_3} \sim \frac{yLb^2}{v} \ , \tag{2.28}$$

and

$$\tau \sim \frac{L}{\lambda} \left[\frac{\lambda^2}{D_1} + \frac{r_{\text{eff}}^2}{D_3} \right] \ . \tag{2.29}$$

Once again, remembering two regimes for the relation between λ and ξ, formula (2.6), and having either first or second term dominate in the total time (2.29), we recover four regimes A, B, C, and D.

Finally, the results for all saturation regimes E, F, G are recovered by replacing the antenna length λ with L in equation (2.27) or (2.29), and replacing equality with inequality in the conditions (2.26) or (2.28).

2.5.2 Comparison with earlier theoretical works

Let us now compare our findings with various statements found in the literature. The most widely known result of the classical work [7] was the prediction, later confirmed experimentally [8], that the rate depends on y (controlled by ionic strength) in a characteristic way, exhibiting a maximum followed by a plateau.

We have recovered this as a possible scenario for some combinations of parameters (regimes), as shown in Fig. 5.4. However, we found also a number of additional features not noticed previously: first, the maximum is in many cases asymmetric; second, the scaling of rate dependence on y exhibits rich behavior, with the possibilities of crossing over from $y^{1/2}$ to $y^{1/3}$ on the way to the maximum, or from $y^{-2/3}$ to $y^{-1/2}$ on the way down; third, there is a possibility of very strong deceleration at large adsorbtion strength y compared at the Smoluchowski rate. All these features have simple qualitative explanation: the rate grows because increasing y increases the antenna; the rate decays when most of the proteins are fruitlessly adsorbed far from target (or, in other language, every protein spends most of the time adsorbed far away); the rate saturates and comes to the plateau because antenna becomes as long as the DNA itself. All of these features are the direct consequence of the fractal properties of DNA, in either coil or globule state.

The work Ref. [11] represents a review of a variety of topics related to protein-DNA interactions, and the issue of search rate is considered only briefly. In the context, the work Ref [11] provides an important insight, used above in presenting the formula (2.27), that subsequent rounds of 1D search are performed on uncorrelated pieces of DNA. In other words, there exists a cross-over from mostly correlated events, earlier combined into one "correlated sliding length λ", to mostly uncorrelated ones. In accord with this insight, the search time is linear

in DNA length in the regime I.

In the paper Ref. [12] antenna length was explicitly identified with the sliding distance (that is, with the bare sliding distance, earlier in this paper denoted as $\ell_{\rm slide} \sim b\sqrt{yd}$), and then essentially formula (2.27) was used to determine the search time. This approach is perfectly valid as long as the antenna is straight, $\lambda = \xi$, and $\lambda = \ell_{\rm slide}$, it predicts the symmetric maximum of $J(y)$ dependence, but it should not be used when DNA antenna is coiled. For the globular DNA, the approximation of straight antenna - implicit in the identification of λ with bare $\ell_{\rm slide}$ - is valid for the right end of the regime A and for the regime D, while of course other globular regimes require going beyond this approximation.

The main emphasis of the article Ref. [13] is on the role of non-uniform sequence of DNA, which may lead to either non-specific adsorbtion strength y, or 1D diffusion coefficient D_1, or both to be "noisy" functions of coordinate on DNA. In their review of the uniform homopolymer case, Ref. [13] employ formula equivalent to our Eqs. (2.27) or (2.29), but instead of the condition like (2.26) or (2.29) they minimize overall time with respect to λ. As we pointed out before, this approach is valid within the cross-over corridor around the line $y \sim v/Lb^2$. In general, the idea to apply variational principle is very interesting. It can be generalized beyond the above mentioned corridor if one minimizes the overall dissipation, which is equivalent to energy minimization in terms of electrostatic analogy, as we show in appendix B. Of course, minimization of dissipation is

equivalent to the diffusion equation as long as diffusion is linear. Alternatively, one can also think, as emphasized in the work Ref. [12], that search mechanism was subject to optimization by biological evolution. To employ this idea, it is obviously necessary first to understand the possible search scenario, or regimes, existing in physics, and then, on the next stage, one could attempt optimization with respect to the parameters, such as DNA packing properties etc, which could be subject to selective pressure in evolution.

BWH [7] and some subsequent authors treated DNA solution in terms of domains. Although this term was never particularly clearly defined, it could be understood as space regions more or less occupied by separate DNA coils in solution. With such understanding, the terminology of domains can be used as long as DNA coil fits into the volume v, or, in other words, better suitable for an *in vitro* experiment, DNA solution is dilute, such that DNA coils do not overlap. The terminology of DNA domains becomes unsatisfactory at larger DNA concentrations.

Work Ref. [10] considered the stochastic approach, which means they did not look at the stationary diffusion, but rather at the trajectory of a single protein. As we pointed out before, these approaches must be equivalent as long as one is only interested in the average time of the arrival of the first of proteins. The important contribution of the work Ref. [10] was the elucidation of the crucial neglect of the correlations between the desorbtion point of a protein and its re-adsorbtion

point. It is because of this crucial and not always justified approximation previous theories appear to have overlooked the mechanism of correlated re-adsorbtion, which is entirely due to the DNA being a polymer and a fractal coil. Correlated re-adsorbtion was anticipated in the experimental works [6].

2.5.3 Experimental situation

Most of the experiments in the field (see review [6] and references therein) involve various ingenious arrangements of two or more target sites on the linear or ring DNA and observation of the resulting enzyme processivity. In the light of our theory, it would be interesting to revive the earlier BWH-style experiments and to look carefully at the theoretically predicted multiple features of $J(y)$ curves, such as asymmetric maximum, various scaling regions, the possible deceleration, etc.

The seeming difficulty is that all our "interesting" regimes start when $y > p^2/b^2 d$, when antenna is longer than DNA persistence length. Since persistence length of dsDNA, p, is fairly large, about 150 base pairs under usual ionic conditions (say, [Na] = 0.2 M), and assuming b is about the diameter of the double helix, we get $p/b \approx 25$ for the dsDNA. Unless d is large, this seems to require fairly large non-specific adsorbtion energies, about $6k_BT$ to $10k_BT$, which is a lot but not impossible. In any case, we would like to emphasize that the maximum

$J(y)$ *has* been observed [8], which, according to our theory, could have happened only at $y > p^2/b^2d$, thus assuring that this range is within reach.

One of the most critical and poorly known parameters of our theory is $d = D_1/D_3$. Of course, D_3, diffusion coefficient of the protein in water, is known pretty well, and can be simply estimated based on its size using Stokes-Einstein relation. The difficult part is about D_1, which involves friction of the protein against DNA in the solvent. It is clear that slow diffusion along DNA would make the entire mechanism of 1D sliding less efficient, and indeed decreasing d systematically reduces the rate that we obtain in almost all regimes. There are only two exceptions to this: one is trivial, it is pure Smoluchowski process not involving any sliding and realized only when there is no non-specific adsorbtion on DNA ($y \leq 1$); another exception is in the regimes E and F - regimes when entire DNA, rod-like or coil-like, serves as an antenna, which means 3D transport to the DNA is the slowest part, the bottleneck of the whole process, so that reducing d does not do any damage - except, of course, pushing away the corresponding regime boundaries.

Experimental data on the 1D diffusion of proteins along DNA are scarce and not completely clear [17].

An interesting spin on the whole issue of 1D transport is added by the proteins, such as, e.g., helicase, which, provided with proper energy supply, can move actively. For us, in the context of our present theory, active movement is likely

to correspond to great increase of D_1, or d, for either actively moving proteins themselves, or for passively diffusing proteins which might receive push or pull from active ones. At the first glance, this sounds like a paradoxical statement, because active motion is not diffusion in the sense that displacement is linear in time. However, this is only true up to a certain time and length scales. At larger scale, we can reasonably assume that it would be diffusion again, albeit with a vastly increased diffusion coefficient. Indeed, first, there is always a probability of thermally activated detachment from DNA, and, second, given that two strands in DNA are antiparallel, the re-adsorbtion is likely to lead to random choice of direction of further sliding. These two ingredients surely correspond to diffusion, in the sense that displacement goes like $t^{1/2}$. Of course, this entire issue of active transport requires further investigation, which naturally brings us to the conclusion of this chapter.

2.6 Conclusion

Many questions remain open. The role of concurrent protein species, the role of non-uniform DNA sequence, the role of DNA motion [18], the probability of unusually long search times, the search on a single stranded DNA or RNA, the role of superhelical structures, the dependence of rate (or search time) on the specific positions of one or more targets on DNA, the related issue of enzyme

processivity, the role of excluded volume for very long DNA and corresponding loop-erasing walks [19] - all of these questions invite theoretical work.

To conclude, we have analyzed all scaling regimes of the diffusion-controlled search by proteins of the specific target site located on DNA. We found many regimes. The major idea can be formulated in terms of the cross-over between 1D sliding along DNA up to a certain length scale and 3D diffusion in surrounding space on the larger length scale. Overall, qualitatively, this idea seems to be in agreement with the intuition expressed in experimental papers. In addition, we have made several theoretical predictions which are verifiable and (even more importantly) falsifiable by the experiments. We are looking forward to such experiments.

Chapter 3

Role of Intersegment Transfer

3.1 Introduction

In the previous chapter, we deal only with proteins with a single DNA binding site and ignore the motion of DNA in solution. Our goal in this chapter is to relax these restrictions.

As pointed out by Berg, Winter and von Hippel [7], in addition to 1D sliding, proteins with two nonspecific DNA binding sites may benefit from another facilitating mechanism termed "intersegment transfer". Indeed, such proteins are capable of transiently binding to two DNA segments when the segments are close in space, even if they are well separated from each other along the DNA contour. The subsequent segmental diffusion of DNA then disrupts these double-bound states, resulting in the protein being transferred to a remote position on the

DNA without net dissociation of protein into the water.

The existence of intersegment transfer in principle has been confirmed by a number of well-designed *in vitro* experiments [23, 24, 25]. These experiments measured the dissociation rate of proteins from a prepared complex of the protein and a short piece of specific DNA. The complex was placed in a solution of short nonspecific DNA molecules, and the dissociation rate was measured as a function of the concentration of nonspecific DNA. All the proteins used in [23, 24, 25], namely lac repressor [23], glucocorticoid receptor DNA-binding domain protein [24] and human Hox-D9 homeodomain [25] are believed to have two DNA binding sites so that the protein-DNA complex can adsorb a second short piece of DNA, allowing the protein to transiently form a double-bound state with two DNA pieces. This double-bound state breaks up quickly (faster than the dissociation of protein to water in the prepared protein-DNA complex) and the protein has a chance to be transferred to the newly adsorbed DNA. As a result, the dissociation rate of the complex grows linearly with the concentration of nonspecific DNA. This phenomenon of inter-DNA transfer is essentially similar to the intersegment transfer of proteins inside a single long DNA strand. Direct observation of intersegment transfer was also achieved by a scanning force microscopy study of the translocation of RNA polymerase in E. coli [26].

In this chapter, we propose a scaling theory of the target search time for proteins with two DNA binding sites, which combines the effects of 3D diffusion,

1D sliding, intersegment transfer and DNA motion.

Our main interest is the search time t for the biologically relevant case of globular DNA. However, its complex geometrical properties combined with the several mechanisms of protein motion make this problem very complicated. Therefore, we start from a relatively simple case, namely the search time in a solution of short, straight double-helix DNA molecules among which only a small fraction carry the specific targets. In this situation we are able to include the effects of intersegment transfer and establish connections with the *in vitro* experiments on short DNA [23, 24, 25]. We characterize the rate enhancement by the acceleration ratio t_s/t, where t_s is the inverse of the previously mentioned Smoluchowski rate

$$J_s = 4\pi D_3 bc. \tag{3.1}$$

Our analysis of this case is detailed in Sec. 3.2, and a summary of the resulting scaling regimes is shown in Fig. 3.3.

In Sec. 3.3 we apply the methods developed for short DNA pieces to the case of a very dense DNA globule as shown in Fig. 3.1. The acceleration rate t_s/t is shown schematically as the solid line in Fig. 3.2, plotted as a function of $y = \exp(\epsilon/k_BT)$, where ϵ is the nonspecific adsorption energy of the protein to DNA. Experimentally, the value of y can be controlled through the salt concentration of the solution, since non-specific absorbtion of proteins is controlled by Coulomb

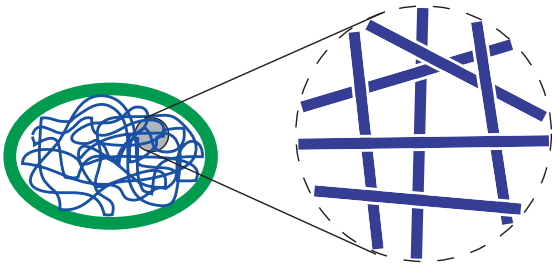

Figure 3.1: A DNA globule. The long DNA is forced to return many times by the wall of a prokaryotic cell. On the right, a blown-up view shows a typical region of the transient network at a scale much smaller than the DNA persistence length p. This figure represents a very dense case, where the nearest neighbor distance between DNA segments, each of length p, is shorter than p.

interaction between negative DNA and the positive patch on the protein surface and may be screened by salt concentration. For comparison, we also plot the main result from chapter 2, which ignores DNA motion and intersegment transfer, as a dashed line. In the latter case, the acceleration rate grows first with y because protein binding to DNA increases the antenna size; then the acceleration rate decays when most of the proteins are fruitlessly adsorbed far from the target (or, in other words, every protein spends most of the time adsorbed far away from the target). Finally, the acceleration rate saturates and comes to a very low plateau (not shown) when the antenna becomes as long as the DNA itself. Hence, when DNA motion and intersegment transfer are not accounted for, there is a very strong deceleration at large ionic strength compared to the Smoluchowski rate. With the help of intersegment transfer, however, the acceleration rate saturates at a much higher level (larger than unity) because adsorbed proteins become much more effective in target search.

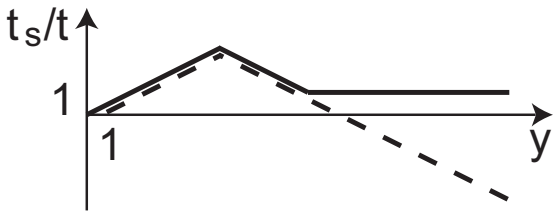

Figure 3.2: Schematic dependencies of the acceleration rate on the adsorption strength y, with (solid line) or without (dashed line) DNA motion and intersegment transfer. Both the acceleration rate t_s/t and y are given in logarithmic scale.

In Sec. 3.4, we conclude with a discussion of the applicability of our model and a comparison to the previous theory [7].

3.2 Simple case: DNA is short

3.2.1 Model and approach

We assume that within some volume v a number of short, rigid (double helix) DNA molecules of length l are confined, among which only one piece of DNA contains a target site of size b. We call this molecule the specific DNA while others are called nonspecific DNA. The system considered here is equivalent to an *in vitro* experiment with specific DNA concentration $1/v$ and much larger nonspecific DNA concentration N.

We further assume that a protein can be adsorbed non-specifically on DNA, and that the nonspecific adsorption energy ϵ, or the corresponding constant $y = \exp(\epsilon/k_BT)$, is the same everywhere on the DNA and does not depend on the

DNA sequence. The only exception is at the target site on the specific DNA, where the binding energy is much larger. We assume that every protein has two sites capable of binding to DNA, so that the protein can be bound to two DNA molecules at the same time.

A non-specifically bound protein is assumed to diffuse (slide) along DNA with the diffusion coefficient D_1, while protein dissolved in the surrounding water diffuses in 3D with diffusion coefficient D_3. In the simplest version of the theory, we assume $D_1 = D_3 = D$. While the protein is diffusing, the DNA molecule itself diffuses through water with diffusion coefficient D_t. Following the Stokes-Einstein relation, $D_t \sim D(b/l)$, where b is the size of the protein.

The quantity of our interest is the mean time t needed for the target site to be found by a protein. We want to look at the situation in terms of a single protein diffusing to its target. In this view, one should imagine that a protein molecule is initially introduced into a random place within volume v (thus the protein concentration c is $1/v$), and then ask how fast the protein diffuses to its target site on the specific DNA. In order to compare the predicted time t to the Smoluchowski time $t_s = 1/J_s = 1/4\pi Dcb$, we shall mainly look at the acceleration rate

$$\frac{t_s}{t} = \frac{1}{t(4\pi Dcb)} \sim \frac{v}{tDb}. \tag{3.2}$$

We note that in our scaling theory we drop away both all numerical factors

and all logarithmic correction factors, which exist in the problem because it deals with strongly elongated cylinders. In this context, we will use the symbol " $\sim$ " to mean "equal up to a numerical coefficient of order one", while symbols $<$ and $>$ mean $<<$ and $>>$, respectively. Along with these simplifications, we also make several assumptions driven by pure desire to make formulae simpler and to clarify major physical ideas. We assume that all "microscopic" length scales are of the same order, namely, the target size b: protein diameter, double helical DNA diameter, and the distance from DNA at which nonspecific absorbtion takes place are all considered to be roughly equal to b.

3.2.2 Search time

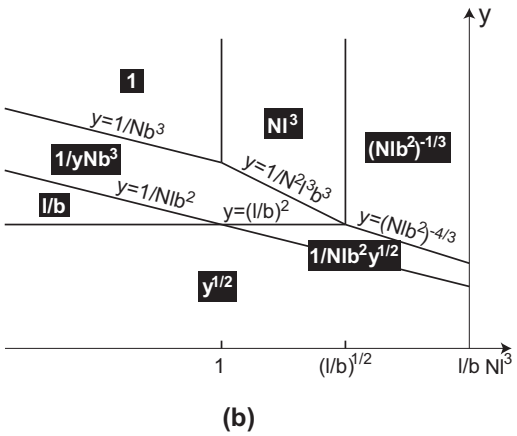

Figure 3.3: "Phase diagram" for the acceleration rate t_s/t in the plane of y and Nl^3, where l is held constant. Both the y and Nl^3 axes are in the logarithmic scale. The ratio t_s/t is shown in black on the background of each region. (a) shows scaling dependencies without inter-DNA transfer; (b) gives results with inter-DNA transfer, where t_s/t saturates at large y.

Let us imagine for a moment that there is no intersegment transfer, as is the case for a protein with only one nonspecific DNA binding site. One protein is introduced into the volume v. The ensuing search process for the given single protein consists of tours of 1D sliding along the nonspecific DNA followed by 3D diffusion in water, followed by 1D sliding, and so on. On its way to the target on the specific DNA, the protein will go through many adsorption and desorption cycles, and therefore the ratio of the typical time for the protein to be adsorbed, t_a, and desorbed, t_d, in a cycle should simply follow the equilibrium Boltzmann statistics:

$$\frac{t_a}{t_d} \sim y(Nlb^2). \tag{3.3}$$

The diffusion time in water per cycle t_d can be estimated as the time a protein needs to find a DNA molecule and bind nonspecifically to it. Using Eq. (3.1), $t_d \sim 1/(1/v)D(Nv)l \sim 1/NDl$, where $1/v$ stands for the protein concentration c and Nv is the number of DNA molecules in the volume v. As a result $t_a \sim t_d y(Nlb^2) \sim y(b^2/D)$.

Let x be the average length of DNA searched by the protein per cycle. Then in order to find the specific site (target) among the total Nvl/b sites on DNA, the protein should perform such searching cycles roughly Nvl/x times. Therefore

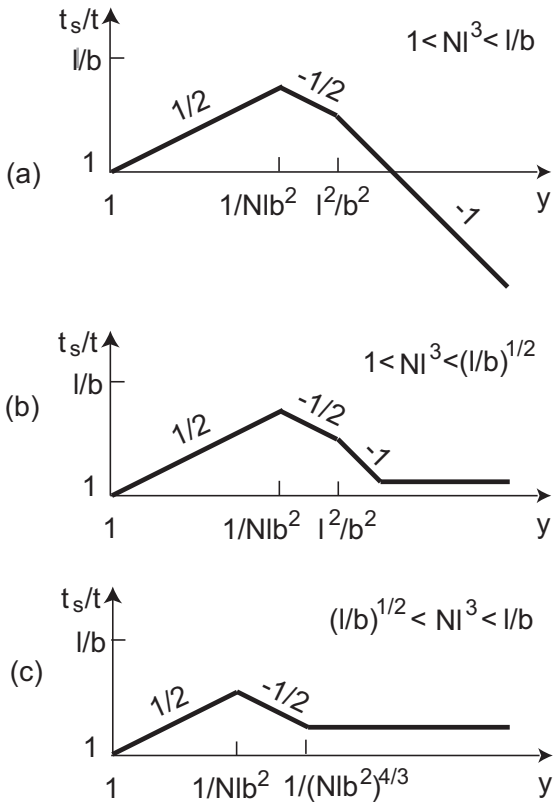

Figure 3.4: Schematic dependencies of acceleration rate on y for a semi-dilute ($Nl^3 > 1$) solution of short DNA pieces. (a) without inter DNA transfer; (b) and (c) with inter DNA transfer. The fraction next to each curve shows its slope (the power dependence of t_s/t on y).

the search time is given by

$$t \sim \frac{Nvl}{x}(t_a + t_d) = \frac{v}{Dx}(1 + yNlb^2). \tag{3.4}$$

Plugging t into Eq. (3.2), we obtain the acceleration rate

$$\frac{t_s}{t} \sim \frac{1}{1 + yNlb^2}\frac{x}{b}. \tag{3.5}$$

We can consider two limiting cases to find expressions for x. At $y < l^2/b^2$, $x \sim (Dt_a)^{1/2} \sim y^{1/2}b$ is just the sliding distance of the protein on one DNA molecule, while at $y > l^2/b^2$, x is limited to the total length of DNA l. There are also two limiting cases for the denominator of Eq. (3.5). When y is relatively small so that $y < 1/Nlb^2$, i. e. the protein spends most of its time desorbed in water, the first term dominates. At $y > 1/Nlb^2$, the protein spends most of its time adsorbed and the second term dominates. As a result we obtain four scaling regimes shown in the phase diagram of Fig. 3.3(a). We terminate the phase diagram at the concentration $Nl^3 = l/b$ because in a denser system liquid crystalline nematic ordering of DNA molecules becomes likely. The dependencies of the acceleration rate on y for a semi-dilute solution of short DNA pieces are plotted in Fig. 3.4(a). The search rate is shown to increase at first due to the increase of x, and then decrease due to the fact that at large y the protein spends most of the time adsorbed on nonspecific DNA molecules, which slows down the diffusion to the target.

Now let us move on to the case of a protein with two DNA binding sites. When a piece of DNA with an adsorbed protein collides with another DNA molecule, the protein has some probability to move directly to the new molecule. If the inter-DNA transfer is faster than the dissociation of protein into water, i.e. if the average time τ_t required for a protein to be transferred from one piece of DNA to another is shorter than the adsorption time t_a, then the protein can explore several

DNA molecules during t_a. As a result, the protein can visit a large number of different sites during adsorption and the efficiency of 1D search on DNA is greatly enhanced. We find below that at large y when $\tau_t < t_a$ and inter-DNA transfer dominates, the protein already spends most of the time adsorbed and $t_a > t_d$. Therefore we neglect the time spent in water t_d and redefine x/b as the number of different sites explored on the same DNA during τ_t. The search time can then be estimated as

$$t \sim \frac{Nvl}{x}\tau_t, \tag{3.6}$$

so that we obtain the acceleration rate

$$\frac{t_s}{t} \sim \frac{x}{NDlb\tau_t}. \tag{3.7}$$

The results are shown in the diagram Fig. 3.3(b). At large y the acceleration rate stops decreasing with y and saturates.

We begin explaining our results by calculating the most important quantity of our theory: τ_t. For a dilute solution of DNA molecules with $Nl^3 < 1$, one can use Eq. (3.1) to find the time for a given DNA molecule to enter the spherical region occupied by another piece of DNA by replacing D_3 and b by the DNA diffusion coefficient $D(b/l)$ and the length l. The result is $1/D(b/l)Nl = 1/DNb$. When the given DNA molecule enters the sphere of another molecule and diffuses

over distance l, on average every site on the DNA has a chance to collide with the second DNA before it leaves the sphere. As a result, a protein adsorbed on one DNA can essentially always get transferred to the new one during a collision. Since in a dilute solution the diffusion time to find such a sphere containing a second DNA piece, $1/DNb$, is larger than the diffusion time within the sphere, $l^2/D(b/l) \sim l^3/Db$, the transfer waiting time τ_t is the order of $1/DNb$. Because $D\tau_t > l^2$, the protein searches l/b different sites during τ_t and $x \sim l$. Using Eq. (3.6), we obtain the search time

$$t \sim \frac{Nvl}{l}\tau_t \sim \frac{v}{Db} \sim t_s. \tag{3.8}$$

When $Nl^3 > 1$, the spheres containing individual DNA molecules strongly overlap. In such a semi-dilute solution, the first collision for a given DNA molecule happens when it diffuses over the nearest neighbor distance r_p. One can find r_p by constructing an imaginary cylinder with radius r_p around each DNA molecule, where the length of the molecule serves as the cylinder's axis. Because the excluded volume of a cylinder is $\sim l^2 r_p$, the radius r_p should satisfy $Nl^2 r_p \sim 1$ and thus scale as $1/Nl^2$. During time

$$\tau \sim \frac{r_p^2}{D(b/l)} \sim \frac{1}{DN^2 l^3 b}, \tag{3.9}$$

the DNA diffuses over a distance r_p, giving every site on some segment of the DNA of length r_p the opportunity to collide once with the nearest-neighboring DNA (see Fig. 3.5). After time τ, the diffusing DNA and its neighbors have moved around enough that the nearest-neighboring region (shown by a dashed circle) may be considered to have shifted to a random place on the DNA.

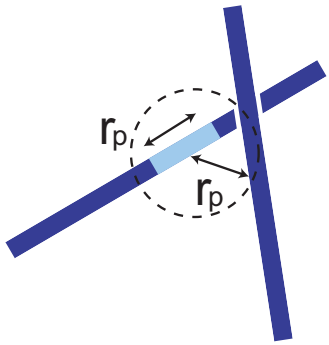

Figure 3.5: Collision of a DNA molecule with its nearest neighbor at distance r_p (other DNA molecules are not shown).

Let us assume that the protein has just arrived at some place on the given DNA molecule. In order to be transferred to another DNA within time τ, the protein must reach the segment of length r_p (see Fig. 3.5) during τ. Since the typical distance between the adsorbed protein and the nearest neighboring region is just proportional to the DNA length l, the protein will change molecules during τ when $D\tau > l^2$, or $Nl^3 < (l/b)^{1/2}$. Therefore $\tau_t \sim \tau$ and we obtain the search time

$$t \sim Nv\tau_t \sim \frac{1}{Nl^3}\frac{v}{Db} \sim \frac{t_s}{Nl^3}, \tag{3.10}$$

from which we can see that the search rate saturates Nl^3 times faster than the

Smoluchowski rate, and that the acceleration rate grows with DNA concentration since denser solution makes inter-DNA transfer easier.

When $Nl^3 > (l/b)^{1/2}$, the 1D sliding distance of protein on a single DNA molecule during τ is $x \sim (D\tau)^{1/2} < l$. Therefore, the probability for the protein to reach the nearest neighboring region on the DNA during τ is $x/l \sim (l/b)^{1/2}/Nl^3 < 1$. In this case the transfer waiting time $\tau_t > \tau$, and it should be calculated self-consistently. During τ_t the sliding distance x of the protein is $(D\tau_t)^{1/2}$, so the probability for the protein to reach a specified nearest neighboring region is on the order of $(D\tau_t)^{1/2}/l$. Since the nearest-neighboring region changes to a random place on the DNA after τ, there are τ_t/τ such regions during time τ. Therefore the probability for the protein to reach any one of these regions and then get transferred should satisfy

$$\frac{(D\tau_t)^{1/2}}{l}\frac{\tau_t}{\tau} \sim 1. \tag{3.11}$$

As a result,

$$\tau_t \sim \frac{1}{D(N^2l^2b)^{2/3}}, \tag{3.12}$$

and the search time is given by

$$t \sim \frac{Nvl}{(D\tau_t)^{1/2}}\tau_t \sim (Nlb^2)^{1/3}\frac{v}{Db} \sim (Nlb^2)^{1/3}t_s. \tag{3.13}$$

The equations for the crossover lines at large y, shown in Fig. 3.3(b), are

obtained by equating τ_t to t_a. This condition determines the range of parameters for which intersegment transfer takes over, i.e. when the time it takes the protein to transfer between DNA molecules is much shorter than the time the protein spends adsorbed on the DNA then we can say that intersegment transfer is the dominant mechanism. The dependencies of the acceleration rate on y for semi-dilute DNA concentrations with $Nl^3 > 1$ are schematically plotted in Fig. 3.4 (b) and (c). For the purpose of comparison, we also show the dependencies for proteins with a single binding site in Fig. 3.4 (a).

A new feature shown by Fig. 3.4 (b) and (c) is that, for proteins with two DNA binding sites, inter-DNA transfer stops the search rate from decreasing and causes it to saturate at large y. It can be shown from equations (3.8), (3.10) and (3.13) that the acceleration rate is constant and ~ 1 when the solution is dilute and y is large. The acceleration rate begins to grow as the concentration is increased past $Nl^3 \sim 1$, peaking when $Nl^3 \sim (l/b)^{1/2}$ and achieving a maximum value of $(l/b)^{1/2}$. After the peak, it decreases again and reaches $(l/b)^{1/3}$ when $Nl^3 \sim l/b$.

Before we move on to next section, we should emphasize that in our calculation we have completely neglected the energy barrier associated with breaking the double-bound state. We have assumed the barrier to be so small that the lifetime of the double-bound state is a small correction to the above calculated τ_t. The search time we have found is therefore the lower limit which can be achieved with

the help of intersegment transfer. In Sec. 3.4, we will return to this issue in more detail.

3.2.3 Dissociation rate

Since in experiments [23, 24, 25] the role of intersegment is inferred from measuring the dissociation rate of the prepared protein-DNA complex, in this section we calculate this rate for a protein adsorbed on a nonspecific piece of DNA dissociating to other nonspecific DNA pieces via inter-DNA transfer. [1]

The calculation is quite straightforward and the results are presented in the phase diagram of Fig. 3.6. The apparent dissociation rate is just $1/t_a+1/\tau_t$, where each term represents a possible relaxation process undergone by the adsorbed protein: either dissociation to water or intersegment transfer to another piece of DNA. The faster process dominates the rate. Since the dissociation rate to water decreases with the adsorption strength y and the intersegment transfer rate

[1] Our model serves as a simple generalization of experimental systems where the protein is specifically adsorbed to its target on the DNA in the complex and the DNA free in solution can be specific or nonspecific [23, 24, 25]. We argue that this generalization does not change the main feature of the problem, which is determined by the frequency at which the free DNA molecules collide with the protein-DNA complex. The difference lies in the transfer probability per collision. On the nonspecific DNA, the protein can slide freely. In contrast, protein on the specific DNA spends most of the time adsorbed to its target. Thus, to experience a transfer the complex should collide with another piece of DNA exactly at the position of target, which results in smaller transfer probability. However the specifically adsorbed protein can first slide into nonspecific sites and then dissociate into the bulk solution or transfer to other DNA molecules [27]. In this way the decreased transfer probability is somewhat compensated, and it becomes closer to the case of dissociation from nonspecific DNA. More importantly, the process of target search involves the protein making direct transfers between nonspecific segments of DNA, so we prefer to study the dissociation rate for this case.

grows with the nonspecific DNA concentration, intersegment transfer dominates the apparent dissociation rate at relatively large y and N. We find that the enhanced dissociation rate grows linearly with nonspecific DNA concentration N when the solution is dilute, in agreement with the experiments [23, 24, 25]. In semi-dilute solution, however, the dissociation rate has power law dependence on N, with power equal to either 2 or 4/3.

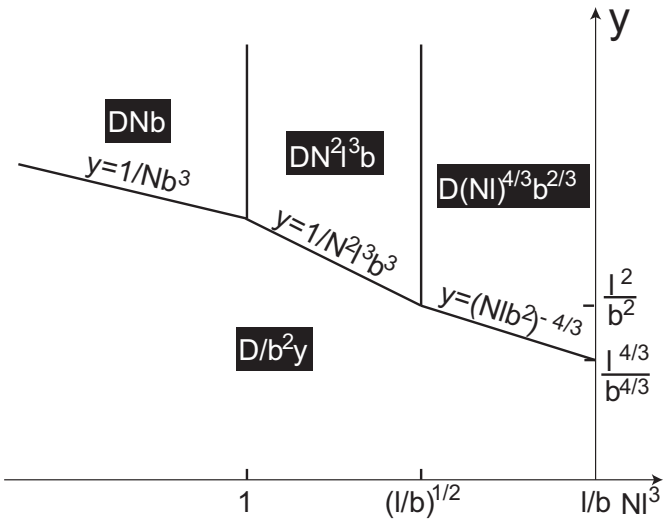

Figure 3.6: "Phase diagram" for the dissociation rate under the influence of inter DNA transfer.

3.3 DNA is a globule

After exploring the particular role of DNA motion and protein intersegment transfer for short DNA pieces, we are well prepared to generalize the above results to the more realistic case of globular DNA (see Fig. 3.1). We focus here on cases

with large y, where the mechanism of intersegment transfer is important. The results for acceleration rate at small y, where intersegment transfer does not help much, can be found in Ref. [28].

We assume that within some volume v, a double helical DNA with contour length L and persistence length $p \gg b$ is confined. We disregard the excluded volume of DNA, considering the DNA coil to be Gaussian and not a swollen coil, described by the Flory index 3/5. This is a reasonable approximation for most realistic cases. Indeed, for many real DNA molecules such as λ-DNA, it is justified because of the large persistence length-to-diameter ratio of the double helix: excluded volume in the coil remains unimportant up to DNA length about $L < p^3/b^2$ (as much as 100000 base pairs under normal ionic conditions). When the DNA is very long for a given volume, specifically, when the gaussian coil size $(Lp)^{1/2} > v^{1/3}$, it cannot remain a Gaussian coil, but must fold back to make several smaller overlapping coils. In other words, it must be a globule which locally resembles a transient network.

In order to simplify our calculation, we can approximate the DNA as a series of freely-jointed straight segments (rods), each with persistence length p. We further restrict our study to a globule so dense that the spheres containing each rod strongly overlap (Fig. 3.1). Except for the connectivity, the globule is quite similar to a semi-dilute solution of short straight DNA pieces of length p and concentration $N = (L/p)/v$ satisfying $Np^3 > 1$. In this case the diffusion distance

r_p for a given rod to experience its first collision with another rod, which may be close in space but far removed along the DNA contour, is shorter than its length p. As a result, one can disregard the correlation of motion between connected rods and treat the motion of each rod over the short distance r_p separately as a normal diffusion process with diffusion coefficient $D(b/p)$.

Let us first look at a simple case where the 1D sliding distance x for a protein on a single DNA rod is shorter than the chain length p. As before, we consider x to be the distance traveled by the protein within a time τ_t, the average waiting time before a protein is transferred from one DNA rod to another, uncorrelated rod. In this situation, the protein does not feel the connection between rods. Therefore, we can simply use the result for short DNA pieces, replacing the length l by p and using the rod concentration $N = (L/p)/v$. Then Eq. (3.13) gives the search time

$$t \sim (Npb^2)^{1/3}(v/Db) \sim (Lb^2/v)^{1/3}t_s. \tag{3.14}$$

From Eq. (3.12), we find $\tau_t \sim 1/D(N^2p^2b)^{2/3}$ and thus $x \sim (D\tau_t)^{1/2} \sim 1/(N^2p^2b)^{1/3}$. So the condition $x < p$ is fulfilled when $Np^3 > (p/b)^{1/2}$ or $L > (v/b^2)(b/p)^{3/2}$. Furthermore, to avoid the liquid crystalline nematic ordering of DNA chains, we assume that $Np^3 < p/b$ or $L < v/pb$.

When the concentration of DNA rods is small enough that it falls within the range $1 < Np^3 < (p/b)^{1/2}$, the separation between DNA rods becomes large.

Therefore, the time between collisions increases. As a result, the transfer waiting time τ_t grows and the 1D sliding distance of the protein x becomes larger than p. In this case, one should be careful in calculating the DNA diffusion distance that results in the first collision between DNA rods. It is no longer equal to the nearest neighbor distance $r_p \sim 1/Np^2$ between DNA rods of length p. To find this distance, let us concentrate on the continuous piece of length $x > p$, which spans several rods. The shortest distance from this piece of DNA to another similar piece is realized at only one of its constituent rods. The first collision that could result in transfer of the protein happens only when this particular rod diffuses over the x-dependent nearest neighbor distance $r(x) \sim r_p p/x \sim 1/Npx$. During time $\tau(x) \sim r^2(x)/D(b/p)$, on average each DNA piece of length x experiences a collision, and the protein slides a distance x across the DNA. Thus, the waiting time for a protein to be transferred to another, uncorrelated DNA piece $\tau_t \sim \tau(x) \sim 1/DN^2x^2pb$ should be equal to the 1D sliding time x^2/D of the protein on a single piece. This self-consistent calculation gives $x \sim (1/Np)^{1/2}(p/b)^{1/4}$ and $\tau_t \sim (1/DNp)(p/b)^{1/2}$. We therefore obtain the search time

$$t \sim \frac{L}{x}\tau_t \sim (Np^3)^{1/2}\left(\frac{b}{p}\right)^{3/4}\frac{v}{Db} \sim \left(\frac{Lb^2}{v}\right)^{1/2}\left(\frac{p}{b}\right)^{1/4} t_s. \tag{3.15}$$

As explained in Ref. [28], without intersegment transfer, large values of y result in the protein spending most of its time adsorbed on DNA far from the

target site. The result is that the search time saturates at $L^2/D \sim (L^2 b/v)t_s$, which is a huge deceleration compared to the Smoluchowski time. From Eqs. (3.14) and (3.15), one can easily find that at large y the search time is greatly reduced below t_s by the combination of 1D sliding, intersegment transfer and DNA motion. Correspondingly, the acceleration rate is enhanced and can be larger than 1, as shown by the solid line in Fig. 3.2. These results remain qualitatively correct for a sparser globule with $p/v^{1/3} < Np^3 < 1$ or $v^{2/3}/p < L < v/p^2$, where the typical mesh size of the transient network is longer than p and thus the piece of DNA inside each mesh is not straight as shown in Fig. 3.1 but rather a small Gaussian coil. To fully account for this kind of geometry, however, one should consider a more complicated correlated segmental diffusion of DNA, and this is beyond the scope of the current paper.

Until now, we assumed that $D_1 = D_3 = D$, where D_1 and D_3 are the diffusion coefficients of protein on DNA and in water, respectively. In fact, the random sequence of DNA and the resulting sequence-dependent nonspecific adsorption energy most likely produces $D_1 < D_3$. To illustrate the role of 1D sliding in conjunction with intersegment transfer, we fix $D_3 = D$ and calculate the acceleration rate for various values of D_1 following the methods explained above. The results for large y, where the intersegment transfer plays an important role, are shown in the plane of D_1/D and Np^3 in Fig. 3.7. The dashed line corresponds to $D_1 = D_3 = D$. We find that the acceleration rate grows as $(D_1/D)^S$ with the

index S increasing from 1/2 to 1.

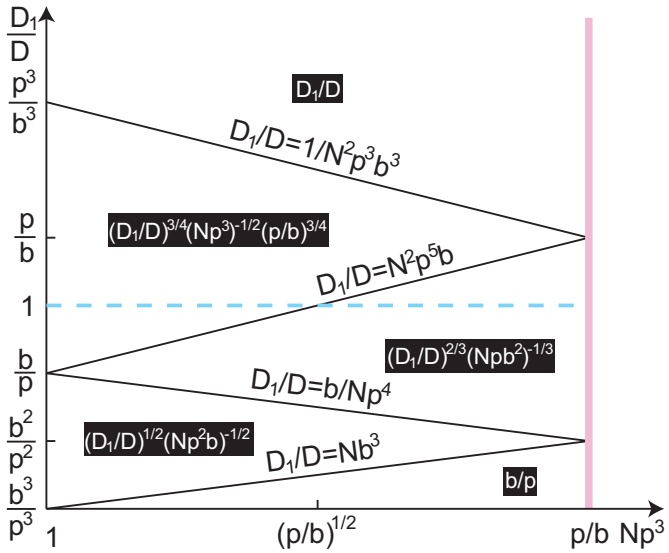

Figure 3.7: "Phase diagram" for the acceleration rate at large y on globular DNA, where the intersegment transfer plays an important role in the target search.

3.4 Discussion

In our theory, we completely neglect the effect of the energy barrier ϵ^* associated with breaking the double-bound state and reverting to a single-bound state. Our results are therefore an upper estimate of the effect of intersegment transfer. On the other hand, a naïve guess of the barrier height is $\epsilon^* = \epsilon$, since to break one of the two contacts the protein has to pay the adsorption energy per binding site on one side. If this were true, the protein would be trapped in the double-bound state for the adsorption time t_a, and therefore the inter-DNA transfer could not do better job in accelerating the dissociation of the protein from the protein-DNA

complex than desorption into water. As a result, adding DNA into the solution of a protein-DNA complex would not increase the dissociation rate of the protein, which clearly contradicts the *in vitro* experiments on various proteins and DNA molecules [23, 24, 25]. This suggests that in the double-bound state, the binding strength per binding site $\epsilon^* < \epsilon$, which could be a result of the excluded volume of close DNA molecules or the Coulomb repulsion between them.

The experiment [23] showed that the dissociation rate increases linearly with the nonspecific DNA concentration and saturates at large concentrations. This implies that at small DNA concentration, the dissociation rate is limited by the diffusion of nonspecific DNA molecules and the resulting collisions that induce inter-DNA transfer. As the DNA concentration is increased, the energy barrier for releasing the protein from the double-bound state becomes the bottleneck of the dissociation. Since the lifetime of the double-bound state does not depend on the nonspecific DNA concentration, the dissociation rate saturates. Having $\epsilon^* < \epsilon$ in mind, one can show that our theory is valid if the transfer waiting time τ_t is larger than the lifetime of the double-bound state. We can estimate this lifetime as the product of the characteristic time scale b^2/D and the binding strength per site in the double-bound state $y^* \sim \exp(\epsilon^*/k_BT)$. Thus our theory works when $y^*(b^2/D) < \tau_t$. When $y^*(b^2/D) > \tau_t$, our main idea is still correct, however one should replace τ_t by the lifetime of the double-bound state $(b^2/D)y^*$ and repeat a similar analysis. The acceleration rate will be diminished as a result but will

remain much larger than in the case without intersegment transfer.

The above discussion of ϵ^* assumes that the double-bound state does not affect the equilibrium Boltzmann statistics represented by Eq. (3.3). This places an additional restriction on ϵ^*. The energy of the double-bound state is $2\epsilon^*$. If one were to take a snapshot of the solution of short DNA pieces at a given time, the number of DNA contacts (where two DNA collide) per DNA strand is on the order of Nl^2b, where l^2b represents the excluded volume of a rod-like DNA. Then the limitation on y^* can be expressed as $\exp(2\epsilon^*/k_BT)(Nl^2b)(b^3) < ylb^2$ or $(y^*)^2 < y/Nlb^2$.

Let us now compare our work with the treatment of intersegment transfer in Ref. [7]. While our work combines both mechanisms of 1D sliding and intersegment transfer, the Ref. [7] treats them separately. Neglecting the mechanism of protein sliding in a description of intersegment transfer results in a huge overestimation of the collision time τ and the subsequent transfer time τ_t. Indeed one can see from Fig. 3.7 that if the protein cannot move on DNA, the acceleration rate is b/p, which is much smaller than the acceleration rate at $D_1 = D_3 = D$. Equivalently, neglecting intersegment transfer results in overestimation of the sliding time, sliding distance and search time. In the later review of Ref. [**?**], the interplay between sliding and intersegment transfer was taken into account. Qualitatively, the conclusions agree with our results, however the dependence of

the intersegment transfer rate on the characteristics of DNA geometry, DNA motion, concentration and the nonspecific adsorption strength of protein to DNA y was not calculated.

Finally, we note that our theory can be easily adapted to study the effective diffusion rate of a protein through a solution of polymers like DNA. This problem was studied in Ref. [29], assuming $D_1 = 0$. Following the ideas of our paper, one can expand on this study to account for the "constructive interference" of 1D sliding and intersegment transfer of protein, which was not addressed in Ref. [29]. As with target search, intersegment transfer enhances the macroscopic diffusion coefficient of proteins at large y, where the protein spends most of its time adsorbed on DNA. We can consider a solution of short DNA molecules, where without intersegment transfer the effective diffusion coefficient of the protein is decreased by nonspecific adsorption to DNA and eventually saturates at the DNA diffusion coefficient $D(b/l)$. In a dilute solution, intersegment transfer does not assist the macroscopic diffusion of proteins, since each DNA molecule is far removed from other molecules and therefore the macroscopic displacement of protein is determined mainly by the motion of the DNA. In a semidilute solution, however, where $1 < Nl^3 < l/b$, 1D sliding on DNA becomes important. When $1 < Nl^3 < (l/b)^{1/2}$, $D\tau_t > l^2$ and the 1D sliding distance of protein during time τ_t is limited to the length of DNA l. In this case $\tau_t \sim \tau$. Using Eq. (3.6), the effective diffusion coefficient is obtained as $l^2/\tau_t \sim N^2 l^6 D(b/l)$. At higher

densities when $(l/b)^{1/2} < Nl^3 < l/b$, $D\tau_t < l^2$. As a result, the nonspecific adsorption of protein on DNA does not hinder the diffusion of protein at all and the macroscopic diffusion coefficient is just D. For $D_1 \neq D_3$, a similar analysis can be performed.

One further application of our theory is to the problem of dynamic (stirred) percolation, e.g., the conductivity of well-conducting wires in some insulating liquid. It is well known that if the wires are randomly frozen in the liquid, the conductivity vanishes below the percolation threshold [30]. However, because of the diffusion of wires in the liquid, the charge carriers are not trapped within finite clusters of wires. Instead, they can hop from one wire to another when the wires approach close to each other. This results in a finite conductivity below the percolation threshold [31]. For such systems, one can find the macroscopic diffusion coefficient of the charge carriers and then map it to the effective conductivity of the system.

Chapter 4

Role of Disorder

4.1 Distribution of nonspecific adsorption energies

Until now, our theory assumes that the nonspecific adsorption energy between proteins and DNA is sequence independent, i.e. the energy profile experienced by the searching protein away from the target is totally flat. This however disagrees with quasi-random character of the natural sequences of DNA. It is known that the nonspecific protein-DNA adsorption energy can be divided into two parts [32, 33]: (i) The sequence independent Coulomb energy of attraction between the positively charged domain of the protein surface and the negatively charged phosphate backbone, and (ii) the sequence specific adsorption energy due

to formation of hydrogen bonds of the protein with the DNA bases. This is done by the recognition α-helix going deep into the major groove of DNA [34]. Suppose the protein encounters l base pairs between positions i and $i+l$. We call this position of the protein *site* i and characterize it by energy $\epsilon_i < 0$, where the energy of the free protein in water is chosen to be 0. Because the sliding protein has a complex nonuniform structure and interacts with a random DNA sequence, the total energy ϵ_i randomly fluctuates along DNA (Fig. 4.1). One can assume that at nonspecific positions on DNA, the protein exploits the same set of potential hydrogen bonds it forms with the target [35]. Since target recognition is often mediated by hydrogen bonds to some of the four chemical groups on the major groove side of the base pair [36], and the recognition α-helix interacts with several base pairs, many hydrogen bonds contribute to ϵ_i. Therefore the distribution of ϵ_i can be approximated by the Gaussian distribution [13, 35, 37] with a mean w and standard deviation $\sigma \ll |w|$:

$$g(\epsilon_i) = \frac{1}{\sqrt{2\pi\sigma^2}} \exp\left[-\frac{(\epsilon_i - w)^2}{2\sigma^2}\right]. \tag{4.1}$$

In this chapter we study the role of disorder on the rate enhancement J/J_s assuming that disorder is strong, i.e. $\sigma > kT$, where k is the Boltzmann constant and T is the ambient temperature.

Similar to the the case of the flat energy profile [28], we assume that transport

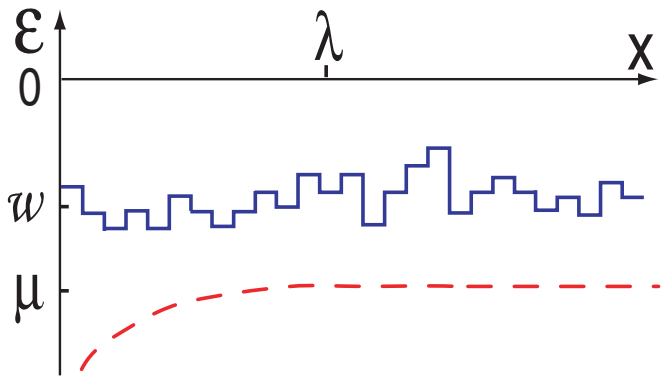

Figure 4.1: Distribution of nonspecific adsorption energies ϵ and of chemical potential $\mu(x)$ along DNA molecule. The target site is located at $x = 0$, λ is the antenna length.

outside the antenna is *mainly* due to the 3D diffusion, while inside the antenna transport is *dominated* by sliding, or 1D diffusion along DNA and we equate the fluxes J_1 and J_3 to find λ. The rate J_3 is given by the Smoluchowski formula for the target size λ and for the concentration of "free" (not adsorbed) proteins c_3, it is $J_3 \sim D_3 c_3 \lambda$. The flux on antenna J_1 strongly depends on σ and also, generally speaking, on DNA sequence in the finite antenna. We show that there is a characteristic length of antenna $\lambda = \lambda_c(\sigma, T)$ such that at $\lambda > \lambda_c$ flux J_1 self-averages and becomes sequence independent. Such a "macroscopic" antenna determines J/J_s for moderate disorder. In this case, the ratio J/J_s decreases exponentially fast with growth of disorder. At stronger disorder we deal with a mesoscopic antenna with $\lambda < \lambda_c$ and strictly speaking J/J_s depends on random DNA sequence. In this paper, we concentrate only on the most probable value of J/J_s. In order to calculate it, we estimate the most probable value of J_1. We

show that in such a mesoscopic situation disorder leads to a weaker reduction of J/J_s.

We assume that within some volume v there is a straight, immobile (double helical) DNA with the length L smaller than $v^{1/3}$, but much larger than any antenna length. For a dilute DNA solution, $1/v$ stands for the concentration of DNA. We also assume that all the microscopic length scales such as the length of a base pair, the size of the target site, the diameter of the DNA etc. are of the same order b. We are mainly interested in scaling dependence of the rate enhancement J/J_s on major system parameters, such as σ, w, L and v. This means that all the numerical coefficients are dropped in our scaling estimates.

To estimate J_1, we assume at each site i on DNA, the protein has some probabilities of hopping to nearest neighboring sites j. We write the probability for the hopping from an occupied site i to an empty site j as

$$\begin{aligned} \gamma_{ij} &= \nu_0 \exp\left(-\frac{\epsilon_j - \epsilon_i + |\epsilon_j - \epsilon_i|}{2kT}\right) \\ &= \begin{cases} \nu_0 \exp(-\frac{\epsilon_j - \epsilon_i}{kT}) & \text{if} \quad \epsilon_j > \epsilon_i \\ \nu_0 & \text{if} \quad \epsilon_j < \epsilon_i \end{cases}, \end{aligned} \tag{4.2}$$

where $\nu_0 \sim D_1/b^2$ is the effective attempt frequency. In Eq. (4.2) we neglected the activation barriers separating two states in comparison with $\epsilon_j - \epsilon_i$. The number of proteins making such transition from site i to j per unit time can be estimated

by $\Gamma_{ij} = \gamma_{ij} f_i (1 - f_j)$, where function f_i is the average occupation number of site i. At small enough c, all $f_i \ll 1$ and thus $\Gamma_{ij} \simeq \gamma_{ij} f_i$. Function f_i is given then by:

$$f_i = \exp[-(\epsilon_i - \mu_i)/kT], \tag{4.3}$$

where μ_i is the chemical potential. Using Γ_{ij} and Γ_{ji}, we can write the net flux from site i to j in the form:

$$J_{ij} = \Gamma_{ij} - \Gamma_{ji} \simeq \nu_0 e^{-\frac{\epsilon_{ij}}{kT}} (e^{\frac{\mu_i}{kT}} - e^{\frac{\mu_j}{kT}}), \tag{4.4}$$

where $\epsilon_{ij} = max\{\epsilon_i, \epsilon_j\}$.

We now argue that as long as the antenna is only a small part of the DNA molecule, every protein adsorbs to DNA and desorbs many times before it locates the target. Therefore, outside the antenna there is statistical equilibrium between adsorbed and desorbed proteins, and hence proteins have uniform chemical potential $\mu_i = \mu = kT \ln(c_3 b^3)$. Within the antenna, μ_i decreases when the site approaches the target and reaches $-\infty$ at the target site (see Fig. 4.1). If we label the border of the antenna as site 1 and the target as site $\lambda/b + 1$, using Eq. (4.4), we can write

$$\sum_{i=1}^{\lambda/b} J_{ij} e^{\frac{\epsilon_{ij}}{kT}} = \nu_0 (e^{\frac{\mu}{kT}} - e^{-\frac{\infty}{kT}}) = \nu_0 c_3 b^3, \tag{4.5}$$

where $j = i + 1$. Since the 1D current J_1 towards the target is the same at any antenna site, i. e. $J_{ij} = J_1$, we can find it as

$$J_1 = \frac{\nu_0 c_3 b^3}{\sum_{i=1}^{\lambda/b} \exp(\epsilon_{ij}/kT)} \simeq \frac{\nu_0 c_3 b^3 \sqrt{2\pi\sigma^2}}{(\lambda/b) \int_{-\infty}^{0} d\epsilon_{ij} R(\epsilon_{ij})}, \tag{4.6}$$

where $R(\epsilon_{ij})$ is given by

$$\begin{aligned} R(\epsilon_{ij}) &= \sqrt{2\pi\sigma^2} g(\epsilon_{ij}) \exp(\epsilon_{ij}/kT) \\ &= \exp\left\{ \frac{\sigma^2}{2(kT)^2} + \frac{w}{kT} - \frac{[\epsilon_{ij} - (w + \sigma^2/kT)]^2}{2\sigma^2} \right\}. \end{aligned} \tag{4.7}$$

One can interpret Eq. (4.6) as the Ohm's law, where the numerator plays the role of the voltage applied to antenna and denominator is the sum of resistances of all pairs (i, j) which are similar to Miller-Abrahams resistances for the hopping transport of electrons [30].

The sharp maximum value of function $R(\epsilon_{ij})$ determining the sum of Eq. (4.6) is reached when $\epsilon_{ij} = \epsilon_{opt} = w + \sigma^2/kT$, and $R(\epsilon_{opt}) \sim \exp[\sigma^2/2(kT)^2 + w/kT]$. Thus

$$J_1 \sim \frac{D_3 c_3 b^2}{\lambda} \exp\left[\frac{|w|}{kT} - \frac{\sigma^2}{2(kT)^2} \right], \tag{4.8}$$

where we assumed for simplicity that $D_3 = D_1 \sim b^2 \nu_0$.

4.2 Macroscopic and Mesoscopic antenna

Before we move forward, we emphasize the crucial assumption already made in above derivation. We assumed λ is so long that within the antenna the sliding protein encounters sites with energy ϵ_{opt} more than once and therefore, the sum in Eq. (4.6) can be replaced by the integral with limits from $-\infty$ to 0. We call such antenna macroscopic. For a short antenna, the probability for such a site to appear inside is very small. Thus the sum in Eq. (4.6) is determined by the largest value of $R(\epsilon_{ij})$ typically available within the antenna. We call such antenna mesoscopic.

Macroscopic antenna—We study macroscopic antenna first. Using J_1 and J_3, our main *balance* equation for the rate J reads

$$J \sim D_3 c_3 \lambda \sim \frac{D_3 c_3 b^2}{\lambda} \exp\left[\frac{|w|}{kT} - \frac{\sigma^2}{2(kT)^2}\right] . \tag{4.9}$$

Thus the antenna length λ is obtained as

$$\lambda \sim b \exp\left[\frac{|w|}{2kT} - \frac{\sigma^2}{4(kT)^2}\right] . \tag{4.10}$$

Next we calculate the free protein concentration c_3. Suppose the one-dimensional concentration of non-specifically adsorbed proteins is c_1. Assuming the antenna

is only a small part of the DNA and remembering that adsorbed proteins are confined within distance of order b from the DNA, we can write down the equilibrium condition as:

$$\frac{c_1}{c_3 b^2} \sim \int f(\epsilon) e^{-\epsilon/kT} d\epsilon \sim \exp\left[\frac{|w|}{kT} + \frac{\sigma^2}{2(kT)^2}\right], \tag{4.11}$$

which must be complemented by the particle counting condition $c_1 L + c_3(v - Lb^2) = cv$. Since volume fraction of DNA is always small, $Lb^2 \ll v$, standard algebra then yields

$$c_3 \simeq \frac{cv}{yLb^2 + v} \sim \begin{cases} c & \text{if} \quad y < v/Lb^2 \\ cv/Lb^2 y & \text{if} \quad y > v/Lb^2 \end{cases}, \tag{4.12}$$

where y is $\exp[|w|/kT + \sigma^2/2(kT)^2]$. Eqs. (4.12) lead to two different scaling regimes, which are denoted as A and B in the diagram Fig. 4.2. In regime A, the non-specific adsorption is relatively weak, $c_3 \sim c$, we arrive at

$$\frac{J}{J_s} \sim \exp\left[\frac{|w|}{2kT} - \frac{\sigma^2}{4(kT)^2}\right]. \qquad \text{(regime A)} \tag{4.13}$$

In the regime B, most proteins are adsorbed. Using the lower line of Eqs. (4.12), we obtain

$$\frac{J}{J_s} \sim \frac{v}{Lb^2} \exp\left[-\frac{|w|}{2kT} - \frac{3\sigma^2}{4(kT)^2}\right]. \qquad \text{(regime B)} \tag{4.14}$$

In both regimes, $|w| > \sigma^2/kT$, thus σ term of $\ln(J/J_s)$ constitutes a correction. The size of antenna grows with $|w|$, however unproductive non-specific adsorption of proteins on distant pieces of DNA, which can slow down the transport to the specific target grows with $|w|$ too. These two effects compete, as a result the rate enhancement J/J_s grows with w in regime A and declines in regime B. On the other hand, growing σ reduces the antenna size and promotes non-specific adsorption. Therefore, J/J_s decreases with σ in both regimes.

The above theory deals with a macroscopic antenna. To be macroscopic, the antenna has to contain at least one site with energy around ϵ_{opt}. The number of sites $n(\epsilon)$ with energy ϵ within the antenna is of the order of $\sim (\lambda/b)\exp[-(\epsilon - w)^2/2\sigma^2]$. Thus a macroscopic antenna requires $n(\epsilon_{opt}) > 1$, which gives $\lambda > \lambda_c = b\exp[\sigma^2/2(kT)^2]$. Since we know λ from Eq. (4.10), this condition can be written explicitly as $|w| > 3\sigma^2/2kT$. Hence, $|w| = 3\sigma^2/2kT$ is the border between the macroscopic regimes (A, B) and mesoscopic regimes (C, D) in Fig. 4.2. We can check that when $|w| > 3\sigma^2/2kT$, the condition $\epsilon_{opt} < 0$ is satisfied for the case of macroscopic antenna. Now we are ready to switch to the case of mesoscopic antenna and explain regimes C and D.

Mesoscopic antenna—In this case, the upper limit of the integral in Eq. (4.6) should be replaced by $\epsilon_\lambda \ll \epsilon_{opt}$ which is the largest energy typically available within the antenna. It can be estimated from $n(\epsilon_\lambda) \sim 1$, it is $\epsilon_\lambda \sim w + \sqrt{2}\sigma\sqrt{\ln(\lambda/b)}$. Using w and ϵ_λ, we can estimate the sum in Eq. (4.6) and

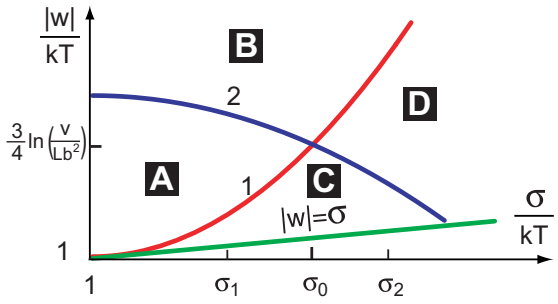

Figure 4.2: The phase diagram of scaling regimes for $|w| > \sigma > kT$. Each line marks a smooth crossover between scaling regimes. The red line $|w| = 3\sigma^2/2kT$ marks the border 1 between macroscopic regimes (A, B) and mesoscopic regimes (C, D). The blue line $|w| = kT\ln(v/Lb^2) - \sigma^2/2kT$ marks the border 2 between weak and strong adsorption regimes. They intersect at $\sigma_0 = kT[(1/2)\ln(v/Lb^2)]^{1/2}$, $|w| = kT(3/4)\ln(v/Lb^2)$.

get typical 1D current for the case of mesoscopic antenna:

$$J_1(\lambda) \sim D_3 c_3 b \exp\left[\frac{|w|}{kT} - \sqrt{2\ln(\lambda/b)}\frac{\sigma}{kT}\right]. \tag{4.15}$$

Eq. (4.15) is apparently different from Eq. (4.8) valid for the macroscopic antenna. This difference is partially related to the rate enhancement of 1D diffusion at small time scale noticed for the Gaussian disorder in computer simulations [35]. Equating $J_1(\lambda)$ to $J_3 \sim D_3 c_3 \lambda$, we obtain the antenna length

$$\lambda \sim b \exp\left[\left(\sqrt{\frac{|w|}{kT} + \frac{\sigma^2}{2(kT)^2}} - \frac{\sigma}{\sqrt{2}kT}\right)^2\right]. \tag{4.16}$$

We can check, with this λ, that the condition $\epsilon_\lambda < 0$ still holds. When $|w| < \sigma^2/2kT$, the antenna length $\lambda \sim b\exp(w^2/2\sigma^2)$. For a given adsorption energy

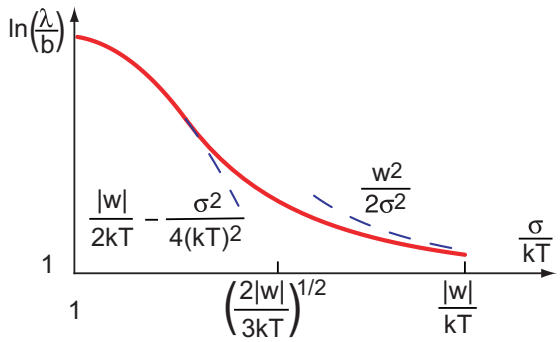

Figure 4.3: Dependence of antenna length λ on the disorder strength σ. Dashed lines represent the asymptotic limits.

w, dependence $\lambda(\sigma)$ is plotted in Fig. 4.3. It shows that the decrease of the antenna length with growing disorder strength slows down when antenna becomes mesoscopic.

The crossover from a relatively weak adsorption to a strong one described by Eqs. (4.12) again leads to the two scaling regimes for the case of mesoscopic antenna. They are labeled C and D in the diagram Fig. 4.2. For relatively weak adsorption, when $|w| < \sigma^2/kT$, we obtain regime C, where

$$\frac{J}{J_s} \sim \exp\left(\frac{w^2}{2\sigma^2}\right), \qquad \text{(regime C)} \tag{4.17}$$

while for strong adsorption we have regime D where

$$\frac{J}{J_s} \sim \frac{v}{Lb^2} \exp\left[-\frac{|w|}{kT} - \frac{\sigma^2}{2(kT)^2}\right]. \qquad \text{(regime D)} \tag{4.18}$$

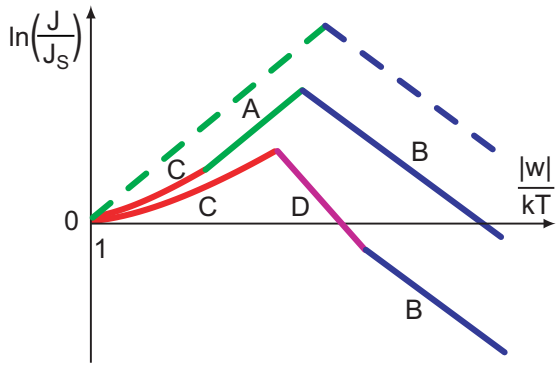

Figure 4.4: Schematic plot of the dependencies of the rate enhancement J/J_s on $|w|$ at $\sigma = \sigma_1$ (upper solid curve) and $\sigma = \sigma_2$ (lower solid curve). Letters A, B, C, D represent the domains of Fig.4.2 they go through. Dashed line shows the limit case of the flat energy profile with $\sigma = 0$.

In experiment, the adsorption energy w can be controlled by the salt concentration changing the Coulomb part of protein-DNA interaction [8]. The dependencies of $\ln(J/J_s)$ on $|w|$ at the two specified values of disorder strength σ_1 and σ_2 marked in Fig. 4.2 are schematically plotted in Fig. 5.4. For comparison, we also plotted the case of the flat energy profile ($\sigma = 0$). In both cases with $\sigma > 0$, $\ln(J/J_s)$ first grows proportional to w^2 (regime C), because the antenna is mesoscopic and thus 1D diffusion is faster, when compared to the normal diffusion at macroscopic antenna. For a relatively small disorder $\sigma = \sigma_1$, this rate enhancement continues to regime A but with a rate proportional to $|w|$ because the antenna grows to be macroscopic. For a larger disorder $\sigma = \sigma_2$, strong nonspecific adsorption of proteins on distant pieces of DNA slows down the search rate, when the antenna is still mesoscopic, and $\ln(J/J_s)$ decreases in regime D

faster than it does in regime B. The antenna in regime B is macroscopic and $\ln(J/J_s)$ decreases proportional to $|w|$ for both $\sigma = \sigma_1$ and $\sigma = \sigma_2$.

The crossover from the weak disorder to the strong one happens at $\sigma \sim \sigma_0 = kT[(1/2)\ln(v/Lb^2)]^{1/2}$ (see Fig. 4.2). If one plugs in the achievable experimental conditions with $L/b \sim 150$ and $v \sim L^3$, estimate of σ_0 is the order of $2kT$, which falls in the range of estimates of σ from $1kT$ to $6kT$ used in the Refs. [13, 35, 37]. Apparently σ grows for proteins with larger number of contacts with DNA and σ_0 decreases with DNA concentration. In order to identify the role of strong disorder, we look forward to more experiments dealing with relatively large concentrations of short straight DNA to guarantee that disorder strength satisfies $\sigma > \sigma_0$.

We know only one observation [8] of the peak in the coordinates of Fig. 5.4 but for a long and definitely coiled DNA for which our theory is not directly applicable. Indeed, in this paper, we concentrated on the case of relatively short and, therefore, straight DNA. In our recent paper [28], we presented a general theory including Gaussian coiled and globular DNA in the absence of disorder. In current paper, we did not touch these cases because of our prejudice that simple questions should be addressed first. We concentrated on the simplest regimes labeled A and D in figure 4a of Ref. [28] and still got rather complicated diagram Fig. 4.2 [1]. That is why we did not try to present our theory for more complicated

[1]We assume $D_3 = D_1$ in the absence of disorder. Thus with disorder, $d = D_1/D_3 < 1$ which corresponds to the case represented by the figure 4a of Ref. [28]

regimes here.

Chapter 5

Self-assembly of Virus

5.1 Introduction

A direct application of our theory on how proteins search for their targets is the kinetics of viral self-assembly. Many viruses can self-assemble from a solution of their identical capsid proteins (CPs) and genome consisting, for example, of a long single stranded (ss) RNA. For a big class of T = 3 viruses capsid proteins have long positive flexible N-terminal tails. We explore the role played by the Coulomb interaction between the N-terminal tails and negative ss RNA molecule in the kinetics of virus self-assembly. Capsid proteins stick to unassembled chain of ss RNA (antenna) and thus can slide on it towards the self-assembly site. We show that due to such one-dimensional diffusion the virus self-assembly is more than ten times faster than the case involving only three-dimensional diffusion. As

a preparation for the theory on kinetics, current chapter starts with an electrostatic theory on the viral structure. In the assembled virus, the ss RNA strongly interacts with the brush of tails rooted at the inner surface of the capsid. We show that viruses are most stable when the total length of ss RNA is close to the total length of the tails. For such a structure the absolute value of total (negative) charge of ss RNA is approximately twice larger than the charge of the capsid. This conclusion agrees with available structural data.

5.2 Electrostatic theory of viral self-assembly

Unlike living cells, viruses do not have any metabolic activity, which may mean that they are in the state of thermal equilibrium. This is one of the reasons why the statistical physics can be used for understanding of viruses. The structure of viruses is also dramatically simple. Inside the protein capsid each virus carries its genome, which consists of one or more DNA or RNA molecules and is used for reproduction in host cells. The focus of this section is on viruses with single stranded RNA (ss RNA) genomes. Detailed image reconstruction of apparently spherical viruses reveals their icosahedral symmetry. This is why such a virus capsid can be viewed as a curved two-dimensional crystal closed on itself [38, 39, 40].

Icosahedral viruses are formed from 60T CPs for only certain triangulation

number T such as 1, 3, 4, or 7, etc [41]. Here we concentrate on the viruses of the so called T = 3 class, in which a capsid is made of precisely 180 identical proteins, or of 60 triangular blocks consisting of three proteins each (see Fig. 5.1). In-vitro studies of solutions of capsid proteins and RNA molecules of a given virus show that under the biological pH and salinity they can spontaneously self-assemble into infectious viruses [42, 43, 44]. This section focuses on the energetics of this amazing protein-RNA self-assembly. In addition to hydrophobic attraction between the proteins it is driven by strong Coulomb attraction between capsid proteins and RNA molecules [40, 43]. Indeed, ss RNA is strongly negatively charged. Its backbone has one negative phosphate per nucleotide or per 0.65 nm. We denote the total ss RNA charge of a virus particle as $-Q_r$. According to Tab. 5.1 of T = 3 viruses Q_r is about several thousand in units of the proton charge. On the other hand, for many viruses their capsid proteins carry substantial net positive charge q_p, which can reach 17. The net positive charge of the capsid of a T = 3 virus $Q_c = 180q_p$ can, therefore, reach 3000. Although, in biological conditions the protein-RNA interaction is screened by monovalent salt at the Debye-Huckel screening radius r_s, attraction energy of such big charges is still very large.

A dramatic feature of the group A of T = 3 viruses collected in the upper part of Tab. 5.1 is that almost all the capsid protein charge is concentrated in the N-terminal tail located inside the capsid (Fig. 5.1). We define such an N-terminal

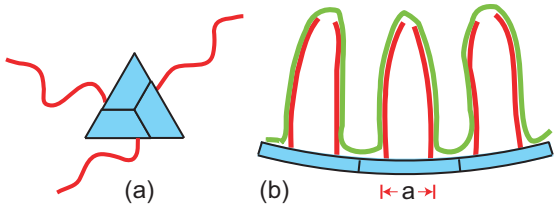

Figure 5.1: Schematic sketch of the protein capsid assembly. (a) Triangular block made of three proteins with their positive flexible N-terminal tails. (b) The brush of positive N-terminal tails rooted at the inner surface of the capsid made of triangular blocks. The ss RNA strongly interacts with the tails and keeps all the blocks together.

tail as the flexible sequence of amino acids, which starts from the N-terminus of the protein and ends at the first α-helix or β-sheet. It looks like evolution created cationic N-terminal tails for the strong interaction with ss RNA genome (Fig. 5.1b).

In this section we concentrate on the electrostatic interaction of the ss RNA with the brush of tails of a group A virus (see Fig. 5.1b). In particular we want to understand a remarkable fact that for these viruses the absolute value of the ss RNA charge Q_r is substantially larger than the total charge of the capsid $Q_c = 180q_p$. The charge inversion ratios $R = Q_r/Q_c$ for them are given in Tab. 5.1. They are scattered with the median value 1.8. This raises a challenging question whether such ratio can be obtained by minimizing free energy of the virus [45] with respect to RNA length. The positive answer to this question was recently given in the framework of the simplest model where positive protein charges are uniformly smeared on the internal surface of the capsid, while the

ss RNA is adsorbed on this surface as a negative polyelectrolyte [45]. As we see from Tab. 5.1 capsid charges of all the group A viruses are concentrated in the tails. That is why we suggest an alternative model of virus self-assembly, namely adsorption of ss RNA on a brush of flexible positive tails, rooted on a neutral surface. Minimizing the free energy of such self-assembly with respect to the total ss RNA length we arrive at the theoretical charge inversion ratios $\Re$, which are quite close to the the factual ones R.

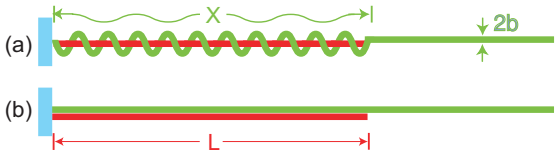

Figure 5.2: Complexes of the long ss RNA with a cationic tail rooted on the internal surface of capsid. L is the length of the tail, X is the length of RNA piece, which complexes with the tail. The structure and the magnitude of X depends on the ratio between the charge densities of the tail and the ss RNA. (a) $X > L$, when $\eta_r < 2\eta_t$; (b) $X = L$, when $\eta_r > 2\eta_t$.

We call our model a toy model because we start from the following two simplifications. (i) First, similar to Ref. [45] we neglect hydrogen bonds between ss RNA bases which lead to the secondary structure of ss RNA. (ii) Second, we assume that each tail is free (does not stick to the capsid surface). Actually for some tails, their part close to the tail root sticks to the capsid surface [41]. Only this part of the N-terminal tail is seen in the X-ray images of the crystallized viruses, while the rest of the tail is missing. Missing part of the tail strongly fluctuates and is called disordered. We call N_d the average number of amino acids in the

Table 5.1: The absolute value of ss RNA charge Q_r, the charge of the capsid protein q_p, the N-terminal tail charge q_t, the number of amino acids in the tail N_t, the ratio of the linear charge densities (in fully stretched state) of the ss RNA η_r and the tail η_t, the ratio N_d/N_t, where N_d is number of amino acids in disordered part of the tail, the actual and predicted charge inversion ratios R and $\Re$. The data are obtained from Refs. [46, 47]. In the group A most of the capsid charges are concentrated in the tails. In the group B the protein charges are large but the tails are practically neutral. In the group C the charges of both capsid proteins and tails are very small.

Virus	Q_r	q_p	q_t	N_t	$\frac{\eta_r}{\eta_t}$	$\frac{N_d}{N_t}$	R	$\Re$
Group A								
Brome Mosaic	3030	10	9	48	2.8	0.44	1.7	2.8
Cowpea Chlorotic Mottle	2980	7	9	49	2.8	0.63	2.4	2.8
Cucumber Mosaic	3214	15	12	66	2.9	0.59	1.2	2.9
Tomato Aspermy	3391	14	12	67	2.9	0.55	1.3	2.9
Nodamura	4540	13	18	52	1.5	0.79	1.9	1.8
Pariacoto	4322	13	14	47	1.8	0.61	1.8	1.9
Sesbania Mosaic	4149	6	6	57	5.0	0.89	3.8	5.0
Rice Yellow Mottle	4450	17	12	52	2.3	0.79	1.5	2.3
Southern Bean Mosaic	4136	16	14	58	2.2	0.89	1.4	2.2
Cocksfoot Mottle	4082	15	13	54	2.2	0.88	1.5	2.2
Carnation Mottle	4003	10	11	81	3.9	1.0	2.2	3.9
Tobacco Necrosis	3700	9	10	79	4.1	0.90	2.3	4.1
Tomato Bushy Stunt	4776	12	13	92	3.7	0.91	2.2	3.7
Group B								
Dengue	10735	9	1	7				
Immature Yellow Fever	10862	14	1	7				
Immature Dengue-2 prM	10703	15	1	7				
Group C								
Norwalk	7654	4	-2	28				
Native Calicivirus	7500	1	-4	26				
Bacteriophage Q Beta	4215	3	1	3				
Bacteriophage Ga	3466	3	0	3				
Bacteriophage MS2	3569	1	0	4				
Bacteriophage Fr	3575	1	0	4				
Bacteriophage Pp7	3588	1	0	3				
Bacteriophage alpha3	6087	-4	-1	8				
Turnip Yellow Mosaic	6318	0	-2	29				
Desmodium yellow mottle	6300	5	1	29				
Physalis Mottle	6673	4	-1	28				

disordered (free) part of the tail. Ratios N_d/N_t are given in Tab. 5.1. We see that on average 76% of the tail length is free. In our toy model we assume that $N_d = N_t$.

Let us first consider interaction of a homo-polymeric ss RNA with a single free cationic N-terminal tail rooted at the neutral internal surface of the capsid (Fig. 5.2a). We assume that in fully stretched state each tail has length L and the positive linear charge density η_t, while the very long ss RNA in fully stretched state has the negative linear charge density $-\eta_r$. The ss RNA piece of the length $X \geq L$ complexes with the tail. Both polymers are modelled as worm-like chains with the same radius b, which is simultaneously of the order of their bare persistence length p_0 (which does not include Coulomb self-repulsion). The third important assumption of our toy model is that (iii) the solution has a moderate salt concentration, so that $b \ll r_s \ll L$. We argue below that even this assumption does not change our results qualitatively.

Due to the strong Coulomb repulsion inside the overcharged complex, the strongly negatively charged ss RNA has a relatively large persistence length $p \sim r_s^2/p_0$ (see Refs. [48, 49, 50]), so that its Coulomb energy can be estimated as the energy of a rigid cylinder of the radius b. Same is true for the complex of the N-terminal tail and the ss RNA, which as we will see has the large negative linear charge density η^*. Self-repulsion of these negative charges makes the complex locally stretched, so that its total length equals L. Therefore, $\eta^* = (-X\eta_r +$

$L\eta_t)/L$. The tail-RNA complex with the long ss RNA shown in the Fig. 5.2a has the large electrostatic energy. Therefore, the contribution to the free energy F from configurational entropy plays a minor role and can be neglected. Since $r_s \ll L \leq X$, the Coulomb interaction is truncated at r_s. As a result, we obtain the following simple expression for the X-dependent part of the free energy

$$F(X) = L\left(\frac{-X\eta_r + L\eta_t}{L}\right)^2 \ln\left(\frac{r_s}{b}\right) - X\eta_r^2 \ln\left(\frac{r_s}{b}\right). \tag{5.1}$$

The first term represents the self-energy of the overcharged N-terminal tail (the complex), while the second term represents the loss of the electrostatic energy of the ss RNA segment with length X. Here we neglect the Coulomb repulsion between the complex and the rest of the ss RNA because $r_s \ll L, X$. Minimizing $F(X)$ with respect to X, we find the optimal $X = X_0 = (\eta_t/\eta_r + 1/2)L$, and the linear charge density of the complex $\eta^* = -\eta_r/2$ [51]. As we expected, η^* is negative, so the N-terminal tail is overcharged by the ss RNA. The above calculation is valid if ss RNA wraps around the tail (Fig. 5.2a) and, therefore, $X_0 > L$. This happens only at $\eta_r/\eta_t < 2$. On the other hand at $\eta_r/\eta_t = 2$, the length of the ss RNA segment in the complex, X_0 reaches the minimum possible value $X_0 = L$ corresponding to stretched ss RNA. At $\eta_r/\eta_t > 2$ both polymers are stretched (Fig. 5.2b) by the Coulomb self-repulsion, $X_0 = L$, and $\eta^* = \eta_t - \eta_r < -\eta_t$. Thus, at $\eta_r/\eta_t > 2$ the tail is overcharged by ss RNA more

than twice.

Until now we assumed that the ss RNA length $\mathscr{L}$ is always larger than X_0, so that X_0 does not depend on $\mathscr{L}$. Let us now imagine that we vary $\mathscr{L}$ at fixed L, η_t and η_r. Then for a short ss RNA, $\mathscr{L} < X_0$, (where X_0 is still the optimum value of X found above) the new optimum value of $X = X_{00}$ equals $\mathscr{L}$ (the N-terminal tail consumes all available ss RNA). This means that at $\mathscr{L} < X_0$ the electrostatic energy decreases with growing $\mathscr{L}$, while for $\mathscr{L} > X_0$ the energy saturates. Thus, complex of ss RNA with an N-terminal tail is most stable if $\mathscr{L} \geq X_0$.

Now we can switch from a single N-terminal tail to the whole brush of 180 tails and a very long ss RNA with the length $\mathscr{L}$ comparable to $180L$. The average distance a between two neighboring tail roots (see Fig. 5.1b) is typically close to 5 nm. We deal with r_s much smaller than a, so that complexes of the nearest neighbor tails with RNA can be treated separately. This means that long enough ss RNA goes from one tail to another consequently overcharging each of them in the way we calculated above for a single tail (Fig. 5.1b).

It is easy to show that if $\mathscr{L} < 180X_0$ ss RNA is shared between tails in equal portions $\mathscr{L}/180 < X_0$. In this case the total electrostatic energy still goes down with growing $\mathscr{L}$. (Here and below we neglect the length of ss RNA per tail necessary to connect the tail roots: it is of the order of $a/2 \ll L$. Indeed, according to Tab. 5.1 $L \sim 15$ nm, while $a/2 \sim 2.5$ nm.) On the other hand, when $\mathscr{L} > 180X_0$ and each N-terminal tail gets the length X_0 of ss RNA, the

electrostatic energy saturates at low level and does not depend on $\mathscr{L}$. At this point in order to find optimal length of ss RNA for given tails, we should recall the excluded volume interaction energy, which is smaller than the electrostatic energy, but provides the growth of the free energy with $\mathscr{L}$ at $\mathscr{L} > 180X_0$. Indeed, one should take into account that due to screening the persistence length of the tail-RNA complex is much smaller than the tail length L and the tail-RNA "arches" are not extended as shown in Fig. 5.1b, but rather tend to make coils. This leads to a noticeable excluded volume interaction. Thus, for given tails the free energy reaches minimum at $\mathscr{L} \simeq 180X_0$. (Similar minimum was obtained earlier for the model of protein charges uniformly smeared on the internal capsid surface [45].) For the theoretical charge inversion ratio $\Re$ we arrive at

$$\Re = \frac{X_0\eta_r}{L\eta_t} = \begin{cases} 1 + \eta_r/(2\eta_t), & \text{when} \quad \eta_r < 2\eta_t \\ \eta_r/\eta_t, & \text{when} \quad \eta_r > 2\eta_t \end{cases} . \tag{5.2}$$

In Tab. 5.1 we calculated the ratio η_r/η_t for the group A viruses using 0.65 nm for the distance between two charges of ss RNA and 0.34 nm for a length of the tail per amino acid. We see that for the most of the viruses $\eta_r/\eta_t \geq 2$ and, therefore, ss RNA is stretched along the N-terminal tails (Fig. 5.1b), so that a simple way to formulate our results for the length of ss RNA is to say that the total length of ss RNA $\mathscr{L}$ is equal to the total length of the tails $180L$. Substituting values of

η_r/η_t from Tab. 5.1 in Eq. (5.2) we arrived at values of $\Re$ listed in Tab. 5.1. We see that most of them are in reasonable agreement with the structural data [53].

This agreement may be interpreted as a result of natural evolution of viruses in the direction of the maximum viral stability. It is desirable, however, to design an in vitro experiment, which verifies our predictions. Before suggesting such experiment let us note that although above we discussed only packaging of a single ss RNA molecule in a virus, our conclusions can be extended to the case, where many shorter ss RNA pieces are packaged in the virus. They just continue each other inside the virus and bind proteins together. Our predictions, therefore, can be verified by experiments with a solution of relatively short homo-polymeric ss RNA with the length $\mathscr{L}$ in the range $2L < \mathscr{L} \ll 180L$. We suggest an equilibrium experiment with a series of solutions, which have a varying ratio ρ of the total charges of short ss RNA and capsid capsid proteins. At $\rho \simeq 1$ in equilibrium all ss RNA molecules are used up in viruses, so that there is no free ss RNA. With growing ρ free ss RNA should appear at the critical point $\rho = \rho_c = \Re$, where, according to our theory, free ss RNA molecules and ss RNA molecules inside the virus are in equilibrium. Using short ss RNA permits to vary amount of ss RNA in a virus almost continuously in order to find ρ_c and compare it with $\Re$.

Let us now discuss the assumptions (i), (ii) and (iii) of our toy model, starting from the assumption (ii), that one can treat the N-terminal tail with a part of it

sticking to the internal capsid surface as a free tail. The picture of RNA going along the one side of the tail without wrapping does not seem to be too sensitive to the fact that the other side of the tail sticks to the capsid. This, (together with the fact that in average only 24% of the tail length sticks to the capsid surface) makes (ii) reasonable. The assumption (iii) is more problematic because biological values of $r_s \sim b \sim 1$ nm. They easily satisfy inequalities $r_s \ll L, a$, but do not literally satisfy assumption that $r_s \gg b$. This assumption was important in order to say that ss RNA and N-terminal tail-RNA complex are stretched and the Coulomb energy dominates the configuration entropy. We argue here that according to numerical simulations [50] for a very flexible polyelectrolyte (with the bare persistence length equal to the Bjerrum length) even for such a small r_s the Coulomb interaction plays a strong role: its persistence length grows three times already at $r_s = 1$ nm. For less flexible polyelectrolyte such as ss RNA or the tail-RNA complex the Coulomb interaction should play even stronger role so that for zero order approximation the configuration of the complex shown in Fig. 5.2b is reasonable. The assumption (i) that ss RNA behaves as a flexible linear polyelectrolyte is not necessary for a homo-polymeric ss RNA or a generic linear polyelectrolyte used for virus self-assembly in-vitro [43]. On the other hand, for the viral ss RNA, the energy of hydrogen bonds should be optimized together with the electrostatic energy. It seems that effect of such global optimization will not differ much from our result, but this remains to be shown.

Up to now we have dealt with the group A. In the group B charges of the capsid proteins are large but tails are practically neutral so that the theory of Ref. [45] is appropriate. In the group C the charges of proteins and tails are very small but it is possible that for some viruses the internal surface of capsid proteins is positively charged, while the negative charges are on the external surface [54]. In this case, one may also redefine R as ratio of ss RNA charge to the total charge of the internal surface of the capsid and use Ref. [45] to estimate R.

In this section we focused on T=3 viruses, because they attract most of physicists attention [40, 45, 55]. As we saw many of their capsid proteins have long positive tails. Capsid proteins of some T=1, 4 and 7 viruses also have positively charged tails. Our theory is applicable to them as well. Detailed analysis of these classes is beyond scope of this section.

In conclusion, the data [46, 47] show that there is a big group of viruses, where practically all positive charges of a capsid protein are concentrated in a long and flexible N-terminal tail. For a given length and charge of the tail we optimized the length of the ss RNA genome by searching for minimum of free energy of the virus. We arrived at the very simple result that a virus is most stable when the total length of ss RNA is close to the total length of the tails. This result is in reasonable agreement with the viral structural data [46, 47]. This may be interpreted as a result of evolution in the direction of viral stability.

5.3 Kinetics of viral self-assembly

In this section we continue to deal with electrostatic interaction of N-terminal tails and ss RNA, but switch our attention from the thermodynamics to the kinetics of in vitro self-assembly. Most of papers on in vitro kinetics study self-assembly of an empty capsid at much higher than biological concentrations of salt, where the Coulomb repulsion of capsid proteins is screened and hydrophobic interactions dominate [56, 57]. In Ref. [57] one can clearly discriminate the initial nucleation "lag phase", followed by the "growth phase", where the average mass of the assembled particles linearly grows with time. The recent study of the kinetics of self-assembly with ss RNA genome emphasizes that CPs stick to ss RNA before the assembly [58, 59], so that a virus is assembled actually from the linear CP-RNA complex. Not much is known about the nucleation and growth phases of such assembly.

The goal of this section is to understand the role of the large length of ss RNA in kinetics of self-assembly at biological salt concentrations. We assume that after nucleation (for example, at one end of ss RNA) the capsid growth is limited by CP diffusion. We calculate the acceleration of self-assembly, which originates from the fact that due to the Coulomb interaction of N-terminal tails with ss RNA, CPs stick to ss RNA and slide on it to the assembly site. In this case, ss RNA plays the role of a large antenna capturing CPs from the solution

and leading them to the assembly site. Figure 5.3b illustrates this process. We show below that for a T=3 virus this mechanism can accelerate self-assembly by approximately 15 times.

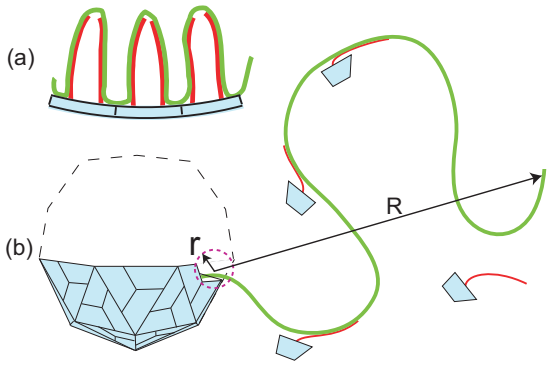

Figure 5.3: (a) A blowup view from the inside of the virus. The brush of positive N-terminal tails (dark gray line) is rooted at the inner surface of the capsid (light gray block). The ss RNA (gray line) strongly interacts with the tails and glues all the CPs together. (b) Schematic model of the capsid self-assembly. The unassembled ss RNA makes an antenna of size R for the one-dimensional pathway of the CPs towards the capsid assembly site at the capsid fragment (dashed circle with radius r of the size of a CP.

We consider a dilute solution of virus CPs with molecules of its ss RNA genome. For the most of this section we assume that concentrations of the protein $c \sim 2Mc_R$, where c_R is the concentration of ss RNA and M is the number of proteins in the assembled virus (for T=3 viruses $M = 60\mathrm{T} = 180$). In this case there are enough proteins in the system in order to assemble the virus around each ss RNA molecule and c changes weakly in the course of assembly. Viruses, however, self-assemble only when the concentration c of CP is larger than some threshold concentration c_1 [45], which is similar to the critical micelle concentration for the

self-assembly of surfactant molecules [60]. The critical concentration c_1 can be estimated as

$$c_1 \approx \frac{1}{v} \exp[-(\epsilon_e + \epsilon_p)/k_B T], \tag{5.3}$$

where v is the CP volume, ϵ_e is the absolute value of the electrostatic adsorption energy of the CP N-terminal tail to ss RNA, and ϵ_p is the absolute value of the CP-CP attraction energy in the capsid (per CP). Both ϵ_e and ϵ_p can be of the order of 10 $k_B T$, so that the critical concentration c_1 can be very small. In this section we always assume that $c \gg c_1$. As shown in Ref. [61], in a partially assembled capsid, CP sticks to a piece of ss RNA of the length equal to the tail length L (Fig. 5.3a). A partially assembled capsid with $m < M$ CPs encapsulates the length mL of ss RNA . To continue this process the next $(m+1)$th CP should attach itself to the partially assembled capsid at the site, where ss RNA goes out of the capsid (see Fig. 5.3b) and this CP gets more nearest neighbors. We call this slowly moving site "the assembly site". It has the size of the order of the size r of CP (see Fig. 5.3b).

CPs diffuse to the assembly site through the bulk water. For $c \gg c_1$ one can neglect the dissociation flux from the assembly site. In this case the net rate of assembly (the number of CP joining the capsid per unit time) is equal to the rate at which diffusing CP find the absorbing sphere with the radius r. It is equal to

the Smoluchowski three-dimensional reaction rate [1]

$$J_3 = 4\pi D_3 r c, \tag{5.4}$$

where D_3 is the diffusion coefficient of CP in water. The rate J_3 as a function of CP concentration c is plotted in Fig. 5.4 by the dashed straight line.

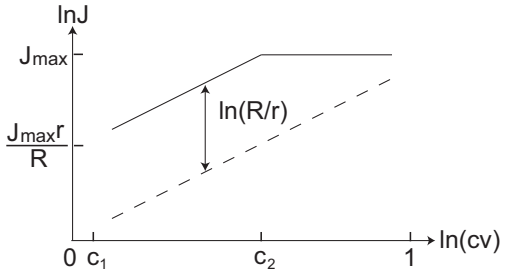

Figure 5.4: Schematic plot of the diffusion limited self-assembly rate J as a function of the protein concentration c. The full line is for the sliding of capsid proteins on ss RNA. The rate for the slower three-dimensional diffusion is shown by the dashed line.

Our main idea is that the long chain of yet unassembled ss RNA outside of the capsid provides an additional route for the diffusion of CPs to the assembly site, in analogy to the well-known faster-than-diffusion locating of the specific site on DNA for a protein [7, 11, 12, 13, 28]. The dramatic enhancement of the assembly rate is achieved because, due to the Boltzmann factor $\exp[\epsilon_e/k_BT]$, the three dimensional concentration of CP on unassembled chain of ss RNA is larger than the bulk concentration c. This concentration can be estimated using the cylinder with cross-section $v^{2/3}$ build around RNA as the axis: it is equal to the

number of CPs per unit length of ss RNA divided by $v^{2/3}$. At large distances the one-dimensional flux of CP sliding on the ss RNA should be balanced by the three dimensional diffusion flux of CP to the ss RNA. This balance determines the radius ξ of the sphere around the assembly site at which two fluxes match each other and the crossover between three-dimensional and one-dimensional diffusions of CP takes place. The ss RNA coil inside this radius is called antenna.

The maximum possible antenna size is the characteristic size $R \sim (p\mathscr{L}_e)^{1/2}$ of the unassembled portion of ss RNA with length $\mathscr{L}_e = \mathscr{L} - mL$. (Here we assume the ss RNA is a flexible Gaussian coil with the persistence length $p \sim 2b \sim 1.5$ nm, where $b \simeq 0.7$ nm is the monomer size, and do not account for the excluded volume interaction.) In the case when $\xi = R$, the whole ss RNA adsorbs CPs arriving by three-dimensional diffusion and provides a path of fast one-dimensional diffusion to the assembly site (See Fig. 5.3). As a result, in this case the size R replaces the protein size r in Eq. (5.4) leading to a much faster rate

$$J = 4\pi D_3 R c, \tag{5.5}$$

which is shown in Fig. 5.4 by the part of the solid line parallel to the dashed one. Equation (5.5) is correct until CPs adsorbed on the unassembled chain of ss RNA are still sparse and do not block each other's diffusion on ss RNA. Let us use the notation c_2 for the concentration c, where the antenna becomes saturated by CPs

and the dependence of the self-assembly rate J on c saturates roughly speaking at the level $J_{max} = 4\pi D_3 r/v$, which is the Smoluchowski rate J_3 at $c \sim 1/v$ (see the solid line in Fig. 5.4). It was shown in Ref. [28] that if $\xi \leq R$

$$c_2 = \frac{1}{v} \exp[-\epsilon_e/k_B T] \approx c_1 \exp[\epsilon_p/k_B T]. \tag{5.6}$$

We see that the largest enhancement R/r of the self-assembly rate J can be achieved in the range of relatively small CP concentrations $c_1 \ll c \ll c_2$. For a typical T=3 virus the ss RNA genome consists of 3000 bases, so that the length $\mathscr{L} \sim 2100$ nm and $R \sim 60$ nm. Using $r \sim 4$ nm, we arrive at the acceleration factor $R/r \sim 15$. One can calculate the assembly time τ_a limited by diffusion. As we said above for $c \sim 2Mc_R$, the concentration of proteins c can be regarded as a constant. Thus, the assembly time with the help of antenna τ_a is given by

$$\tau_a \approx \int_0^M \frac{dm}{4\pi c D_3 [(M-m)Lp]^{1/2}} = \frac{2M^{1/2}}{4\pi c D_3 (Lp)^{1/2}}, \tag{5.7}$$

while according to Eq. (5.4), the assembly time without antenna is simply $\tau_0 = M/(4\pi c D_3 r)$. Since $(Lp)^{1/2} \sim 4$ nm, we can neglect the difference between $(Lp)^{1/2}$ and r, and arrive at the assembly time with the help of antenna $M^{1/2} \approx 14$ times shorter than τ_0.

Strictly speaking, these estimates are correct only for self-assembly with a

homopolymeric ss RNA or a synthetic negative polyelectrolyte [43]. For these cases, a small additional acceleration by a factor 2 or 3 can be provided by the excluded volume effect. On the other hand, the native ss RNA is more compact than gaussian one due to hydrogen bonds forming hairpins and thus the estimated acceleration rate can be reduced by a factor between 2 or 3. Above we for simplicity replaced ξ by its maximum value R. The actual calculation of the antenna size ξ can follow the logic of the scaling estimate for the search rate of the specific site on DNA by a protein in Ref. [28]. In our case, the assembly site plays the role of the target site (diffusion sink) for the protein, the unassembled chain of ss RNA plays the role of DNA and the Coulomb attraction energy of N-terminal tails to the unassembled ss RNA is analogous to the non-specific binding energy of diffusing protein on DNA. One may argue that the virus self-assembly problem is different, because ss RNA plays a dual role. It is not only an antenna for the sliding CPs, but ss RNA itself also moves to the assembly site, where it gets packed inside the capsid (each newly assembled CP consumes the length L of ss RNA). However, for a small concentration c in the range $c_1 \ll c \ll c_2$, where the unassembled ss RNA chain is weakly covered by CPs, the velocity of ss RNA drift in the direction of assembly site is much smaller than the average velocity of CP drift along ss RNA. Thus, for the calculation of the assembly rate at a given length of the unassembled ss RNA chain we can use the approximation of static ss RNA. This brings us back to the problem of proteins searching for the specific

site on DNA [28]. Note that this means that the idea of self-assembly from the prepared linear ss RNA-protein complex [58, 59] is literally correct only at $c > c_2$.

It is shown in Ref. [28] that for a flexible ss RNA, the antenna size reads $\xi \sim b(yd)^{1/3}$, where $y = \exp(\epsilon_e/k_BT)$, $d = D_1/D_3$ and D_1 is the one-dimensional diffusion coefficient of the protein sliding on ss RNA. This result remains correct as long as the antenna size ξ is smaller than the ss RNA coil size R. The energy ϵ_e of adsorption of the N-terminal tail with approximately 10 positive charges on ss RNA can be as large as $10k_BT$. For $d = 1$ we get $\xi \sim 30$ nm, while $R \sim 60$ nm. Thus, a simple estimate leads to the antenna length ξ somewhat smaller than R.

There are, however, two reasons why ξ may easily reach its maximum value R. First, some viruses self-assemble from dimers [57, 59]. Naturally dimers with their two positive tails bind to ss RNA with the twice larger energy $2\epsilon_e$. This easily makes $\xi > R$. ii) The theory of Ref. [28] assumes that a sliding protein molecule has only one positive patch, where it can be attached to a double helix DNA. Even if two distant along the chain pieces of DNA come close in the three-dimensional space, such protein can not simultaneously bind both pieces and, therefore, can not crawl between them without desorbing to water and losing the binding energy $-\epsilon_e$. For a globular protein this is quite a natural assumption. On the other hand, for CP attached to ss RNA by a flexible N-terminal tail, the tail can easily cross over (crawl) between the two adjacent pieces of the same ss RNA molecule losing only small fraction of the energy $-\epsilon_e$. This should lead to

faster protein diffusion on ss RNA and may easily push ξ up to R.

Let us discuss ideas of three in vitro experiments, which can verify the role of ss RNA antenna in virus self-assembly. In the first experiment, one breaks ss RNA molecule into $K \gg 1$ short pieces of approximately equal length. It was shown [62, 63] that the assembly is possible even when $K \sim M/2$, because in order to glue CPs short ss RNA should bind two N-terminal tails of neighboring proteins in the capsid. Virus assembly from short ss RNA pieces goes consecutively through two different diffusion limited stages. In the first stage, capsid fragments (CFs) made of M/K proteins self-assemble on each short ss RNA molecule. According to Eq. 5.7, the time necessary for this stage is proportional to $(M/K)^{1/2}$ and is much shorter than the assembly time τ_a with the intact ss RNA. The second stage, where CFs aggregate to form the whole capsid takes much larger time τ_{as} (s stands for short). In order to calculate τ_{as} we assume that when two CFs with n CPs each collide, they can relatively fast rearrange their ss RNA and CPs in order to make one bigger CF with $2n$ CPs. We also assume that at any time t all CFs are approximately of the same size $n(t)$. Then the concentration of such CFs is $c(n) = c_R M/n(t)$, where c_R is the concentration of original intact ss RNA. Therefore, the time required for doubling of a CF can be estimated from Eq. (5.4)

$$\tau(n) = \frac{1}{4\pi D_3(n) r(n) c(n)} = \frac{n}{4\pi D_3(n) r(n) c_R M}, \tag{5.8}$$

where $D_3(n)$ and $r(n)$ are diffusion coefficient and effective radius of a CF with n CPs. Since the diffusion coefficient is inversely proportional to the droplet radius, the product $D_3(n)r(n) = k_BT/6\pi\eta$, (where η is the water viscosity), is the same constant as D_3r for a single protein. One collision of droplets transfers n CPs to the growing CF. Therefore, the average time needed to add one CP to the growing CF $\tau_1 = \tau(n)/n = 1/4\pi D_3 r M c_R$ does not depend on n. In other words, the number $n(t)$ of CP per CF increases at a constant rate. The assembly ends when n reaches M. Therefore, the assembly time is given by

$$\tau_{as} \simeq M\tau_1 \simeq \frac{1}{4\pi c_R D_3 r}. \tag{5.9}$$

Above equation shows the assembly time depends on Mc_R which stands for the concentration of CP involved in the CF aggregation. However τ_{as} has no dependence on K. Comparing Eqs. 5.7 and 5.9, we obtain that at $c \sim 2Mc_R$

$$\frac{\tau_{as}}{\tau_a} \sim M^{1/2}\frac{(Lp)^{1/2}}{r} \sim M^{1/2} \gg 1. \tag{5.10}$$

We see that the virus assembly time with short ss RNA pieces is much larger than that for the intact ss RNA. This happens due to the breaking of big antenna of the original ss RNA.

In the second experiment, we return to the intact ss RNA and discuss what

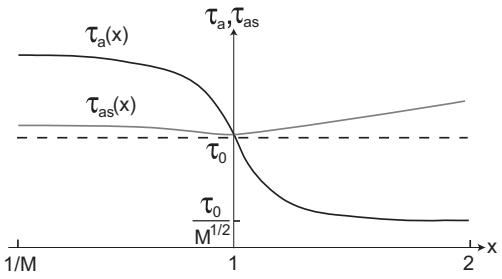

Figure 5.5: Self-assembly times plotted schematically as a function of $x = c/Mc_R$. $\tau_0 = M/(4\pi c D_3 r)$ is the assembly time without the effect of ss RNA at $x > 1$. The dark and gray lines correspond to intact ss RNA and short RNA pieces respectively.

happens when we vary relative concentrations of CP and ss RNA $x = c/Mc_R$, for example, keeping $c = const$ and changing c_R. Until now we assumed that $x \sim 2$, i.e. we have marginally more proteins than it is necessary to assemble a virus at every ss RNA. If $x \gg 1$ the assembly time τ_a is practically the same as that at $x \sim 2$ and is given by Eq. 5.7. Let us now consider much larger c_R, for which $x \ll 1$. Here situation changes dramatically. There are two assembly stages. In the first stage, a CF is assembled with part of each ss RNA molecule, leaving the rest of the ss RNA molecule as a tail. This assembly uses up all the proteins and stops, when all CFs are still much smaller than the complete capsid and their ss RNA tails are long (see, for example, Fig. 5.3b). This state is essentially a kinetic trap. If energies ϵ_e and ϵ_p are much larger than $k_B T$, CFs on different ss RNA molecules can not exchange CPs trough the solution or via collision of their ss RNA tails. They can grow only via CF-CF collisions, while merging on one ss RNA and releasing the other empty one. We explained above, at $x > 1$

(CPs are in excess), CFs without RNA tails produce a capsid during time given by Eq. 5.9. On the other hand, at $x < 1$, only occupied by CP ss RNA molecules take part in the aggregation and in order to get the assembly time, c_R in Eq. 5.9 should be replaced by c/M, which does not depend on x. However, due to the long ss RNA tail, a CF diffuses slower than it does without a tail. The time $\tau_a(x)$ grows substantially with decreasing x, because with more ss RNA, the initial CFs have fewer CPs and longer ss RNA tails. This time saturates at $x \sim 1/M$, where $c = c_R$ and each CF has only one protein and the longest ss RNA tail. Thus, a long antenna accelerates assembly at $x > 1$ and decelerates it at $x < 1$. This behavior of $\tau_a(x)$ is schematically plotted in Fig. 5.5.

In the third experiment we can combine the first two and break ss RNA into pieces at several different values of x. At $x < 1$ a CF gets a shorter tail of ss RNA and larger mobility, so that assembly is faster than for intact ss RNA. When $x > 1$, the assembly time grows according to Eq. (5.9) with decreasing c_R (increasing x). This is because the smaller the ss RNA concentration, the harder for the CFs to collide with each other and form larger CFs. In other words, kinetics is determined only by CPs already assembled in CFs and their number decreases with growing x. We illustrate such nontrivial role of broken ss RNA in Fig. 5.5.

Now let us give some numerical estimates for c_1, c_2 and τ_0 for the in vitro assembly. Using the radius of CP $r \sim 4$ nm, we obtain $c_1 \sim 0.1$ nM and $c_2 \sim 1$

μM from Eqs. (5.3) and (5.6). For $c \sim 1$ nM and the diffusion coefficient $D_3 \sim 2 \times 10^{-7}\text{cm}^2/\text{s}$, the assembly time τ_0 is about 10 min. At excess of CP, ss RNA antenna reduces it to $\tau_a \sim 1$ min. At excess of ss RNA roughly speaking τ_a increases to $2\tau_0$. One can make τ_a even larger using much longer than native ss RNA.

In conclusion, we studied the role played by unassembled tail of ss RNA, which we call antenna. We showed that one-dimensional diffusion accelerates the virus self-assembly more than ten times when proteins are in excess with respect to RNA. On the other hand when RNA is in excess long tail of ss RNA slows down the assembly. We discussed several experiments which can verify the role of antenna. Although in this section we focus on viruses for which CPs have long positive N-terminal tails, our idea can be also applied to the case where a CP binds to ss RNA by its positive patch. Our ideas are applicable beyond icosahedral viruses, for example, to the assembly of immature retro-viruses such as RSV or HIV [58, 62, 63].

Chapter 6

Macroscopic Diffusion and Effective Conductivity

6.1 Introduction

Equilibrium and transport properties of composites are of great interest because of their importance both in nature and technology. One usually wants to characterize the composite macroscopically, determining its effective properties such as conductivity, dielectric constant, magnetic permeability etc., in terms of properties of the respective constituents. Most of the theoretical literature on this subject dealt with spherical (or single scale) inclusions [64, 65, 66, 67, 68, 69, 70]. At the same time, Monte-Carlo simulations and experiments reveal[71, 72, 73, 74, 75, 76, 77] that elongated, needle or stick like inclusions, can be very effective in modifying

the properties of materials even at small volume fractions. For example, composites made of metallic wires with aspect ratio $a/l \ll 1$ (a is the radius of the wire and l is its length) immersed in a good insulator exhibit record values of the dielectric constant [78]. The transport properties of such composites were studied in many works [71, 74, 75, 76]. A comprehensive review of these works and a thorough study of the dielectric response of conducting stick composites can be found in Ref. [78], but only in the asymptotic regime of very large conductivity of wires.

Recently, another system attracted a lot of attention. It consists of carbon nanotubes dispersed in ceramic or plastic material. It was shown that nanotubes can greatly enhance the electrical and thermal conductivities of the material [74, 79, 80, 81, 82, 83].

In this chapter we present scaling theory of the macroscopic conductivity σ of the suspension of well conducting wires with conductivity σ_1 in poorly conducting medium with a finite conductivity $\sigma_2 \ll \sigma_1$. The wires can be rigid sticks or flexible and coiled like conducting polymers. We imagine that they are dispersed, randomly oriented and frozen in the medium.

On the first glance, the problem of macroscopic conductivity of the composite seems to belong to the realm of percolation [69]. Indeed, this would be true for the conducting wires in perfectly insulating medium, $\sigma_2 = 0$, where macroscopic conductivity could only be realized through the direct contacts between wires. In

this chapter, we are interested in a different problem - we assume that the medium does conduct, $\sigma_2 \neq 0$, albeit poorly ($\sigma_2 \ll \sigma_1$). In this case, although overall macroscopic current is carried mostly along the wires, it is still able to switch from wire to wire through the medium, depending on the random disordered configuration of the wires. Accordingly, we mostly consider volume fraction of wires ϕ to be not only small $\phi \ll 1$, but actually smaller than the corresponding percolation threshold $\phi \sim a/l$, such that the direct contacts between wires are rare and completely negligible. We show later how our results properly cross over to that of percolation at larger ϕ.

For very dilute system of wires, when the distance between wires is much larger than the length of the wire, the effective conductivity σ is trivially close to the conductivity of the medium σ_2. We therefore mostly deal with larger concentrations with $\phi > a^2/l^2$ where the spheres containing each wire strongly overlap (see Fig. 6.1). In the parlance of polymer science, we study the *semidilute* system [14] of wires. In terms of increasing concentration, our theory continues as long as there remains enough room to distribute wires isotropically. We show that although ϕ is small in semi-dilute system of wires, macroscopic conductivity σ is dramatically enhanced when compared to σ_2.

The useful image to think about is a single typical current line in the system. It follows inside one wire for a long distance and then bridges to a neighboring wire over a more-or-less narrow gap in the medium, and then continues again

in the wire for a long distance. We denote λ the length scale of one continuous stretch of current line in one wire, it can be called *correlation* length. This is the key concept of the chapter. With the increase of wire conductivity σ_1, the correlation length λ increases, and so does macroscopic conductivity σ, until λ gets as large as the wire length l, then macroscopic conductivity σ saturates at values independent on σ_1. Remarkably, for flexible wires there are wide scaling regimes, where $\sigma \propto (\sigma_1\sigma_2)^{1/2}$. Such dependence is known for a narrow vicinity of percolation threshold in two dimensional isotropic mixtures [64, 65] but, to the best of our knowledge, has never been claimed for a broad range of parameters.

Our theory of effective conductivity of composites can be easily applied to a completely different problem, for which the meaning of the correlation length λ is particularly obvious. Namely, we speak of diffusion of proteins through the semi-dilute system of dsDNA molecules. Many proteins have positively charged domains on their surfaces, which provide for nonspecific attraction to the negatively charged surface of the double helical DNA. Such proteins stick to DNA and diffuse along DNA for some time, then get desorbed and wander in 3D, then get adsorbed for another tour of 1D diffusion, and so on. These phenomena are believed to be behind the ability of proteins to locate their specific functional targets on DNA faster than simple 3D diffusion [6, 7, 28, 84]. As regards macroscopic diffusion of proteins through semi-dilute DNA solution, we show later in this chapter that this problem can be easily reduced to that of conductivity in

the composite with nanowires. As a result, Fig. 6.2, part of Figs. 6.3 and 6.4 (which is redrawn in the Fig. 6.5) can all be understood in terms of macroscopic diffusion if one uses translation keys provided in the captions of these figures. The results are also summarized in Table 6.1. Clearly, in the case of protein diffusion λ is the length of one tour of protein diffusion along DNA (including episodes of activated desorbtion if they are followed by correlated re-adsorbtion).

Our results are presented by the "phase diagrams" in the log-log plane of parameters ϕ vs. $s = \sigma_1/\sigma_2$ shown in Figs. 6.2, 6.3 and 6.4. They specify scaling regimes of different power laws formulae for σ listed in the Table 6.1. Relatively simple phase diagram of Fig. 6.2 presents results for straight wires, while more complicated phase diagrams of Figs. 6.3 and 6.4 are constructed for semi-flexible wires characterized by a large persistence length p, such that $a \ll p \ll l$.

The plan of this chapter is as follows. In section 6.2 we first consider the relatively simple case when each wire is straight. In this situation we explain the main idea of our theory and identify several scaling regimes. We then consider a more complicated case when wires are flexible and coiled (section 6.3). We continue in section 6.4 by using these results for the macroscopic diffusion constant of proteins in semidilute DNA system. Finally, we conclude with the discussion of other possible applications of our work (section 6.5).

In this chapter restrict ourselves to scaling approximation for the conductivity and to delineating the corresponding scaling regimes. In our scaling theory, we

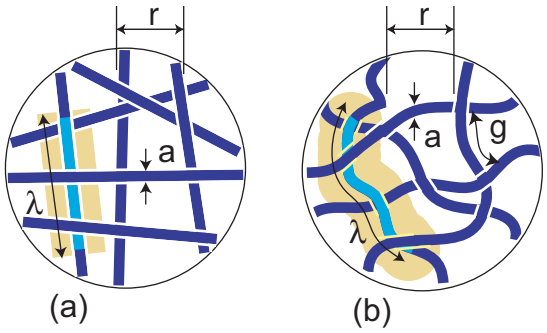

Figure 6.1: Local view of the semidilute solutions of wires. The correlation length along the wire is shown in lighter color than the rest of the network. The conducting channel is shadowed. In a), wires are straight sticks. In b), wires are flexible Gaussian coils. If the mesh size is not longer than persistence length, so the wire within each mesh is essentially straight. At lesser density, the mesh size is longer than the persistence length, and then the wire in the mesh would be wiggly.

drop away both all numerical factors and, moreover, also all logarithmic factors, which do exist in the problem, because it deals with strongly elongated cylinders.

6.2 Straight wires

In this section, we concentrate on the system of straight well conducting sticks, such as, e.g., carbon nanotubes, suspended in the medium of lower conductivity - see Figure 6.1a. First of all let us note that percolation through the wires and the direct contacts where wires touch each other starts in such system when volume fraction of wires exceeds a critical value which is of the order of $\phi \sim a/l$ (see Ref. [74, 76]). It is not a coincidence that at about the same concentration it becomes

impossible to place wires randomly and isotropically [85] - both percolation and nematic ordering occur at the concentration at which there are on average about two contacts per each stick.

As stated in the introduction, we consider the range of concentrations $a^2/l^2 < \phi < a/l$. Only in the very end we comment on the role of percolation in our system. As long as $\phi \ll a/l$ wires are still oriented isotropically and the contacts of wires can still be neglected, i.e., we are below percolation threshold; the latter means that overall macroscopic conductivity is entirely due to the fact that the medium does conduct, $\sigma_2 \neq 0$, albeit maybe not too well. On the other hand, the spheres containing wires already overlap strongly ($\phi > a^2/l^2$). The latter condition means that we deal with semidilute solution of sticks - the system that locally looks like a network with certain mesh size r (see Figure 6.1a). In the scaling sense, r is the same as the characteristic radius of density-density correlation function, and can be estimated by noticing that one stick within one mesh makes density about $\sim ra^2/r^3 \sim \phi$, therefore $r \sim a\phi^{-1/2}$.

Let us start with the simplest case when σ_1 is not significantly larger than σ_2. Then current basically has no incentive to concentrate into the wires, instead it flows all over the place, and effective conductivity is simply that of the medium:

$$\sigma \simeq \sigma_2 \ . \qquad \text{(regime A)} \tag{6.1}$$

In the diagram Figure 6.2, this regime is denoted as A.

It is also quite easy to find perturbative corrections to the result Eq. (6.1) assuming small "conductivity contrast" $(\sigma_1/\sigma_2) - 1 \ll 1$. In this case $\sigma \simeq \sigma_2 + (\sigma_1 - \sigma_2)\phi$, which follows from the fact that to the first order in perturbation the current lines remain unaffected by the difference between σ_1 and σ_2, they remain parallel straight lines (assuming for simplicity the simplest geometry of a uniform current field), and each of them runs through σ_1 material instead of σ_2 over the fraction ϕ of its length. This perturbative result suggests that regime A continues as long as $\sigma_1\phi \ll \sigma_2$.

Let us now switch to the more challenging case, when σ_1 is so much larger than σ_2 that the current is mostly carried by the wires. To imagine the flow of current through the composite material in this case, it is useful to think of a single current line. As stated in the introduction, such line typically consists of long stretches along one wire followed by relatively short switches from wire to wire, and the important parameter is the typical length over which current line follows inside one wire, we denote it as λ.

Our plan is to consider λ as a variational parameter. That means, we first imagine the current distribution at some given value of λ, determine the resistance (or conductance) of the macroscopic sample as a function of λ, and then try to optimize λ accordingly. The justification of this procedure comes from the fact that all parts of our material obey linear Ohm's law (linear response theory), so

that the requirement of minimal dissipation, or maximal overall conductance, is mathematically exactly equivalent to the Kirchoff's laws determining distribution of currents in the network of resistors [86].

To begin with, let us consider the most interesting case when λ is much shorter than total length of one wire, but still larger than the mesh size r: $r \ll \lambda \ll l$. Consider then a cube of the size about λ inside our macroscopic sample. On the one hand, overall conductivity on the scale of this cube is already about the same as that of a macroscopic body, we denote it σ; the resistance of one λ-size cube is, in other words, about $1/\lambda\sigma$. On the other hand, we can estimate this resistance considering wires inside the cube. There are about $\lambda^3/\lambda r^2$ of the wires crossing the cube, because the distance between wires is about r and, therefore, each wire can be thought of as dressed in a sleeve of the thickness about r and volume about λr^2 (see Fig. 6.1a). The sleeve can be thought of as a weakly leaking insulation for the wire. Each piece of the sleeve of the length about r bridges given wire to another one through the resistance about $r/\sigma_2 r^2$, and about λ/r such bridges are connected in parallel, yielding overall resistance connecting the given wire as $(1/\sigma_2 r)(r/\lambda) = 1/\sigma_2\lambda$. This is connected in series with the wire itself, producing a conducting channel with resistance $\lambda/a^2\sigma_1 + 1/\sigma_2\lambda$. Since all (or sizeable fraction of all) λ^2/r^2 conducting channels in the cube are in parallel, we finally arrive at the cube resistance as $(r^2/\lambda^2)\,(\lambda/a^2\sigma_1 + 1/\sigma_2\lambda)$. Equating this to $1/\lambda\sigma$, we arrive

at the following estimate of effective macroscopic conductivity

$$\sigma \sim \frac{a^2/r^2}{1/\sigma_1 + a^2/\sigma_2\lambda^2} \ . \tag{6.2}$$

Let us now analyze this result. As a function of λ, macroscopic conductivity does not appear to have maximum at any finite λ. This does not necessarily mean that λ is going to increase *ad infinum*; rather, it suggests that more accurate calculation is required to determine λ. Luckily, such more accurate calculation is not necessary to determine the quantity of our interest - macroscopic conductivity σ. Indeed, as soon as λ exceeds certain threshold, namely

$$\lambda > a\sqrt{\sigma_1/\sigma_2} \ , \tag{6.3}$$

the second term in denominator of formula (6.2), which describes resistance of wire-to-wire bridges, becomes subdominant, and must be neglected within the accuracy of our scaling estimates. This yields

$$\sigma \simeq \sigma_1\phi \ . \qquad \text{(regime B)} \tag{6.4}$$

As expected, regimes A and B cross over smoothly on the line $\sigma_1/\sigma_2 \sim \phi$.

In the regime B, macroscopic conductivity does not depend on σ_2, conductivity of the medium. This happens because σ_1/σ_2 is so large that current mostly flows

through the wires, but at the same time σ_1 is not large enough to make resistance of wires insignificant and thus unmask the resistances of narrow gaps between wires. This is also why the resulting macroscopic conductivity is in this regime insensitive to the exact value of λ: overall distance travelled by any particular line of current through the wires scales simply as the sample size and, to the scaling accuracy, does not depend on how frequently current switches from wire to wire - precisely because wires are straight.

To complete our analysis of the regime B, let us note that the quantity $a\sqrt{\sigma_1/\sigma_2}$ which appears in the formula (6.3) can be understood in the following way. Imagine one straight wire in an infinite medium, and suppose we somehow feed current into a certain point 0 of this wire. Current will flow away from 0, mostly along the wire, but also slightly leaking into the environment. Due to this leaking the current remaining in the wire will decay exponentially as we move away from 0, with the decay length equal to $a\sqrt{\sigma_1/\sigma_2}$. Indeed, the length of current decay for a single wire is estimated by the condition that the resistance of wire over the length λ, which is about $\lambda/\sigma_1 a^2$, should be about the same as the resistance of the medium "in perpendicular direction", which is about $1/\sigma_2\lambda$; equating these two returns the result (6.3).

Let us now switch to the next regime H, which arises because of the finite length of sticks. Indeed, the length λ, over which current flows in one wire, cannot exceed the wire length l. According to formula (6.3), this crossover happens along

the border $s = l^2/a^2$. Indeed, starting from this s, we get even $a\sqrt{\sigma_1/\sigma_2} > l$, and so λ cannot satisfy Eq. (6.3). To find conductivity in the regime H, we should replace λ by l in Eq. (6.2). Since the second term in the denominator dominates, we arrive at

$$\sigma \sim \phi(l/a)^2\sigma_2 \ . \qquad \text{(regime H)} \tag{6.5}$$

We get the same l^2 dependence as predicted in reference [78]. This effective conductivity has no dependence on σ_1 because σ_1 is so high that overall resistance is entirely concentrated in the narrow gaps where current should switch from wire to wire. As a result, σ_1 does not enter the formula.

If we decrease ϕ and look at the dilute regime $\phi < a^2/l^2$, our scaling theory suggests that $\sigma \simeq \sigma_2$. More accurate analysis of this regime was performed in the work [87] using first order perturbation theory in powers of ϕ, which is applicable in the dilute regime, as long as current field around one wire does not affect the neighboring wires. The achievement of that work is that the authors were able to take into account, to the first order in their perturbation theory, both numerical coefficients and logarithmic factors proportional to $\ln(l/a)$ (in our notations). Up to these factors, which we systematically neglect, all our scaling results cross-over smoothly with the results of the work [87]. Moreover, the simplified expressions of perturbation results are given in the work [87] in the form of three formulae, describing the dilute solution in the ranges (in our notations) $l \gg a\sqrt{\sigma_1/\sigma_2}$,

$l \approx a\sqrt{\sigma_1/\sigma_2}$, and $l \ll a\sqrt{\sigma_1/\sigma_2}$; this sheds an additional light on the importance of the lengths scale $a\sqrt{\sigma_1/\sigma_2}$ introduced by us here in the present work.

Thus, we have completed our consideration of the phase diagram up to the concentration about $\phi = a/l$. It would be frustrating to stop at this point, because, for example, the experiments with suspensions of carbon nanotubes often use loadings with $\phi > a/l$ to achieve larger electrical and thermal conductivities. Let us therefore discuss what happens to conductivity if one can manage to create isotropic suspension with $\phi > a/l$. Suppose the length of wire between direct contacts, or the mesh size of the percolating network, is ζ. Then, the number of electrically parallel wires within a cube of size ζ is of the order of $\zeta^3\phi/(\zeta a^2)$, each with the resistance about $\zeta/(\sigma_1 a^2)$. Therefore the total resistance of the cube scales as $1/(\sigma_1\zeta\phi)$, yielding the effective conductivity about $\sigma_1\phi$. In the scaling sense, this is the same σ as that in Regime B. Thus, regime B continues to higher concentrations $\phi > a/l$. Trivially, the lower bound of this continued regime B remains to be the condition $s > 1/\phi$, since at lower s current does not concentrate in wires, percolation gives no help. More interestingly, percolation produces no effect on conductivity σ as long as $s < (l/a)^2$ because the percolating network gives no advantage over the conducting channels made of combination of wires and surrounding medium. Percolation does have effect when $s > (l/a)^2$, where conductivity as a function of concentration ϕ changes rapidly from $\sigma \sim \phi(l^2/a^2)\sigma_2$ below percolation to $\sigma \sim \phi\sigma_1$ above. This change occurs around the threshold

$\phi = \phi_c \simeq a/l$, over the interval of width of order ϕ_c, which is schematically plotted as the shaded cone in the diagram Fig. 6.2. In this range, the conductivity has critical behavior similar to that discussed in Ref. [65]. The detailed structure of this range is beyond the scope of this chapter.

We should emphasize that in all our considerations we completely disregard the resistivity of the contacts, either between a wire and surrounding medium, or between two wires in contact. In particular, everything we said about percolation assumes that whenever there is a touch between two wires, it presents an electrical contact of vanishing resistance. In fact, this assumption is model sensitive and it is not necessarily good in practical cases. For instance, our theory predicts that above percolation threshold, when $\phi > a/l$, effective electric conductivity σ grows linearly with ϕ, independently of s being larger or smaller than $(l/a)^2$. Similar prediction holds also for thermal conductivity. However it is not compatible with the apparently super-linear growth of effective electrical or thermal conductivity observed in experiments [80, 81, 82, 83]. It is not clear whether interfacial resistance can help to explain these experimental data.

6.3 Gaussian coiled wires

When wires are flexible (e.g. conducting polymer), our theory developed in section 6.2 needs modifications to account for different fractal properties of the wires. We

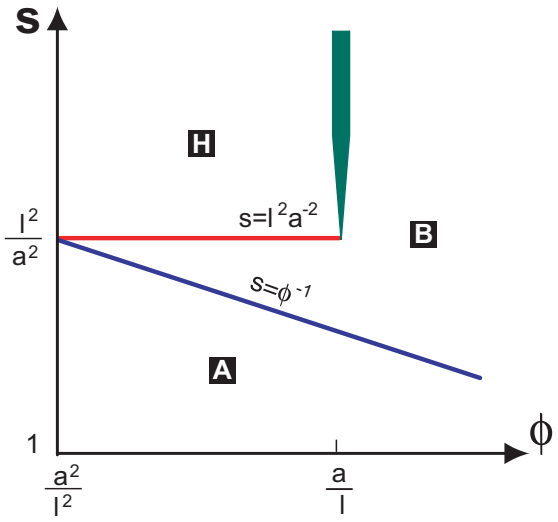

Figure 6.2: Diagram of scaling regimes for the case of straight wires (e.g. carbon nanotubes). Both volume fraction of the wires ϕ and $s = \sigma_1/\sigma_2$ axes are in the logarithmic scale. Each line on this plane marks a cross-over between scaling regimes. The widened line at $\phi = a/l$ shows the location of conductivity jump around the percolation threshold. Summary of the conductivities is provided in Table 6.1. If s is replaced by yd, the diagram represents macroscopic diffusion constant of protein discussed in section 6.4.

Table 6.1: The summary of macroscopic conductivities and diffusion constants in various regimes.

Regime	σ	D
A	σ_2	D_3
B	$\sigma_1\phi$	$D_1 y\phi$
C	$(p/a)\phi(\sigma_1\sigma_2)^{1/2}$	$(p/a)y^{1/2}\phi(D_1D_3)^{1/2}$
D	$(p/a)^2\phi^{3/2}(\sigma_1\sigma_2)^{1/2}$	$(p/a)^2y^{1/2}\phi^{3/2}(D_1D_3)^{1/2}$
E	$(lp/a^2)\phi\sigma_2$	$(lp/a^2)\phi D_3$
F	$(lp^3/a^4)\phi^2\sigma_2$	$(lp^3/a^4)\phi^2 D_3$
G	$(p/a)\phi^2\sigma_1$	no correspondence
H	$(l^2/a^2)\phi\sigma_2$	$(l^2/a^2)\phi D_3$

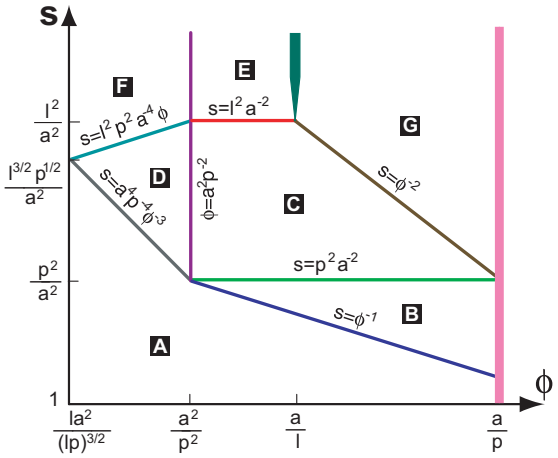

Figure 6.3: Diagram of scaling regimes for the case of flexible Gaussian coiled wires (e.g. conducting polymers) with length $p < l < p^2/a$. Summary of the conductivities is provided in Table 6.1.

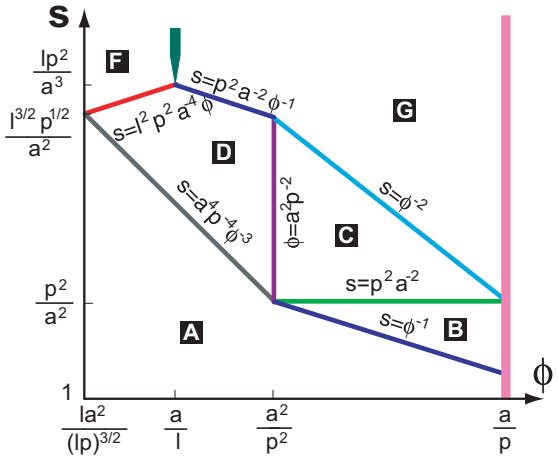

Figure 6.4: Diagram of scaling regimes for the case of flexible Gaussian coiled wires with length $p^2/a < l < p^3/a^2$.

consider the system of semi-flexible conducting polymers as an example (see Fig. 6.1b). We assume that each polymer has contour length l, relatively large persistence length p and the radius (thickness) a. We assume $l \gg p \gg a$. Throughout this work we require $l < p^3/a^2$ and this lets us disregard the effect of excluded volume on the polymer statistics, considering polymer coil as Gaussian. Therefore, if we take a piece of polymer of the contour length λ, then its size in space scales as

$$\xi \sim \begin{cases} \lambda & \text{when} \quad \lambda < p \\ \sqrt{\lambda p} & \text{when} \quad \lambda > p \end{cases} . \tag{6.6}$$

The overlap of coils starts when the volume fraction of polymers exceeds volume fraction of the chain inside one coil: $\phi \sim la^2/(lp)^{3/2} = a^2/(l^{1/2}p^{3/2})$. The nematic ordering of wires starts at a larger volume fraction $\phi \sim a/p$. The percolation threshold can be estimated from following argument. Percolation happens when each wire has roughly two direct contacts with other wires. Following Ref. [14], the number n of contacts per wire is of the order of

$$n \sim \phi l/a \tag{6.7}$$

(each piece of the polymer of the length a has probability ϕ to be in touch). Requiring that n is of the order of 1, we obtain the percolation threshold $\phi_c \sim a/l$. Percolation starts earlier than the nematic ordering and ϕ_c, because percolation

requires a couple of contacts per wire, while nematic ordering requires a contact per a smaller length of a statistical segment ($\sim p$). Therefore, ϕ_c divides into two parts the range of concentrations when the system is semi-dilute but isotropic $a^2/(l^{1/2}p^{3/2}) < \phi < a/p$: $a^2/(l^{1/2}p^{3/2}) < \phi < \phi_c$ where we neglect the effect of direct contacts; and $\phi_c < \phi < a/p$ where the effect of the percolating wires must be included in our theory.

Let us start with determining the mesh size r [14]. Suppose that the polymer within each mesh has a contour length g. It makes a density about $\sim ga^2/r^3$ which must be about the overall average density ϕ. Thus, $ga^2/r^3 \sim \phi$. Second relation between g and r depends on whether mesh size is bigger or smaller than persistence length p:

$$r \sim \begin{cases} g & \text{if} \quad g < p \\ \sqrt{gp} & \text{if} \quad g > p \end{cases} . \tag{6.8}$$

Accordingly, one obtains

$$\begin{array}{llll} g \sim a\sqrt{\frac{1}{\phi}} , & r \sim a\sqrt{\frac{1}{\phi}} & \text{if} & \frac{a}{p} > \phi > \frac{a^2}{p^2} \\ g \sim \frac{a^4}{\phi^2 p^3} , & r \sim \frac{a^2}{\phi p} & \text{if} & \frac{la^2}{(lp)^{3/2}} < \phi < \frac{a^2}{p^2} \end{array} , \tag{6.9}$$

The upper line corresponds to such a dense network that every mesh is shorter than persistence length and polymer is essentially straight within each mesh (see Fig. 6.1b). The lower line describes much less concentrated network, in which every mesh is represented by a little Gaussian coil. Depending on the relation

between l and p, percolation can start before or after $\phi \sim a^2/p^2$. Our results for these two cases are summarized in Figs. 6.3, 6.4 and in the Table 6.1.

When the correlation length $\lambda < p$, the polymer within correlation length is straight. So we can directly apply what we got for the straight wire case and obtain regimes A and B.

For other regimes with $\lambda > p$, the derivation has to be performed from the beginning. So, we consider a typical cube inside the composite with size ξ such that every polymer enclosed in this cube has contour length of the order of correlation length λ. There are about $\frac{\xi^3}{r^3(\lambda/g)}$ electrically parallel conducting channels in this cube (because λ/g is the number of meshes visited by one wire, and r^3 is the volume of each such mesh). Each channel consists of the wire itself, with resistance $\lambda/(\sigma_1 a^2)$, and the wire is connected in series with the group of λ/g parallel connected bridges, each of resistance $r/(\sigma_2 r^2)$. Thus, the resistance of the cube scales as

$$\frac{\lambda/(\sigma_1 a^2) + g/(\sigma_2 \lambda r)}{g\xi^3/(\lambda r^3)} \ , \tag{6.10}$$

which should be equated to $1/(\sigma\xi)$. Therefore we obtain:

$$\sigma \simeq \frac{a^2 g/r^3}{\lambda^2/(\sigma_1 \xi^2) + g a^2/(\sigma_2 r \xi^2)} \ . \tag{6.11}$$

Once again, if the wire remains straight over the length λ, so that $\xi \simeq \lambda$, we

are back at the situation described by formula (6.2), and we can reproduce the corresponding result for the regime B, (6.4). More interestingly, we can now consider the case when $\lambda > p$ and the polymer of the length λ is the Gaussian coil: $\xi \sim \sqrt{\lambda p}$. In this case we obtain

$$\sigma \sim \frac{pa^2 g/r^3}{\lambda/\sigma_1 + a^2 g/(\sigma_2 r\lambda)} \ . \tag{6.12}$$

Now conductivity has the well defined maximum at the well defined value of λ:

$$\lambda \sim a \left(\frac{\sigma_1 g}{\sigma_2 r}\right)^{1/2} \ . \tag{6.13}$$

Not coincidentally, this result for the correlation length λ corresponds to equating two terms in the denominator of Eq. (6.12) - the resistance of wire with correlation length λ and the resistance of the surrounding "sleeve" of thickness r in the medium.

Plugging λ from Eq. (6.13) back into Eq. (6.12) and applying Eqs. (6.9), we obtain the following two scaling regimes:

Regime C, where polymer on the scale λ is Gaussian (lower line in the Eq. (6.6), but the polymer within each mesh is still straight;

Regime D, where polymer is Gaussian even within each mesh (lower lines in the Eqs. (6.9)).

When λ reaches the entire length of the polymer l, we should replace λ by l in Eq. (6.12). Then the second term in the denominator dominates. Since we have two different kinds of meshes represented by formulae (6.9), we have two more regimes:

Regime E, where $\lambda = l$ and the polymer within each mesh is straight (upper lines in the Eq. (6.9));

Regime F, where $\lambda = l$, but the polymer within each mesh is Gaussian (lower lines in the Eq. (6.9)).

We should emphasize that regime E exists only in the case where $l < p^2/a$ (see Fig. 6.3). If $l > p^2/a$, percolation starts so early that the polymer within each mesh is a Gaussian coil. This case is plotted in Fig. 6.4.

When we increase σ_1/σ_2, the effective conductivity grows from σ_2 (regime A) and finally saturates in regimes E and F with values having no dependence on σ_1. As we discussed, for regime A, transport through wires is not at play while in regimes E and F, σ_1 is so large compared to σ_2 that the wires are effectively *"super-conducting"*. More interestingly, for broad ranges of ϕ and σ_1/σ_2 (regimes C and D), σ is proportional to $\sqrt{\sigma_1\sigma_2}$. Such dependence is known for a narrow vicinity of percolation threshold in isotropic mixtures [64] but, as far as we know, it has never been noticed for a broad range of parameters. The width of the range grows as l^2.

When the volume fraction is larger than the percolation threshold, the effect of

percolating wires can not be neglected. If σ_1/σ_2 is relatively small, the transport of current is mainly realized through the conducting channel we have discussed. But when σ_1/σ_2 is large enough, percolation through the directly connected wires dominates. The crossover is determined by equating the conductivity due to the untouched wires and surrounding medium and the conductivity due to percolating wires. We have already calculated the first conductivity. The later one can be calculated by the following argument. Let us denote the length of wire between contacts by ζ. It can be estimated as $\zeta \sim l/(\phi/\phi_c) \sim a/\phi$. Because we require $\phi < a/p$, ζ is larger than the persistence length p and thus the distance it covers in space scales as $\sim (\zeta p)^{1/2}$. Within a cube with size $(\zeta p)^{1/2}$, there are $(\zeta p)^{3/2}\phi/(\zeta a^2) \sim (p/a)^{3/2}\phi^{1/2}$ electrically parallel wires. So the conductance scales as $\sigma_1 pa/\zeta$. It can be also expressed using effective conductivity, it is $\sigma(\zeta p)^{1/2}$. Comparing these two conductances, we obtain $\sigma \sim (p/a)\phi^2\sigma_1$, which is the effective conductivity in regime G. It crosses over smoothly to the regimes E and F (E only exists for case $l < p^2$, which is represented in Fig. 6.3). One can also obtain the border by equating the correlation length λ to the length between direct contacts ζ. Since we assume the current can switch wires freely at the contacts, λ can not grow above ζ. On the other hand in the scaling approach we use, there is a conductivity jump around the percolation threshold $\phi_c \sim a/l$, which is plotted as the widened line in both figures. Actually the jump of conductivity is eliminated when we consider the critical behavior of conductivity at $\phi - \phi_c \ll \phi_c$

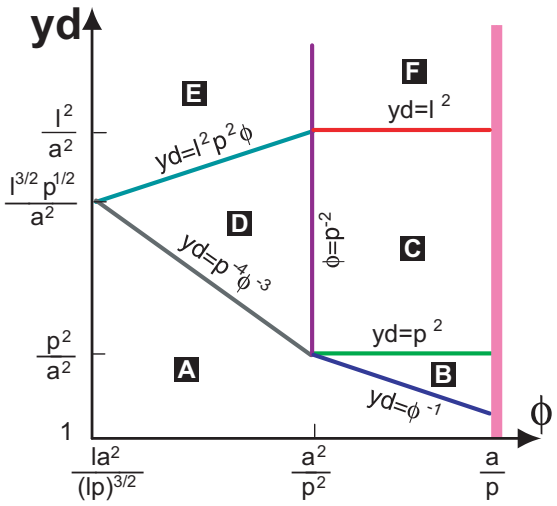

Figure 6.5: Diagram of scaling regimes for the case of protein diffusion in Gaussian coiled DNA solution. Summary of the macroscopic diffusion constants is provided in Table 6.1.

but our scaling theory is not designed to see such details.

6.4 Macroscopic diffusion constant of proteins in semidilute DNA system

The theory we have developed for the effective conductivity of composites can be used to study the macroscopic diffusion constant of the nonspecific DNA-binding proteins in semidilute DNA solutions.

For simplicity, we make the following assumptions: (i) protein can be non-specifically adsorbed on any place of DNA; (ii) non-specific adsorption energy ϵ, or the corresponding constant $y = e^{\epsilon/k_BT}$, are the same everywhere along

DNA (sequence-independent); (iii) every protein molecule has just one surface patch capable to stick to the DNA, so proteins do not serve as cross-linkers for the DNA; (iv) non-specifically bound protein can diffuse along DNA with the diffusion coefficient D_1, while protein dissolved in surrounding water diffuses in 3D with diffusion constant D_3; (v) while protein is diffusing, the DNA remains immobile.

To make the dictionary of translation between conductivity and diffusion languages, the easiest way is to step up the generality in writing down the expressions for current density $\mathbf{j}$ in either conductivity or diffusion problem. In both cases, as long as we consider stationary process, current is subject to the no-divergence condition: $\mathrm{div}\mathbf{j} = 0$. For the electric current driven by the potential gradient, Ohm's law reads $\mathbf{j} = -\sigma(\mathbf{x})\nabla\phi$; and for the the diffusion problem, current driven by the gradient of total chemical potential is described by similar Smoluchowski equation: $\mathbf{j} = -D(\mathbf{x})c(\mathbf{x})\nabla\left(\ln c(\mathbf{x}) - \epsilon(\mathbf{x})/k_BT\right)$. Here, we assume for a moment, that electrical conductivity, diffusion coefficient, protein concentration c, and binding energy ϵ or $y = e^{\epsilon/k_BT}$ have all some general dependence of space coordinates $\mathbf{x}$. In fact, for our case, this space dependence is very simple: within narrow regions along the wires or along DNA, we have $\sigma(\mathbf{x}) = \sigma_1$, and similarly $D(\mathbf{x}) = D_1$ and $y(\mathbf{x}) = y$ (remember that $y = e^{\epsilon/k_BT}$); for all other places $\mathbf{x}$ we have $\sigma(\mathbf{x}) = \sigma_2$, $D(\mathbf{x}) = D_3$ and $y(\mathbf{x}) = 1$. As regards concentration, diffusion equation also implies (since chemical potential is continuous) that locally there

is the equilibrium relation between the 1D concentration of non-specifically adsorbed proteins, c_1, and concentration of proteins remaining free in the nearby solution c_3:

$$c_1/(c_3 a^2) = y \ , \tag{6.14}$$

where a is the length scale such that c_1/a^2 is the 3D concentration of proteins within the region around DNA where proteins are adsorbed. Comparing the equations, we see that complete mapping is achieved by the substitutions $\sigma_1 \leftrightarrow D_1 c_1/a^2$, $\sigma_2 \leftrightarrow D_3 c_3$. Similarly writing the effective macroscopic equations in terms of macroscopic conductivity σ and macroscopic diffusion coefficient D, one finds $\sigma \leftrightarrow D c_3$. In terms of more convenient dimensionless quantities, and taking into account the local adsorbtion equilibrium (6.14), these rules read:

$$\frac{\sigma_1}{\sigma_2} \leftrightarrow \frac{D_1}{D_3} y \quad , \quad \frac{\sigma}{\sigma_2} \leftrightarrow \frac{D}{D_3} \ . \tag{6.15}$$

We can, therefore, directly address macroscopic diffusion based on our results for macroscopic conductivity. Substituting Eq. (6.15) into our results for σ, we obtain the macroscopic diffusion constants of the proteins in the DNA solution expressed in terms of D_1 and D_3 for all the regimes except regime G, for which the applicability of percolation results to the DNA case is doubtful. [1]

[1] As we mentioned, even for the wires the idea of direct contact is very much model-dependent. It is even more so for the protein and DNA case, because in this case "contact between wires" should mean the possibility for the protein to switch from one DNA to the other without

Thus, Fig. 6.2 can be used for the macroscopic diffusion constants for the straight DNA case if we replace σ_1/σ_2 by yD_1/D_3. However, for the gaussian coiled DNA case, without regime G, Figs. 6.3 and 6.4 should be modified. Resulting phase diagram is shown in Fig. 6.5. One can easily get this figure from Fig. 6.3 by removing the borders the regime G makes with other regimes and extending the border line between regimes E and C to the right boundary of the phase diagram. The results for various scaling regimes are also summarized in the right most column of Table 6.1.

Measuring macroscopic diffusion of proteins is a promising way to test our predictions. It is therefore useful to comment a little deeper on the nature of macroscopic diffusion coefficient D. The way it is defined above is adequate for a macroscopic experiment, because D establishes the proportionality between the flow of proteins and the gradient of concentration of *dissolved* proteins. In such experiment, the presence of a large number of proteins adsorbed on DNA is not directly relevant. However, in a different experiment, for instance, in tracking the random walks of a single protein molecule, a different diffusion coefficient, $\tilde{D}$, will be relevant, such that $\tilde{D}c = Dc_3$, where c is total concentration of proteins, including the adsorbed ones: $c = (c_1/a^2)\phi + c_3(1-\phi)$. Using (6.14), one then gets

activation. It might be possible in some systems but impossible in others; besides, there are quite a few other effects which are beyond our theory, such as excluded volume constraints for the proteins which becomes significant when two DNA pieces are close by - protein may have difficulties diffusing along one of them, like a big truck under a low bridge on a highway. We do not consider all these questions in this chapter and only consider DNA system well below percolation threshold.

$\tilde{D} = D/\left(1 - \phi + y\phi\right)$. The difference between these two diffusion coefficients is marginal when absorbtion is weak ($y \ll 1$ and $\phi \ll 1$), but it becomes very much pronounced when the absorbtion is strong, or y is large: $\tilde{D} \simeq D/(y\phi) \ll D$. This result has simple physical meaning: every particular protein will be adsorbed most of the time, so its diffusive motion will be slow, but overall flow of proteins will not be that slow because of a large number of proteins.

Using the macroscopic diffusion constant, we can also re-derive the results of the work [28] concerning the rates of protein searching for specific places on globular DNA. Thus, measuring D or $\tilde{D}$ is another way to verify the results of Ref. [28] in those crowded regimes.

6.5 Conclusion

In this chapter we studied a plethora of different scaling regimes for conductivity of a suspension of wires in poorly conducting medium. Our results are applicable to suspensions of metallic wires in poorly conducting medium at room temperature. In this case our generic description of the system only by two macroscopic local conductivities is valid, because typically the surfaces of nanowires are so dirty that any surface barrier for electrons of the metal is sufficiently well conducting due to hopping through localized states.

We also mention carbon nanotube suspensions as a possible application of our

theory. In this case one may worry about the role of the surface resistance on the nanotube-medium interface, so that our theory strictly speaking only estimates the effective conductivity from above. Including surface resistance or allowing for influence of environment on conductivity of nanotubes would require new parameters in the theory, making it much more complicated. We believe that both real and computer experiments should be first compared with the simplest and generic model presented here in this paper before one starts developing more complicated theories.

The serious advantage of our generic theory is that it can be applied in a variety of different problems beyond electric conductivity, for instance, to thermal conductivity of well thermally conducting wires in a weaker thermally conducting medium, to macroscopic dielectric constant of suspended metallic wires and to wires with large magnetic susceptibility. We also applied our theory to the calculation of the macroscopic diffusion constant of the nonspecific DNA-binding proteins in semi-dilute DNA solution.

The latter application is also promising in terms of computational tests of our theory along the lines of the recent work [84, 88].

References

[1] Smoluchowski,M.V., 1917, Z. Phys. Chem., 92, 129-198.

[2] Riggs, A.D., S.Bourgeois, and M.Cohn, 1970, Journal of Molecular Biology, 53, 401-417.

[3] Richter, P.H., and M. Eigen, 1974, Biophysical Chemistry, 2, 255-263.

[4] Adam, G., and M. Delbrück, 1968, Structural Chemistry and Molecular Biology. A. Rich, and N. Davidson, editors., pp. 198-215, W. H. Freeman, San Francisco, CA.

[5] A. Zangwill, 1988, Physics at Surfaces, Cambridge University Press, Cambridge.

[6] Halford, S.E., and M.D.Szczelkun, 2002, European Biophysical Journal, 31, 257-267.

[7] Berg,O.G., Winter,R.B. and von Hippel,P.H., 1981, Biochemistry, 20, 6929-6948.

[8] Winter,R.B., Berg,O.G. and von Hippel,P.H., 1981, Biochemistry, 20, 6961-6977.

[9] S. Cunha, C.L. Woldringh and T. Odijk., 2005, J. Struct. Biol. 150, 226-232.

[10] Coppey, M., O.Benichou, R.Voituriez, M.Moreau, 2004, Biophys. J., 87, 1640-1649.

[11] Bruinsma, R. F., 2002, Physica A 313, 211-237.

[12] Halford, S.E. and Marko, J.F., 2004, Nucleic Acids Res., 32, 3040-3052.

[13] Slutsky, M., and L. A. Mirny., 2004, Biophys. J., 87, 4021-4035.

[14] Grosberg, A., and A. Khoklov, 1994, Statistical Physics of Macromolecules, AIP Press, New York, NY.

[15] PG deGennes, 1979, Scaling Concepts in Polymer Physics, Cornell University Press, Ithaca.

[16] S. Redner, 2001, A Guide to First Passage Processes, Cambridge University Press, Cambridge.

[17] H.-J. Ehbrecht, A. Pingoud, C. Urbanke, G. Maass and C. Gualerzi, 1985, J. Biol. Chem. 260, 6160-6166.

[18] von Hippel, P. H. and Berg, O. G., 1989, J. Biol. Chem. 264, 675-678.

[19] G.F.Lawler, J. Phys. A: Math. & Gen., **20** 4565-4568 (1987).

[20] A. Parsegian, Nature **221**, 844 (1969); P. C. Jordan, Biophys J. **39**, 157 (1982).

[21] A. Kamenev, J. Zhang, A. I. Larkin, B. I. Shklovskii, Physica A **359**, 129 (2006).

[22] A. V. Finkelstein, O.B. Ptitsyn "Protein Physics", Elsevier (2003); see also: A. V. Finkelstein, D. N. Ivankov, and A. M. Dykhne, in preparation; S. Teber, J. Stat. Mech. P07001, (2005).

[23] M. G. Fried and D. M. Crothers, J. Mol. Biol. **172**, 263 (1984).

[24] B. A. Lieberman and S. K. Nordeen, J. Biol. Chem. **272**, 1061 (1997).

[25] J. Iwahara and G. M. Clore, J. Am. Chem. Soc. **128**, 404 (2006).

[26] C. Bustamante, M. Gutholdi, X. Zhu and G. Yang, J. Biol. Chem. **274**, 16665 (1999).

[27] N. Shimamoto, J. Biol. Chem. **274**, 15293 (1999).

[28] Tao Hu, A. Yu. Grosberg and B. I. Shklovskii, Biophys. J. **90**, 2731 (2006).

[29] O. G. Berg, Biopolymers, **25**, 811 (1986).

[30] B. I. Shklovskii and A. L. Efros, *Electronic Properties of Doped Semiconductors* (Springer-Verlag, Berlin, 1984).

[31] G. S. Grest, I. Webman, S. A. Safran and A. L. R. Bug, Phys. Rev. A, **33**, 2842 (1986).

[32] O.G. Berg and P.H. von Hippel. J. Mol. Biol. **193**, 723 (1987).

[33] U. Gerland, J.D. Moroz and T. Hwa. Proc. Natl. Acad. Sci. USA. **99**, 12015 (2002).

[34] M. Ptashne and A. Gann, *Genes and signals* (Cold Spring Harbor Laboratory Press, Cold Spring Harbor, NY, 2001).

[35] M. Barbi, C. Place, V. Popkov and M. Salerno. Phys. Rev. E **70**, 041901 (2004); J. Biol. Phys. **30**, 203 (2004).

[36] K. Nadassy, S.J. Wodak and J. Janin. Biochemistry **38**, 1999 (1999).

[37] M. Slutsky, M. Kardar and L.A. Mirny. Phys. Rev. E **69**, 061903 (2004).

[38] Encyclopedia of Virology Plus CD-ROM. Edited by R. G. Webster and A. Granoff. Academic Press (1995).

[39] A. Scheneemann, Annu. Rev. Microbiol, **60**, 51 (2006).

[40] R. F. Bruinsma, Eur. Phys. J. E, Soft Matter. **19**, 303 (2006).

[41] S. J. Flint, L. W. Enquist, V. R. Racaniello and A. M. Skalka, *Principles of Virology* 2nd ed (ASM, Washingtion DC, 2004).

[42] P. P. Hung, C. M. Ling and L. R. Overby, Science. **166**, 1638 (1969).

[43] J. B. Brancroft, E. Heibert and C. E. Bracker, Virology **39**, 924 (1969).

[44] K. W. Adolph and P. J. Butler, Philos Trans R. Soc Lond B (Biol Sci.) **276**, 113 (1976).

[45] P. van der Schoot and R. Bruinsma, Phys. Rev. E **71**, 061928 (2005).

[46] http://www.ncbi.nlm.nih.gov.

[47] http://viperdb.scripps.edu.

[48] T. Odijk, J. Polym. Sci., Polym. Phys. Ed. **15**, 477 (1977).

[49] J. Skolnick and M. Fixman, Macromolecules **10**, 944 (1977).

[50] T. T. Nguyen and B. I. Shklovskii, Phys. Rev. E **66**, 021801 (2002).

[51] For similar but not identical problem of flexible polyelectrolyte wrapping oppositely charged rigid cylinder, this result was previously obtained in Ref. [52].

[52] T. T. Nguyen, B. I. Shklovskii, Phys. Rev. Lett. **89**, 018101 (2002); H. Borodjerdi, Y-W. Kim, A. Naji, R. R. Netz, X. Shlagberger, A. Serr, Phys. Rep. **416**, 129 (2005).

[53] One can see strong deviations from our predictions for viruses in the third, fourth and the last three lines of the group A. They have anomalously long tails with strongly non-uniform distribution of charges in the tail [46, 47]. Heavily charged domains occupy roughly speaking only half of the tail length. Because of the salt screening neural pieces are not stretched by the Coulomb repulsion of the neighboring charged domains and acquire coil-like configurations. As a result, a charged tail has twice larger linear charge density. Therefore, according to Eq. (5.2) predicted $\Re$ should be roughly speaking twice smaller, in a reasonable agreement with R. In essence in these cases, we can not neglect the configurational entropy.

[54] T. T. Nguyen and R. F. Bruinsma attracted our attention to this possibility.

[55] J. Rudnick and R. Bruinsma, Phys. Rev. Lett. **94**, 038101 (2005).

[56] A. Zlotnick, R. Aldrich, J. M. Johnson, P. Ceres and M. J. Young, Virology, **277**, 450 (2000)

[57] G. L. Casini, D. Graham, D. Heine, R. L. Garsea and D. T. Wu, Virology, **325**, 320 (2004).

[58] S. Campbell and V. M. Vogt, J. Virol. **69**, 6487 (1995).

[59] J. M. Johnson, D. A. Willis, M. J. Young, and A. Zlotnick, J. Mol. Biol. **335**, 455 (2004).

[60] D. F. Evans and H. Wennerstrom, *The Colloidal Domain* 2nd ed (Wiley-VCH, New York, 1999).

[61] Tao Hu, Rui Zhang, B. I. Shklovskii, Physica A **387**, 3059 (2008).

[62] S. Campbell and A. Rein, J. Virol. **73**, 2270 (1999).

[63] M. Y. Ma and V. M. Vogt, J. Virol. **76**, 5452 (2002); **78**, 52 (2004).

[64] A.M. Dykhne, Zh. Eksp. Theor. Phys. **59**, 111 (1970).

[65] A.L. Efros and B.I. Shklovskii, Phys. Stat. Sol. B **76**, 476 (1976).

[66] D.J. Bergman and D. Stroud, Solid State Phys. **46**, 147 (1992).

[67] G.A. Niklasson and C.G. Granqvist, J. Appl. Phys. **55**, 3382 (1984).

[68] J.P. Clerc, G. Giraud and J. M. Luck, Adv. Phys. **39**, 191 (1990).

[69] D. Stauffer and A. Aharony, *Introduction to Percolation Theory*, 2nd ed (Taylor & Francis, London, 1992).

[70] F.G. Shin and Y.Y. Yeung, J. Mater, Sci. Lett. **7**, 1066 (1988).

[71] I. Balberg, N. Binenbaum, C. H. Anderson, Phys. Rev. Lett. **51**, 1605 (1983).

[72] I. Balberg, Phys. Rev. B **31**, 4053 (1985).

[73] I. Balberg, Phys. Rev. B **33**, 3618 (1986).

[74] M. Foygel, R.D. Morris, D. Anez, S. French and V.L. Sobolev, Phys. Rev. B **71**, 104201 (2005).

[75] C.A. Zuev and A.F. Sidorenko, Teor. Mat. Fiz **62**, 76 (1985); 253 (1985).

[76] A.N. Kolesnikov, A.N. Lagardov, L.N. Novogrudskiy, S.M. Matitsin, K.N. Rozanov, and A.K. Sarychev, in *Optical and Electrical Properties of Polymers*, edited by J. A. Emerson and J. M. Torkelson, MRS Symposia Proceedings No. 214 (Materials Research Society, Pittsburgh, 1991), p. 119.

[77] Y. Yagil, P. Gadenne, C. Julien, G. Deutscher Phys. Rev. B **46**, 2503 (1992).

[78] A.N. Lagarkov and A.K. Sarychev, Phys. Rev. B **53**, 6318 (1996).

[79] R. Andrews, D. Jacques, A. M. Rao, T. Rantell, F. Derbyshire, Y. Chen, J. Chen and R. C. Haddon, Appl. Phys. Lett. **75**, 1329 (1999).

[80] S. Choi, Z.G. Zhang, W. Yu, F.E. Lockwood and E.A. Grulke, Appl. Phys. Lett. **79**, 2252 (2001).

[81] C. Park, Z. Ounaies, K.A. Watson, R.E. Crooks, J. Smith, Jr., S.E. Lowther, J.W. Connell, E.J. Siochi, J.S. Harrison and T.L. St. Clair, Chem. Phys. Lett. **364**, 303 (2002)

[82] M.B. Brynning, D.E. Milkie, M.F. Islam, J.M. Kukkawa, A. G. Yodh, Appl. Phys. Lett. **87**, 161909 (2005).

[83] B.E. Kilbride, J.N. Coleman, J. Fraysse, P.Fournet, M.Cadek, A. Drury, S. Hutzler, S. Roth and W.J. Blau, J. Appl. Phys. **92**, 4024 (2002).

[84] K.V. Klenin, H. Merlitz, J. Langowski and C.X. Wu, Phys. Rev. Lett. **96**, 018104 (2006).

[85] L. Onsager, Ann. N.Y. Acad. Sci. **51**, 627 (1949).

[86] I. Prigogine, *Thermodynamics of Irreversible Processes* (Interscience, New York, 1961).

[87] X. Zheng, M.G. Forest, R. Lipton, R. Zhou and Q. Wang, Adv. Funct. Mater. **15**, 627 (2005).

[88] H. Merlitz, K.V. Klenin, C.X. Wu, J. Langowski, J. Chem. Phys. **125**, 014906 (2006).

Appendix A

Simple scaling derivation of the Smoluchowski rate and the Smoluchowski time

Classical Smoluchowski theory [1] treats the diffusion-controlled process of irreversible absorbtion of diffusing particles by an immobile sphere of a given radius, call it b. As in our proteins problem, Smoluchowski theory can be formulated either in terms of stationary rate J_s, assuming concentration c is fixed, or in terms of mean first passage time τ_s for a single protein.

Let us imagine that a protein diffuses within a volume v, and its diffusion coefficient is D_3. Let us further define the time interval t_b such that over time

t_b protein moves the distance of order b: $D_3 t_b \sim b^2$. Then, over a longer time t protein visits t/t_b spots of the size b each, and, given that $b^3 \ll v$, the probability that none of this spots is the target, or the probability to keep missing target for the time t obeys Poisson distribution and decays exponentially with t: $(1 - b^3/v)^{t/t_b} \simeq \exp\left[-tb^3/(vt_b)\right]$. The mean first passage time is read out of this formula, it is $\tau_s \sim v/(D_3 b)$.

The corresponding stationary rate is obtained by inverting this time, assuming overall concentration of proteins $c = 1/v$. Thus, $J_s \sim D_3 cb$.

Of course, more accurate derivation, available in a number of textbooks (and easily formulated in terms of electrostatic analogy, see appendix B), is necessary to complement the result with the correct prefactor of 4π.

Appendix B

Electrostatic analogy

Here, we re-derive the results of the section 2.2 using the fact that stationary diffusion equation is the same as Laplace equation in electrostatics. Specifically, the problem of diffusion into the target of the size b is equivalent to the problem of finding the electric field around a charge of the size b. The key relatively non-trivial point of this analogy is to realize that the potential well for diffusing particles is equivalent in electrostatic language to the region in space with very high dielectric constant. In our case the potential well is located all around DNA, and the target is also somewhere on the DNA. Therefore, it is equivalent to the electrostatic problem in which we have a channel, of the diameter about b, filled with high dielectric constant material, for instance - water, and surrounded by a low dielectric constant material. Specifically, it is easy to check that y of the diffusion problem is exactly equivalent to ϵ_w/ϵ_m - the ratio of dielectric constants

of water and surrounding medium: $y = \epsilon_w/\epsilon_m \gg 1$.

Thus, we have to address the problem of a charge Q located inside the water filled channel in, let say, a thick lipid membrane. For the straight channel, this is a well known problem in membrane biophysics. It was first studied by Parsegian [20], and the recent most detailed exposition is given in the article [21]. Here, we give only simple scaling consideration.

Since $\epsilon_w/\epsilon_m \gg 1$, field lines prefer to remain inside the channel for as long as possible. This gives the picture of electric field equivalent to the Fig. 2.1, a or b. In other words, we should say that there is some length scale λ along the channel, and within this scale electric field lines are predominantly confined in the channel. At the same time, outside of the sphere of radius ξ, electric field is close to that of a spherical charge in unrestricted space. Thus, electric field energy can be approximated as the sum of two parts, one due to the uniform field in the volume about $b^2\lambda$ in the channel, and the other around the ξ-sphere in the medium. Since E-field in the channel is about $Q/b^2\epsilon_w$ while D-field is Q/b^2, the part of energy due to the field inside the channel is about $(Q/b^2\epsilon_w) \times (Q/b^2) \times (b^2\lambda) = Q^2\lambda/b^2\epsilon_w$. At the same time, energy of the field in the outer zone is about $Q^2/\xi\epsilon_m$. Thus, total electrostatic energy (self-energy of the charge Q) is

$$E \sim \frac{Q^2\lambda}{b^2\epsilon_w} + \frac{Q^2}{\xi\epsilon_m} \ . \tag{B.1}$$

To begin with, let us assume that the channel is straight. Then, $\lambda = \xi$, and minimization of the energy (B.1) gives $\lambda \sim b\sqrt{\epsilon_w/\epsilon_m} \gg b$. This formula can be found in the book ref. [22]. Given that $y = \epsilon_w/\epsilon_m$, this formula is equivalent to our result for the antenna length in the straight antenna regime A (assuming $d = 1$).

Consider now coiled channel; such problem was never considered in electrostatic context, but one can imagine, for instance, a flexible fiber of high dielectric constant material surrounded by air. Formula (B.1) still applies, but $\xi \sim \sqrt{\lambda p}$. Minimization then yields $\lambda \sim b^{4/3}p^{-1/3}\left(\epsilon_w/\epsilon_m\right)^{2/3} = b^{4/3}p^{-1/3}y^{2/3}$, which is our result for the antenna length in the regime B.

To conclude, we note that minimization of energy in the electrostatic language is translated to minimization of dissipation in the diffusion language.